Titre: Title:	Investigation on the Mixing Performance in a Superblend Coaxial Mixer
Auteur: Author:	Xiao Wang
Date:	2014
Type:	Mémoire ou thèse / Dissertation or Thesis
Référence: Citation:	Wang, X. (2014). Investigation on the Mixing Performance in a Superblend Coaxial Mixer [Thèse de doctorat, École Polytechnique de Montréal]. PolyPublie. https://publications.polymtl.ca/1409/

UNIVERSITÉ DE MONTRÉAL

INVESTIGATION ON THE MIXING PERFORMANCE IN A SUPERBLEND COAXIAL MIXER

XIAO WANG

DÉPARTEMENT DE GÉNIE CHIMIQUE

ÉCOLE POLYTECHNIQUE DE MONTRÉAL

THÈSE PRÉSENTÉE EN VUE DE L'OBTENTION

DU DIPLÔME DE PHILOSOPHIAE DOCTOR

(GÉNIE CHIMIQUE)

MARS 2014

UNIVERSITÉ DE MONTRÉAL

ÉCOLE POLYTECHNIQUE DE MONTRÉAL

Cette thèse intitulée:

INVESTIGATION ON THE MIXING PERFORMANCE IN A SUPERBLEND COAXIAL MIXER

présentée par: WANG Xiao

en vue de l'obtention du diplôme de : Philosophiae Doctor

a été dûment acceptée par le jury d'examen constitué de :

M. BERTRAND François, Ph.D., président

M. TANGUY Philippe A., Ph.D., membre et directeur de recherche

M. FRADETTE Louis, Ph.D., membre et codirecteur de recherche

M. TAVARES Jason-Robert, Ph.D., membre

M. CHOPLIN Lionel, Ph.D., membre

Dedicated to my dad and my mom

--you are my everything

ACKNOWLEDGEMENTS

There is a Chinese saying says: do not say ’thank you’ if one received an enormous kindness from the other. Indeed, the two words are too plain to express my gratitude to these people for their consistent supports and encouragements.

Dr Tanguy, my mentor, brought me to URPEI. We first met in Beijing in 2008. He was invited by Bruce Gao, my previous supervisor, who guided me to the world of mixing, for a mixing speech in my previous university, Beijing University of Chemical Technology. If I have to name some people that I really worship, he is always the one on the top. Every time he talks to me, it is like opening a door to another world in my face. I am so desperate for hearing the intriguing industrial experiences he has gained through his world tours. I always ponder that when and how I could be like him. Frankly, I do not expect to catch up with him, but I believe with all my efforts I can get closer to him step by step.

Dr Fradette, my mentor, has been guiding and inspiring me ever since the first day we met. This gentleman told me on that day: ‘My office door is always open for you’, but I didn’t expect he was serious. In the passing years every time I need help and support from him, he is always ready for helping me out with his ‘power-cube’ filled with innovation and erudition, no matter where he is and when it is. No wonder all my friends at Poly envy me so much for being his student. I know he knows he is wonderful, like everybody does.

Dr Bertrand, the mentor of every student in URPEI, has been caring and encouraging me in the past years. The greatest lesson he has taught me is not GCH 6914, but an advice he gave us in the course: ’if one wants to learn something, just go teach it.’ This advice is very useful, and I indeed give the credit to him every time I cite it.

Dr Kresta, the jury member for my Ph. D proposal, has been concerning about my study progress all the time. She gave me a broad vision for mixing and shared with me the cool things occurred in industry.

Dr Inci Ayranci, the co-author of my two papers, has been my teacher and good friend ever since she came to URPEI. Having her around, I don’t need to look up the reference on solid-liquid mixing anymore. I sincerely appreciate her understanding and suggestions during our discussions on my research and the chaotic ideas in my head. Best wishes for her bright future.

Émir, my close colleague, the translator of the abstract, has been a good accompany both in the office and laboratory. His attitude to the experiment and research has been inspiring me, and his food supply to me is also an important support for my hard working.

There are still so many people I would love to list, including my dear colleagues in URPEI, the teachers, technicians and administrative staff in department and all my dear friends at Poly. All the accomplishments I have obtained so far belong to them as well.

I am blessed in having them all around ☺

RÉSUMÉ

Le mélange est une opération unitaire très courante dans les procédés industriels qui trouve son application dans divers domaines tels que la dispersion de liquides, la suspension de solides, les réactions chimiques (polymérisation, fermentation…) et d'autres applications. Par ailleurs, dans beaucoup de cas impliquant des systèmes monophasique ou multiphasique, d'importantes variations de la viscosité peuvent être observées durant le procédé en raison des comportements rhéologiques complexes des systèmes mis en jeu. Cela se traduit notamment par une très grande déviation par rapport aux principes considérés lors de la conception d'un mélangeur standard. Ainsi, le choix d'un type de mélangeur pouvant assurer une efficacité élevée tout au long du procédé peut être une opération relativement complexe nécessitant beaucoup d'innovation. Dans cette optique, différents types de mélangeurs ont été considérés dont le mélangeur coaxial « Superblend » qui a donné les résultats extrêmement prometteurs. Ce mélangeur se compose de deux agitateurs : Un ruban hélicoïdal et un Maxblend. Ainsi, grâce à cette combinaison, différentes conditions de fonctionnement peuvent être considérées dans un seul récipient pour faire face aux problèmes liés aux comportements rhéologiques complexes des fluides mis en jeu.

Ayant pour objectif d'apporter plus de compréhension des performances de mélange, des principes de conception et des lignes directrices des opérations de scale up de ce type de mélangeur, une caractérisation complète de l'hydrodynamique du Superblend a été réalisé en considérant des fluides Newtonien et non-Newtoniens dans des systèmes monophasique ou multiphasique. Les résultats obtenus ont montré que le champ d'écoulement, les performances de mélange en termes de puissance consommée et de temps de mélange ainsi que la contribution de chaque agitateur dépendaient fortement du comportement rhéologique, de la taille des particules et de leur concentration dans les suspensions de solides, du rapport de vitesse des agitateurs ainsi que du mode de rotation. La vitesse caractéristique proposée par Farhat et al. (2008) pour les mélangeurs coaxiaux a notamment été appliquée à d'autres mélangeurs multi-arbres qui n'ont pas été considérés dans les précédents travaux et le domaine d'application et limitations ont été discutés. Ainsi, en comparant les résultats avec les données disponibles, la puissance consommée, le temps de mélange et l'énergie de mélange de différents types de mélangeurs ont été présentés et une approche globale pour prédire la puissance consommée des mélangeurs multi-arbre a été proposée. En conclusion, il a été trouvé que le Superblend surclassait tous les autres mélangeurs en termes de temps et d'énergie de mélange.

ABSTRACT

Mixing is a ubiquitous unit operation in the process industries with numerous applications in reaction (polymerization, fermentation), distribution of solids and liquids, and blending (manufacturing of formulated products). In many cases of single-phase and multi-phase systems, widely and rapidly varying viscosities over the processing time occur along with the development of complex rheological behaviors. Since there is a huge gap between the design principle of the standard mixing approach and the mixing mechanism in rheologically complex systems, the resulting mixing inefficiencies have roused the innovations in mixer design and optimization.

Among a variety of equipments and geometries designed to fill this gap, a recently emerged mixer concept Superblend coaxial mixer is one of the very promising candidates. Superblend coaxial mixer consists of two impellers: a helical ribbon as outer impeller and a Maxblend impeller as inner impeller. This combination allows a synergy between impeller geometries in different operating conditions in a single vessel to tackle the problems in rheologically complex mixing. Aiming at providing comprehensive scientific information on mixing performance, process design principles and scale-up guidelines, a full characterization of the single-phase and multiphase hydrodynamics in the Superblend mixer with both Newtonian and non-Newtonian fluids was carried out. Results exhibited that various experimental parameters such as rheological behavior, particle size and concentration, speed ratio and rotating mode have significant influence on the mixing performance in terms of flow pattern, power consumption, mixing time and evolution, contribution of each impeller and the optimal operating conditions.

New definition of characteristic speed proposed by Farhat et al. (2008) for coaxial mixers were extended to some other multi-shaft mixers not considered in previous works, and the applicability and limitations were discussed. Based on the comparison and analysis of existing resource, the power consumption, mixing time and mixing energy of different mixers were presented and a general approach to predict the power consumption in multi-shaft mixer was introduced. The Superblend mixer outperforms all the other mixers from the perspective of mixing time and mixing energy despite the lack of power-efficiency.

TABLE OF CONTENTS

LIST OF TABLES

LIST OF FIGURES

LIST OF SYMBOLS AND ABBREVIATIONS

Roman letters

c	Clearance between the ribbon and tank wall (m)
D	Impeller diameter (m)
$D_{helical\ ribbon}$	Diameter of helical ribbon (m)
D_i	Diameter of the inside impeller (m)
$D_{Maxblend}$	Diameter of Maxblend impeller (m)
D_o	Diameter of the outside impeller (m)
D_s	Shaft diameter (m)
E_{mix}	Mixing energy (-)
h	Height of helical ribbon (m)
H	Liquid height (m)
I	Electrical current (I)
G’	Storage modulus (-)
k	Consistency index (-)
K	Geometrical parameter (1/m)
K_P	Power constant (-)
K_P’	Characteristic power constant (-)
$K_P{'}_{MB}$	Characteristic power constant of Maxblend (-)

$K_{P'Total}$	Total characteristic power constant of Superblend (-)
K_S	Metzner constant (-)
L	Blade length (m)
M	Torque (N·m)
M_c	Corrected torque (N·m)
M_m	Measured torque (N·m)
M_r	Residual torque (N·m)
n	Power-law index (-)
n_b	Number of blades (-)
N	Rotational speed (1/s)
N'	Characteristic rotational speed (1/s)
$N_{co\text{-}rotating}$	Rotational speed in co-rotating mode (1/s)
$N_{helical\ ribbon}$	Rotational speed of helical ribbon (1/s)
N_H	Homogenization speed (rpm)
N_i	Rotational speed of inside impeller (1/s)
N_{js}	Just suspended speed (1/s)
$N_{Maxblend}$	Rotational speed of Maxblend impeller (1/s)
N_o	Rotational speed of outside impeller (1/s)
N_P	Power number (-)

N_P'	Characteristic power number (-)
p	Pitch (m)
P	Power consumption (W)
$P_{helical\ ribbon}$	Power consumption of helical ribbon (W)
$P_{Maxblend}$	Power consumption of Maxblend impeller (W)
$P_{Superblend}$	Power consumption of Superblend (W)
Pv	Specific power consumption (W/m^3)
R	Resistance (Ω)
Re	Reynolds number (-)
Re_{liquid}	Reynolds number of the liquid (-)
Re_η	Reynolds number for shear-thinning fluids (-)
Re'	Characteristic Reynolds number (-)
Re'_η	Characteristic Reynolds number for shear-thinning fluids (-)
R_N	Speed ratio N_i / N_o
t	Time (s)
t_H	Mixing time for homogenization (s)
t_m	Mixing time (s)
T	Tank diameter (m)
V	Voltage difference (V)

$V_{ø}$	Hindered settling velocity (m/hour)
w	Blade width (m)
$wt\%$	Weight percentage

Greek letters

ρ	Density (kg/m^3)
ρ	Resistivity (Ω /cm)
a	Dependence constant (-)
λ	Time constant (-)
ρ_{liquid}	Liquid density (kg/m^3)
ρ_s	Solid density (kg/m^3)
μ	Viscosity (Pa.s)
μ_{liquid}	Liquid viscosity (Pa.s)
μ_a	Apparent viscosity (Pa.s)
$\dot{\gamma}$	Shear rate (1/s)
$\dot{\gamma}_{av}$	Average shear rate (1/s)
σ	Electrical conductivity (S/m)
Θ	Dimensionless mixing time
Θ_0	Plateau value of Θ at low Reynolds number
Θ_∞	Plateau value of Θ at large Reynolds number

Abbreviations

CFD	Computational fluid dynamics
CMC	Carboxymethylcellulose
ERT	Electrical resistance tomography
LBP	Linear back projection
OAT	Optical attenuation technique
PIV	Particle image velocimetry
rpm	Revolutions per minute

CHAPTER 1: INTRODUCTION

1.1 Mixing research

Mixing operations are widely used in chemical engineering industry as well as biotechnology, and environmental remediation. The efficiency of mixing is associated with the results of the corresponding process and the cost of products. Meanwhile, mixing is also a unit operation that not fully-developed in the theoretical research, which leads user to more rely on the practical experience. For different operation occasions, even for analogical operation purpose, different mixing setups are basically applied. Due to the lack of the common standard for the comparison between the performances of equipments, it causes the huge inconvenience to determine the most effective approach for specified mixing task.

Therefore, the design of mixing installation becomes the key on the evaluation of a new technology or even a new production line. A proper design of agitation system is capable of diminishing the investment, decreasing the production cost, and obtaining the satisfactory process results. However, all this is based on the good understanding of mixing theory and being familiar with the rich experience and important research achievement that the previous researcher have accumulated up to now.

The mixing has been studied systematically as an individual unit operation for merely 60 years. In 1950's, the theoretical foundation of mixing was built on the basis of fluid dynamics and mass transfer principles by dimension analysis and similarity theory. Nevertheless, the similarity theory was unable to touch the core to this complex process, which resulted in the lasting problem that the design and scale-up of mixing system could not be handled in a content manner.

As the further development of mixing theory, the study on the turbulent phenomenon has partly discover the essential of mixing process. Especially in the past two decades, the theoretical research has improved remarkably benefiting from the innovative research method, for example CFD (computational fluid dynamics), and experimental techniques such as PIV (Particle Image Velocimetry). Although it is impossible to establish a new system of mixing theory, certain latest research achievement has already been utilized for the more reasonable design and scale-up.

Due to the development of the industrial demands, however, fluids mixing with diverse viscosities and rheological behaviors such as shearing-thinning effect, as well as homogeneous distribution of solids in liquids, keep arising in this field. Compared with the turbulent mixing, this kind of mixing process belongs to another system of mixing theory.

Referring to this case, if conventional mixing setup is used, which is characterized by a single or multiply impellers (as shown in Figure 1.1), it is obvious that the mixing performance and efficiency is unable to be satisfied, or even it is impossible to achieve the mixing effect. This is all because of the guideline that followed in the design process of these mixers.

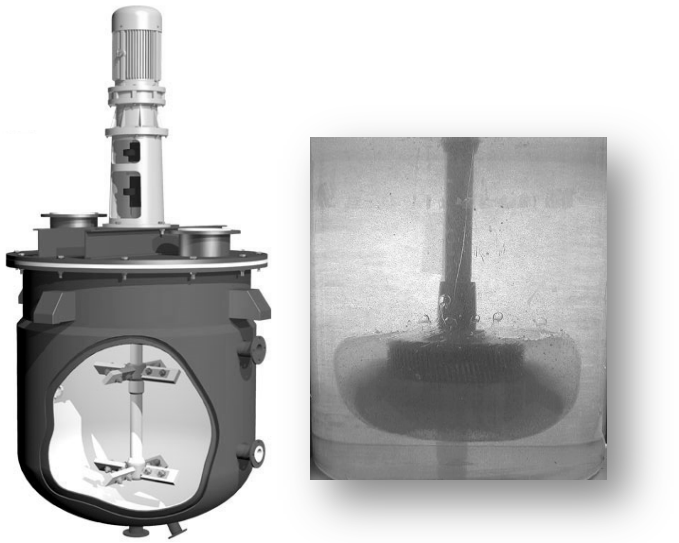

Figure 0.1: Conventional mixing setup and the cavern it causes

As mentioned above, based on the relatively full development of turbulent theory, numerous mixers in industry are designed under turbulent theory, so that those mixers are merely suitable for the turbulent mixing. Therefore, a variety of drawbacks such as stagnancy, segregation, cavern and even mechanical damage are observed in the applications. It was reported that the overall consumption for such poor mixing was approximately $ 10 billion in the US chemical industry in 1989.

Being aware of this current situation, researchers throughout the world have started to study and design proper mixing setups for fluid mixing with complex rheological behavior and homogeneous solid-liquid distribution, which is also the emphasis of this work.

1.2 Structure of the thesis

This thesis is composed of seven chapters. The first chapter provides a general view of mixing research. Chapter 2 reviews the previous studies in multi-shaft mixers, and states the objectives of this investigation. Chapter 3 experimentally investigates the effect of operating parameters such as speed ratio and rotating mode on the power consumption and mixing time in the Superblend coaxial mixer with viscous Newtonian fluids. The highlights lie in the variation of flow patterns in different rotating mode, the power contribution of each impeller and the distinct optimal operating condition in each flow regime. Chapter 4 compares and analyzes the power consumption, mixing time and mixing efficiency of three types of multi-shaft mixers with Newtonian fluids, and assesses the applicability of new definitions of characteristic speed and diameter in a series of multi-shaft mixers. The Superblend mixer outperforms all other mixers based on comprehensive evaluation of both power consumption and mixing time. Chapter 5 extends the research to non-Newtonian fluid mixing, and thoroughly investigates the effect of speed ratio, rotating mode and rheological behavior on the power consumption, mixing time and mixing evolution in the Superblend mixer. A promising outcome is that the mixing efficiency of the Superblend mixer with non-Newtonian fluids even excels that with Newtonian fluids. Chapter 6 quantitatively explores the effect of particle size and concentration and operating parameters on the mixing performance of the Superblend mixer for homogeneous solids distribution with viscous Newtonian fluids. Chapter 7 generally discusses the conclusions on the results and technologies, and provides recommendations for the future researches.

CHAPTER 2: LITERATURE REVIEW

2.1 Mixing theory of highly viscous fluid

Being different from lowly viscous fluid mixing, due to the lack of diffusion phenomenon, the primary mixing principle of highly viscous fluid mixing is shearing mixing and convection mixing. The shearing effect produced by the impeller keeps stretching the target fluid (the cyan phrase) into thin flow layers. As the layers become thinner and thinner, the folding effect starts working. With the continuous stretching and folding actions, the target fluid finally gets broken and achieves the homogeneous mixing with the main fluid in the tank (the yellow phrase in Figure 2.1).

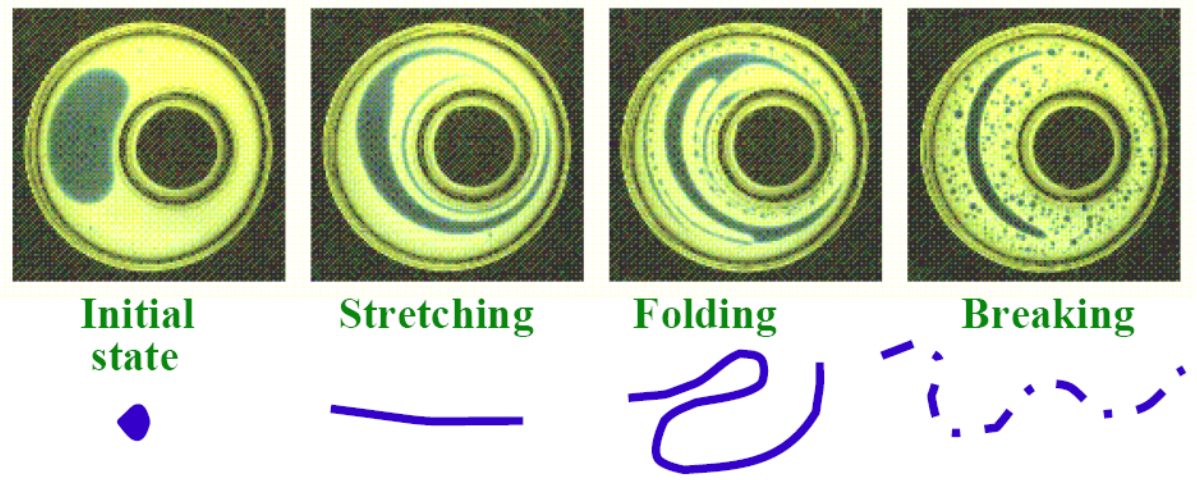

Figure 2.1: The schematic of mixing in laminar regime

With regard to the folding process in the highly viscous mixing, the existence of shear force is not sufficient as the driving force. Since the distribution of shear rate throughout the tank is not uniform, there is supposed to be a circulation effect that could transfer this shear force across the whole tank, namely the liquid elements in high shearing region and low shearing region should be exchanged continuously. The performance of this circulation will determine the efficiency of converting all the driving forces in this tank into effective driving forces.

To sum up, the performance of such mixing lies on whether sufficient shearing is generated near the impeller and the fluid in both high and low shearing regions can be fully circulated. Therefore, traditional mixing installations typified by a single impeller or multi-ply impellers can hardly deal with rheologically complex mixing with satisfying efficiency, restricted by bad regions, stagnancy, segregations and even complete failure of getting full-tank mixing. A variety of mixers are introduced to tackle viscous fluid mixing in a large variation range, such as dual shaft mixers, coaxial mixers, Maxblend and Superblend.

2.2 Maxblend

In the 1990's, a wide impeller named Maxblend as shown in Figure 2.2 was designed by SHI Mechanical & Equipment and was characterized by good mixing performance, low power dissipation, easy to clean, and most significantly capabilities of operating in a wide range of fluid viscosities (Takenaka et al., 2006). Compared with traditional turbine impellers, the Maxblend impeller produces more uniform shear rate distribution for the mixing system (Iranshahi et al., 2007).

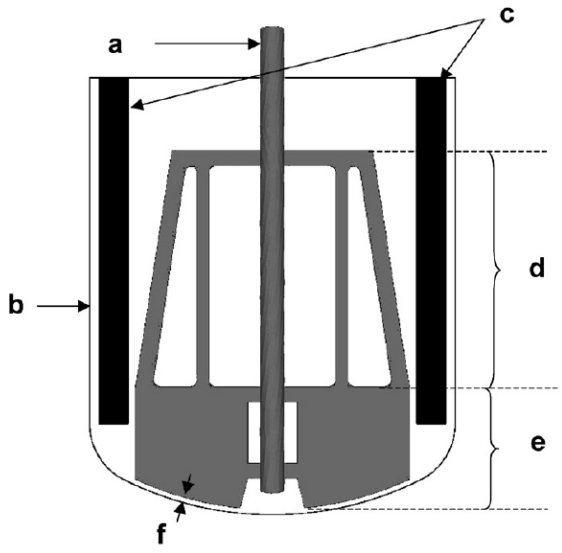

Figure 2.2: Schematic of the Maxblend (Arash Iranshahi et al., 2007)

(a) Maxblend impeller; (b) tank ; (c) baffles; (d) grid (e) paddle (f) bottom gap

The effect of tank scale, rheological behavior, baffle installation and bottom clearance on the power consumption, mixing time, mixing evolution and mixing energy has been reported by Fradette et al. (2007). They introduced a decolorization method for the Maxblend mixer and carried out a comprehensive investigation on the mixing characteristics of the Maxblend impeller in the laminar, transitional and turbulent regimes with both viscous Newtonian and Non-Newtonian fluids at three different scales. On the basis of the comparison between different mixing configurations, the Maxblend impeller is proven to be very efficient for the viscous fluids mixing in light of short mixing time and low power consumption.

The pumping evaluation of the Maxblend impeller can be realized by using an equation proposed by Guntzburger et al. (2013). It is featured by the slope of the mixing curve to express the global pumping effect from the comprehensive behaviour of the axial, radial and tangential flows rather than the simple integration of the single flows. It is noted that the pumping capacity with shear-thinning fluid decreases noticeably due to the 'pathological mixing situation' emerged at low Reynolds number ($Re < 80$), and even the segregation phenomenon occurs when $Re < 10$.

2.3 Dual shaft mixers

Figure 2.3 shows a combination of a centered low-speed low-shear Paravisc impeller and an off-centered high-speed high-shear Deflo (Barar Pour et al., 2007). The power consumption of Paravisc decreases as the speed ratio of the high-speed impeller to the low-speed impeller increases, which can be explained as the influence of the drag force imposed by Deflo. However, the Paravisc has no evident influence on the power consumption of Deflo. The power constant K_P ($K_P = N_P \times Re$) is an important index to describe the power consumption in the mixer in laminar regime. K_P of Deflo is found higher than that in Foucault's study, which can be explained as the existence of strong interaction between the tank wall and Deflo, due to the closer location to the wall after being off-centered. Referring to the mixing time, it decreases remarkably as the speed of Deflo impeller increases. But when the rising of the Deflo rotating speed goes further, the increasing effect will not be noticeable.

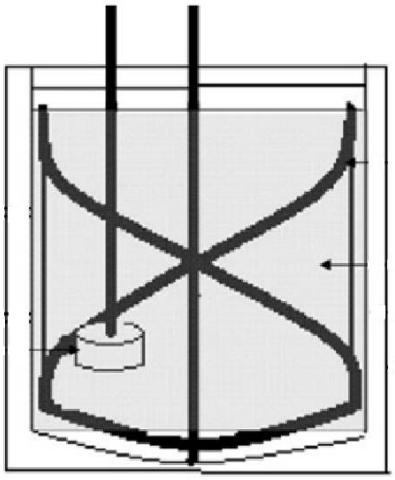

Figure 2.3: The configuration of a dual shaft mixer. (Barar Pour et al., 2007)

Figure 2.4 shows two different types of dual shaft mixers (Cabaret et al., 2007). An eccentric shaft would be helpful to break the segregated region in the tank, but have no effect on the prevention of compartmentalization. On the contrary, the dual shaft system is capable of avoiding that. The power consumption of the dual shaft mode is lower than single shaft mode. The dimensionless mixing time of counter-rotating mode is much smaller than that of co-rotating mode. It must to be noted that as the drawback of co-rotating mode, there is a pressure barrier between impeller B and shaft A. It is this pressure barrier that leads to the presence of little compartmentalization region.

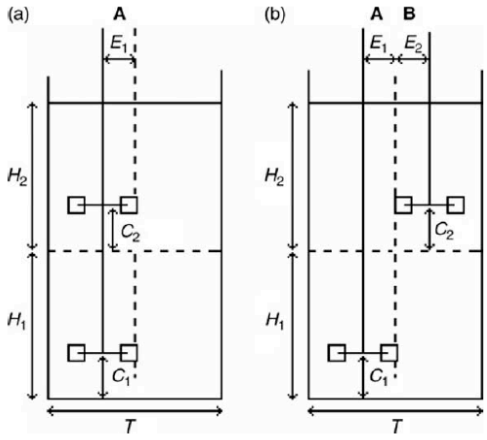

Figure 2.4: Geometries of two different dual shaft mixers. (Cabaret et al., 2007)

2.4 Coaxial mixers

The mixing mechanisms for the highly viscous fluids were pointed out by Tanguy and Thibault, (1997): intensive dispersion at low viscosity and good homogenization at high viscosity, which is regarded as an important reference to the selection of mixing system. They chose Rushton turbine as a source of good dispersion and helical ribbon as an approach to create good homogenization (Figure 2.5).

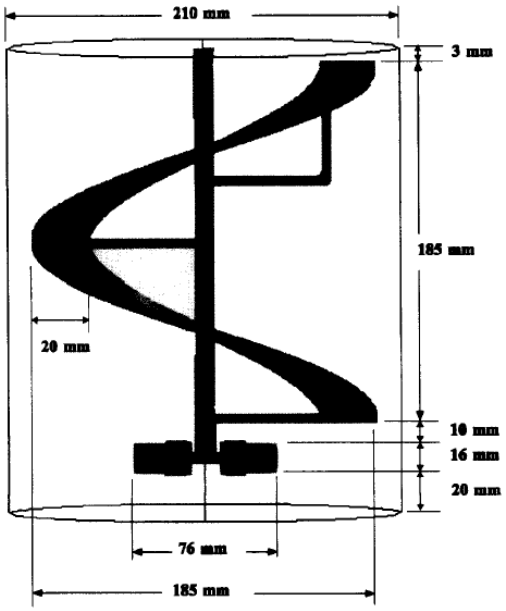

Figure 2.5: The schematic of coaxial mixer. (Tanguy and Thibault, 1997)

Six Newtonian fluids and six shear-thinning fluids were applied as the experimental liquids. Results showed that with the addition of Rushton turbine, the aggregated region can successfully be broken. For the shear-thinning fluids, the dispersion capability of Rushton turbine is even enhanced. The pumping pattern generated by this configuration will not vary from different rheology, which makes this coaxial mixer as a promising system to handle the fluid mixing of complex rheology. On the aspect of power consumption, they claimed that the K_P of Rushton turbine is not affected by the presence of helical ribbon.

Figure 2.6 shows a coaxial mixer consisting of a pitched-blade turbine with wetting rods and a vessel wall-scraping anchor (Thibault et al., 2002; Tanguy et al., 2002). The rods can bring pre-dispersion at the liquid surface at the cost of remarkably low power. The primary consumption of

power in the coaxial mixer is from the high-speed inner impeller and the power number increases along with the speed ratio. The relationship between the speed ratio and threshold of transition regime is: the higher the speed ratio is, the lower the threshold is. The power constant K_P of the anchor depends on the speed ratio quadratically for the Newtonian fluid. For non-Newtonian fluid, the power constant varies along the parabolic curve while the increase of speed ratio, and decreases exponentially when the power law index increases.

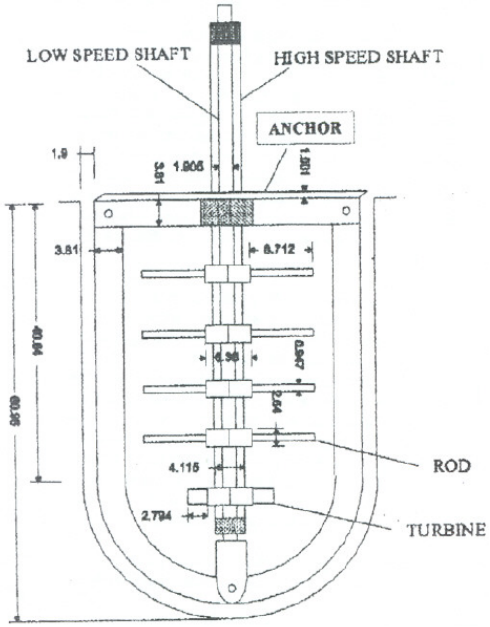

Figure 2.6: Experimental setup. (Thibault et al., 2002)

Figure 2.7 shows the combinations of various impellers and an anchor (Foucault et al., 2004, 2005, and 2006). The power numbers of dispersion impellers were not affected by the anchor speed, while the anchor power consumption is affected by high-speed impellers. From the power curve of single impellers, it was noted that the critical Reynolds number from laminar regime to transition regime was 100 when single anchor was rotating, while this number changed into 20 with respect to the single Rushton turbine and the threshold for the turbulent regime was 1000. For the dispersion impellers, the laminar regime stopped at Re = 10, and the turbulent regime started from Re = 4500. In the coaxial mixer, however, the threshold for the transition regime decreases as the speed ratio rises when the system is under counter-rotating mode. In addition, this phenomenon does not happen in the co-rotating mode. The power consumption from anchor increases along with the Rushton turbine in counter-rotating mode and decreases in co-rotating

mode. This observation was explained as the addition and subtraction of different pressure forces imposed on the anchor.

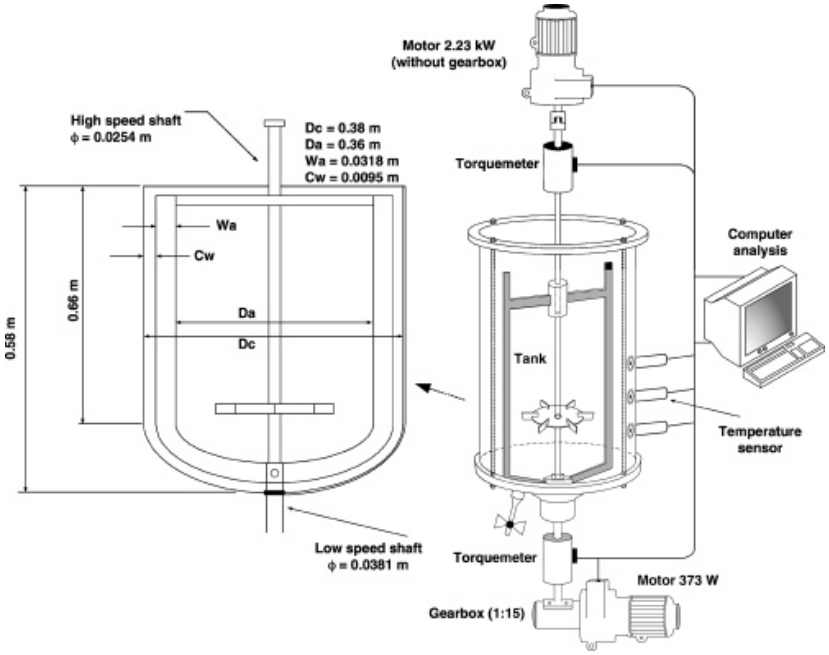

Figure 2.7: Experimental system. (Foucault et al., 2004)

The flow pattern produced by a coaxial mixer is affected by the speed ratio between two impellers. Referring to the mixing time in this system, the mixing time increases along with the anchor speed before a certain speed, and then decreases as the anchor speed rises in counter-rotating mode. In co-rotating mode, the mixing time decreases rapidly as the anchor speed rises. The co-rotating mode was more effective than the counter-rotating mode under the same power consumption (Espinosa-Solares et al., 2001). However, the ability of breaking segregation is stronger in counter-rotating mode. When the speed ratio is high, in the counter-rotating mode the mixing performance is more efficient (Bonnot et al., 2007), which is consistent with the numerical results obtained by Rivera et al. (2006).

The hydrodynamics of a co-rotating coaxial mixer with a combination of A200 impeller and an anchor was investigated by Rudolph et al. (2007). They agreed with the results obtained by Thebault and Tanguy (1997) and Köhler et al. (2003) about the effects of the speed ratio on the power consumption, and successfully drew the single master power curve for both Newtonian and Non-Newtonian fluids with modified Reynolds number.

A coaxial mixer that composed of a radial or an axial impeller mounted with an anchor was introduced by Farhat et al. (2007). It's showed that the axial impeller-anchor system exhibited less power consumption and lower mixing time than that obtained by the combination of radial impeller and anchor.

To study and compare the hydrodynamics of the multi-shaft system instead of single impeller, a new universal correlation for characteristic rotational speed of the coaxial mixer (equation 2.1) was proposed by Farhat et al. (2008). Compared with the correlations proposed by Foucault et al. (2005) (equation 2.2), the new correlation can be used to obtain single power curve for different coaxial mixers regardless of the diameter difference of the inner impellers.

$$N = \frac{(N_i D_i + N_0 D_0)}{D_i}$$

(2.1)

$$N_{co-rotating} = N_i - N_o;\ N_{counter-rotating} = N_i + N_o \qquad (2.2)$$

On the basis of the new correlation, the effects of diameters of inner impellers on the mixing time in a coaxial mixer composed of an anchor can be seen in Figure 2.8 (Farhat et al., 2008). Four Rushton turbines with different diameters (9, 12.5, 15.8, 20 cm) were used. The dimensionless mixing time of the Rushton turbine with 12.5 cm is the least in the range of laminar and early transition regime. Subsequently, the 20 cm Rushton turbine has the least mixing time. This observation was also found in the counter-rotating mode. While the Rushton turbine was working only, the 20 cm impeller, showed the smallest dimensionless mixing time due to its largest diameter in this investigation. The 9 cm Rushton turbine has the largest mixing time in any rotating mode. For a certain diameter, the co-rotating mode requires the least mixing time and counter-rotating the most in the laminar and early transition regime.

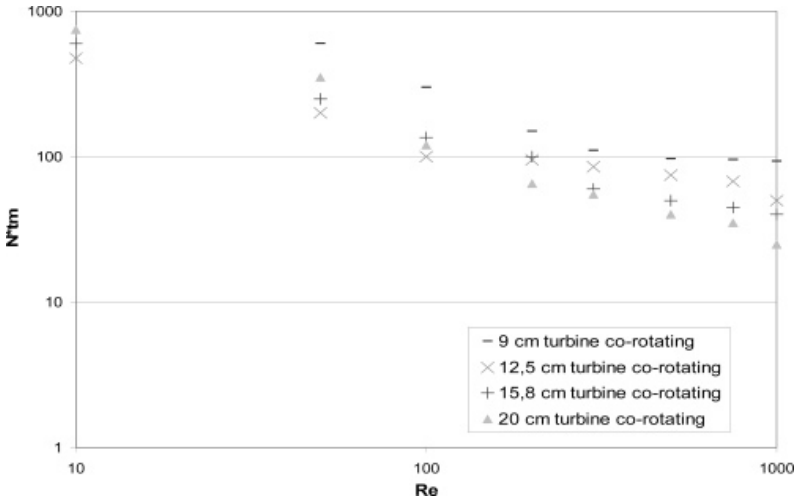

Figure 2.8: Influence of turbine diameter on the mixing time. (Farhat et al., 2008)

2.5 Superblend

Due to the increasing application of highly viscous mixing, many new mixers are designed for satisfying the industrial requirement. Superblend coaxial mixer as shown in Figure 2.9 is a mixing instrument designed by SHI Mechanical & Equipment that characterized by a combination of a Maxblend impeller (generating high shearing and good circulation effects) and a helical ribbon (generating intensive shearing effect). This system has been proposed as a promising technology for viscous fluid mixing with large viscosity variation (Kuratsu et al., 1994; Farhat et al., 2009).

Using the correlation of the characteristic rotational speed proposed by Farhat et al. (2008), single power curve for Newtonian fluids can be obtained regardless the viscosity, speed ratio and rotating mode. When the speed ratio is above 10 in Superblend mixer, the co-rotating mode is more efficient than counter-rotating mode in the laminar and early transitional regimes. Although the Superblend mixer requires more power than some classical coaxial mixers (coaxial Rushton - Anchor mixer and coaxial Mixel TT - Anchor mixer), it exhibits higher mixing efficiency in terms of mixing time and mixing energy (Farhat et al., 2009).

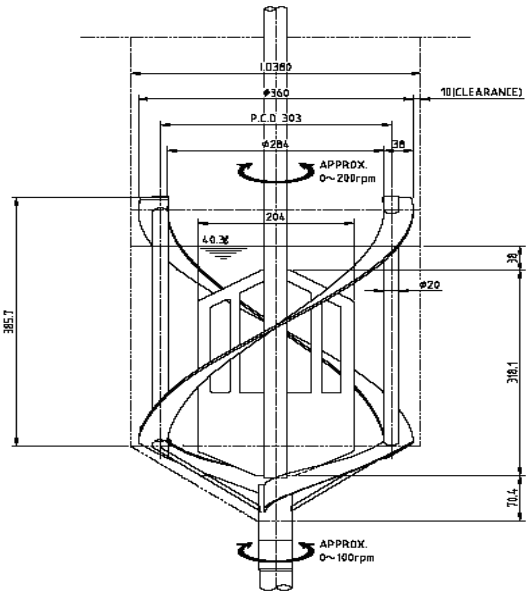

Figure 2.9: Configuration of the Superblend mixer.

2.6 Solid-liquid mixing

2.6.1 Solid-liquid suspension

Generally, solid-liquid suspension is classified into three situations: on bottom motion, complete off-bottom suspension and uniform suspension as shown in Figure 2.10.

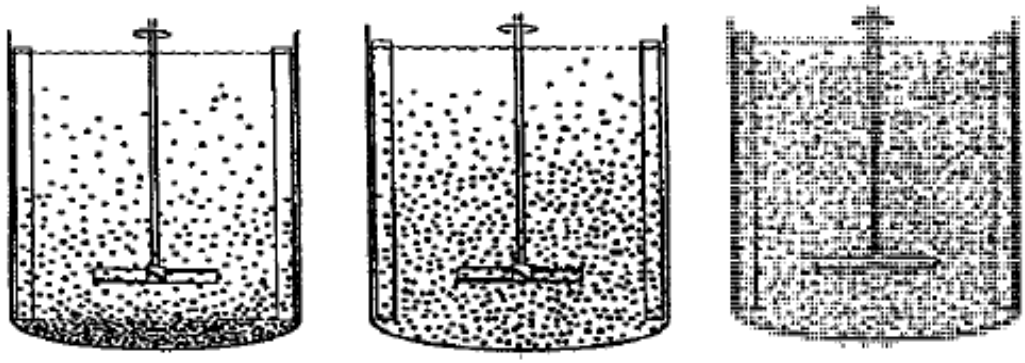

on-bottom motion complete Off-bottom suspension uniform suspension

Figure 2.10: Different situations of suspension.

On-bottom motion suspension

This situation can be described as the complete motion of all the solid particles in the whole tank, regardless of the aggregations of particles nearby the bottom of the tank, which means there are still some particles are in the motion that has contact with the tank bottom. In this case, the surface area of particle cannot be totally calculated for the chemical reaction and transfer. It is suitable for dissolution of solids with high solubility.

Complete off-bottom suspension

This situation can be described as a complete motion of particles that no particle lays on the tank bottom for 1 s to 2 s, even though the suspension throughout the tank might not be uniform. Due to this whole motion, the surface area reaches the maximum level for the chemical reaction and a diversity of transfer. Since this situation is the minimum mixing requirement in the most solid-liquid systems, just suspended speed N_{js} is always chosen as an important parameter in the study of solid-liquid system.

Uniform suspension

This situation can be described as the formation of both uniform particle concentration and particle size distribution in the whole tank.

$$\text{Suspension percentage} = \frac{\text{the weight percentage of the solids in sampling spot}}{\text{the averge weight pencentage of the solids in the whole tank}} \times 100\% \tag{2.3}$$

here, the suspension percentage might greater, equal to or smaller than 100%. As for the uniform suspension, the suspension percentage is 100%. Basically, the particle distribution does not obviously improve if increasing the power input or rotating speed. This suspension is required in processes such as crystallization process and solid catalyzed reaction, where uniform solids concentration is vital to the efficiency of an operation unit or even the continuity of a whole production line. Of course, this ideal scene is based on more power input, more effective equipment configuration and certain operating conditions.

2.6.2 Distribution and dispersion in the solid-liquid mixing

Distribution and dispersion are discussed when the quality of solid-liquid mixing is studied. The uniform suspension depends both on good distribution and dispersion.

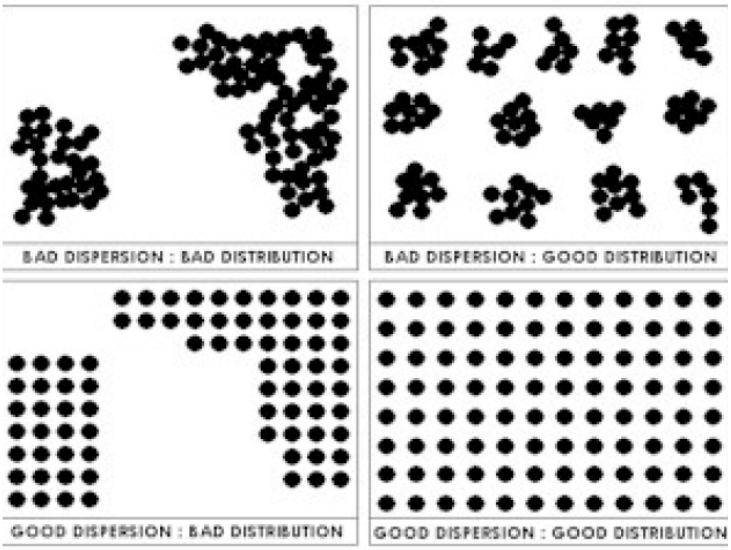

Figure 2.11: Difference between dispersion and distribution

The difference between distribution and dispersion can be observed in Figure 2.11. It can be seen that the appearance of aggregations in the first row. The difference of those conditions is the distribution of aggregations. In the first case, the particles aggregate randomly, while the aggregation distributes orderly in the second case. So the latter situation is called good distribution but bad dispersion.

In the first picture of the second row, we can see that there are still some aggregations from the macroscopic perspective. But for each aggregation, the distribution of particles is uniform. This is locally good dispersion but bad distribution in the whole container.

Finally when we notice the last picture, we can claim that this is exactly the ideal condition we expect in the solid-liquid system: no aggregation and uniform particle distribution everywhere in the tank, which is the uniform suspension. Therefore, both the distribution and dispersion of particles in the tank should be taken into account when the solid-liquid suspension is investigated.

2.6.3 Previous investigations on solid-liquid mixing

Referring to the solid-liquid suspension operation in industry, the most important concern is the specific power input and impeller speed needed to achieve the expected suspension states.

Taking just-suspended state as an example, it shows that when the agitation speed is greater than the just-suspended speed, the effect of agitation speed on the suspension degree is slight, while the power consumption increases dramatically. Thus, in order to get the expected effect without energy waste, the agitation speed should stay at approximately the just-suspended speed as this suspension state is required.

Since the critical impeller speed and power input for each suspension state has remarkable influence on the performance of the solid-liquid system, numerous studied on critical speed and power consumption have been carried out and published by researchers.

Oldshue (1983) pointed out that the achievement of the target suspension states lies on the agitation power input: more energy is required as the target state shifts from on-bottom suspension to off-bottom suspension and finally to uniform suspension (as shown in Table 2.1).

Table 2.1: The influence of power input and operating conditions on the situation of solid-liquid suspension. (Oldshue, 1983)

		Power Ratio at Settling Velocity (ft/min)		
Suspension Criteria	Speed Ratio	16–60 Difficult	4–8 Moderate	0.1–0.6 Easy
On-bottom motion	1	1	1	1
Complete off-bottom suspension	1.7	5	3	2
Total uniformity	2.9	25	9	4

The solid-liquid dispersion can be evaluated on the basis of power consumption evolution. A study on solid-liquid dispersion in a dual shaft Deflo - Paravisc mixer was carried out by Barar Pour et al. (2007) using power consumption evolution.

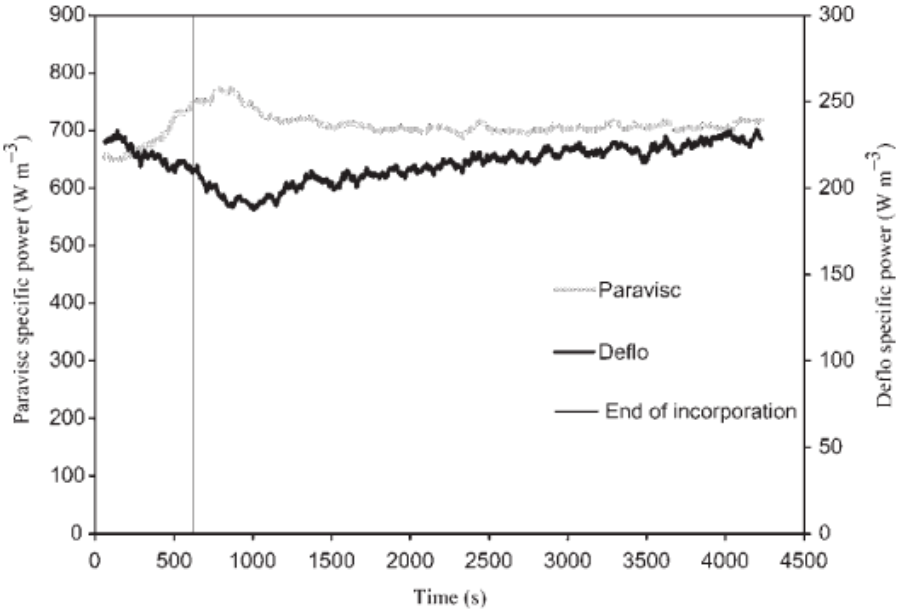

Figure 2.12: Power consumption evolution in solid-liquid dispersion. (Barar Pour et al., 2007)

The evolution of power consumption in solid-liquid dispersion can be seen in Figure 2.12. Results showed that as the solids concentration increases, the power consumption of Paravisc increases; a short period after the incorporation of solid, there appears a peak for this trend. Then the power consumption goes down and forms a plateau eventually. This plateau can be explained as a symbol of achievement of final dispersion. On the contrary, the Deflo shows a minimum value where the maximum value appears for the Paravisc. It was concluded that the formation of agglomerates causes this power drop as the "shear-thinning" effect. The influence of agitation speed on the solid-liquid dispersion can be seen in Figure 2.13a. With the increasing of agitation speed for each impeller, the time takes to transfer to the plateau decreases and the influence of Paravisc on this is much more important than the Deflo. For the effect of continuous phrase viscosity on the solid-liquid dispersion as shown in Figure 2.13b, they revealed that the viscosity has no effect on the position of the power consumption peak. But there is a phenomenon that must be noted is the starting point of continuous phrase with higher viscosity is longer than dispersion media with lower viscosity.

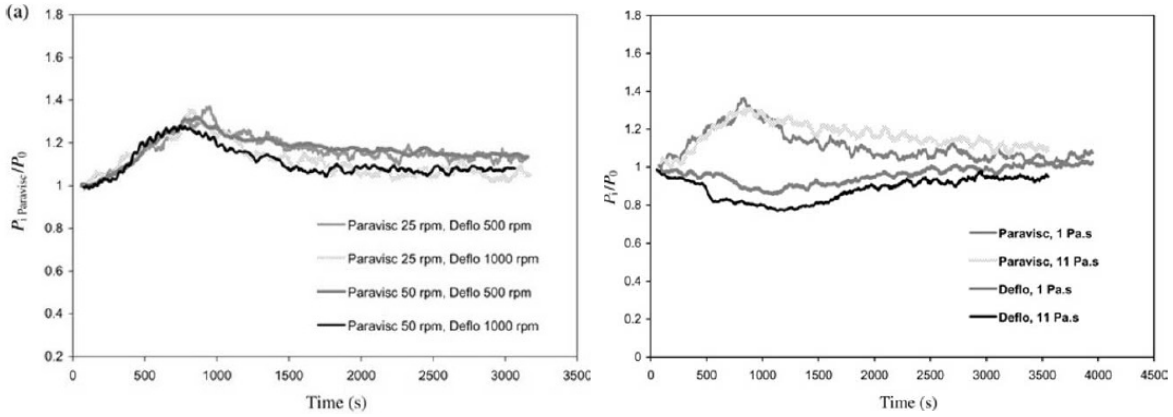

(a) (b)

Figure 2.13: The influence of different factors on the solid-liquid dispersion:

agitation speed; (b) continuous phrase viscosity. (Barar Pour et al., 2007)

Optical attenuation technique (OAT) is a non-intrusive technique to determine the solids concentration in the solid-liquid dispersion process (Fajner et al., 1985). A light beam is emitted out of a light source and goes horizontally across the tank by avoiding the shaft and baffles, then get received by a light receiver. During this process, due to the presence of solid particles, the phenomenon of intensity attenuation is utilized as the detection of solids concentration on the whole horizontal plane. With several measurements on different elevations, the solids concentration profile throughout the tank could be able to be obtained without any intrusion. Taking advantage of this technique, a few researchers (Pinelli et al., 2004; Fajner et al., 2008; Ochieng et al., 2006) have done several works on the solid-liquid dispersion field in terms of the effects of particle size, impeller speed and solids loading on solids concentration distribution, solid dispersion features and the like.

Although OAT has been proved that this technique is reliable and precise, it still has spacial limitation that makes it only able to offer the information on a single line, but not qualified to display the real details on the whole plane. To overcome this drawback, electrical resistance tomography (ERT) is currently applied in many application fields and regarded as the promising technology to measure and analyze the solids concentration in solid-liquid system. The primary

advantage of this technique is the realization of three-dimensional imaging in solid-liquid environment.

ERT is a tomographic system for the phrase concentration and velocity distributions measurement that characterized by non-invasive and soft-field. The principle of this measurement is according to Ohm's law:

$$V = RI \tag{2.4}$$

where the voltage difference V [V] between pairs of adjacent electrodes mounted around the outside wall of aiming object is equal to the product of resistance R [Ω] and the electrical current I [A].

On the other hand, the resistance is inversely proportional to the electrical conductivity σ, [S/m]:

$$R = \frac{K}{\sigma} \tag{2.5}$$

here K is a geometrical parameter, [1/m]. For ERT, K is related to the geometry of electrodes, the distance between them, and the diameter of the object. Since the electrical conductivity for each electrode pair can be obtained, image reconstruction algorithms then are used to compute a cross-sectional image. Finally, the tomogram of conductivity is able to display the situation of solids distribution as shown in Figure 2.14.

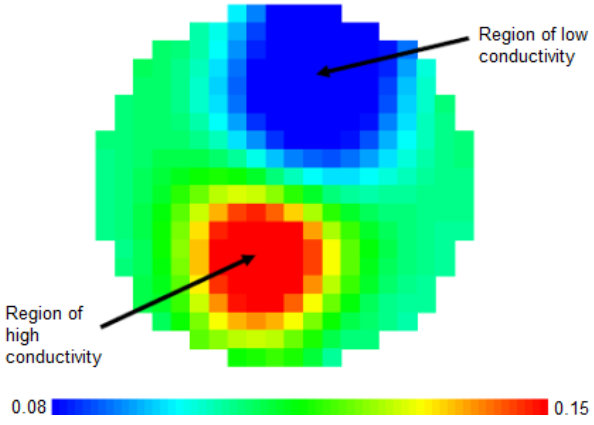

Figure 2.14: Tomogram of conductivity

ERT measurement outperforms other tomograghic approaches on the faster data capture rate and finer spatial resolution (Williams and Beck, 1995). Numerous researcher have done a lot of works on the application of ERT in the study of solid-liquid system, liquid-liquid system, and gas-liquid system in pipe flow (Giguère et al. 2008, Stevenson et al. 2006, Norman et al. 2005), bubble columns(Vijayan et al. 2007, Jin et al. 2007) and LS riser (Razzak et al. 2009).

Reginald Mann (1997) pioneered in introduction this 3-D imaging technique for stirred tank and high anticipation was addressed for its innovative and promoting impact on the visualization of the mixing process inside the stirred tank.

Recently, ERT technique was utilized to investigate the homogeneous solids distribution in water in different geometries. Results proved that the degree of homogeneity in the mixer increases along with the impeller speed. When the homogeneity reaches a maximum degree, the further increase of the impeller speed is detrimental on the homogeneity (Hosseini et al., 2010; Tahvildarian et al., 2011; Harrison et al., 2012). Rather than being consistent throughout the tank, the axial and radial distributions of solids concentration are correlated to the operating conditions (Harrison et al., 2012). The diameter of impeller and the particle size have significant influence on the degree of homogeneity (Tahvildarian et al., 2011). Higher impeller speeds are required for larger particle (1.5 mm) to obtain homogeneous distribution compared to smaller particles (210 and 500 μm) (Hosseini et al., 2010).

2.7 Literature summary and contributions of this thesis

As reviewed above, the studies on the viscous mixing of both Newtonian and non-Newtonian fluids and solid-liquid system with a diversity of configurations have been widely published in open literature. However, there are still several problems that need to be noted and solved:

1. The working fluids might appear extremely high viscosity or cover a large range of viscosity, especially for the highly viscous non-Newtonian fluids used in food and polymerization industry. Single impeller or simple combination of impellers is unable to handle these complex cases. Therefore, a versatile mixer is strongly required in practical industry. The Superblend coaxial mixer is specifically designed for rheologically complex mixing

processes. In this thesis the investigation on the mixing performance in this mixer in both single-phase and multi-phase systems will provide a promising solution for the complex mixing task.

2. The definition of the characteristic rotational speed of the multi-shaft mixers has been a controversial research subject. In this thesis, to validate the applicability of a new correlation for characteristic rotational speed, the extensive investigation of the new correlation in more types of multi-shaft mixers was carried out.

3. The studies on the solid-liquid mixing are mostly confined to the complete off-bottom suspension level. In spite of the fact that some works have carried out on the uniform suspension, they merely used simple approaches such as correlation calculation, sampling measurement and simple optical approach to determine the solids concentration in the tank. In addition, water and low viscosity liquids have appeared as continuous phase in the uniform suspension in some works. However, in the mixing industry, solids distribution in the high viscosity liquids is more common and significant. In this thesis, to provide concrete and practical reference to industrial needs, the investigation of homogeneous solids distribution in viscous continuous phase in a coaxial mixer was first carried out by means of an advanced and reliable technique: electrical resistance tomography. In addition, quantitative measurement using this technique in solid-liquid system is introduced.

2.8 Objectives of the research

2.8.1 General objective

Characterization of mixing performance with high viscosity, shear-thinning fluids and solid-liquid distribution in Superblend mixer

2.8.2 Specific objectives

- Characterization of the mixing performance with highly viscous Newtonian in Superblend mixer in terms of power consumption and mixing time. One journal paper has been published after the accomplishment of this objective (Chapter 3).

- Analysis and comparison of mixing performance in multi-shaft mixers in terms of power consumption and mixing time. One journal paper has been published after the accomplishment of this objective (Chapter 4).

- Characterization of the mixing performance with Non-Newtonian fluids in Superblend mixer in terms of power consumption and mixing time. One journal paper has been submitted after the accomplishment of this objective (Chapter 5).

- Characterization of the hydrodynamics of homogeneous solid-liquid distribution in Newtonian continuous phrase in Superblend mixer in terms of homogeneous speed and mixing time. One journal paper has been submitted after the accomplishment of this objective (Chapter 6).

CHAPTER 3: ARTICLE 1: EFFECT OF OPERATING PARAMETERS ON THE MIXING PERFORMANCE OF THE SUPERBLENDTM COAXIAL MIXER

Article history: Submitted 4 April 2011, Accepted 8 September 2011, Published online 8 September 2011, Industrial & Engineering Chemistry Research.

Authors: Xiao Wang, Louis Fradette, Katsuhide Takenaka and Philippe A. Tanguy

3.1 Abstract

The mixing performance of a Superblend coaxial mixer, which combines a Maxblend™ impeller as the central impeller and a helical ribbon, was investigated experimentally in terms of power consumption and mixing time. The objective was to better understand the influence of the operating conditions on the mixing performance with Newtonian fluids. The experiment setup used allows each shaft to be driven independently. Taking advantage of individual torque-meter on each shaft and a well-developed decolorization technique, it was shown that the speed ratio R_N ($N_{Maxblend} / N_{helical\ ribbon}$ = 1, 2, 4, 6, 8) and the rotating mode (up- and down-pumping of the helical ribbon) have the largest influence on the mixing performance and that there is no universal operating mode for minimizing power and mixing time in all conditions or flow regimes. The results are presented in terms of the power consumption and mixing time throughout the laminar, transitional and turbulent regimes. The contribution of each impeller, the variation of flow patterns, the determination of the optimal operating conditions, and the comparison of power constant are discussed.

3.2 Introduction

Due to the demand for new processes able to handle extreme conditions of viscosity and rheological behaviors, fluid mixing remains an engineering challenge. Coaxial mixers have been designed to handle such difficult conditions. The fundament of the design is to take advantage of a wall-scraping impeller rotating at low speed (anchor or helical ribbon) to generate the bulk flow

and a high shear impeller (turbine of all kinds) rotating at higher speed to break and disperse the bulk.

Anchor blades and helical ribbons with wall-scraping effect have been commonly studied and used. Compared with anchor agitators that are limited in heat transfer application, helical ribbons have been widely used because of their ability to generate axial pumping with relatively low energy consumption. In order to achieve higher efficiency and avoid the drawbacks brought by conventional mixers such as stagnancy, segregation and cavern, coaxial mixers have been developed based on the empirical consideration.

In the literature, the combination of a Rushton turbine and a helical ribbon was proposed by Tanguy et al. Subsequently, this type of mixers was studied with different kinds of radial or axial impellers with an anchor or a helical ribbon. Generally, it is agreed that the power consumption of high-speed inner impeller is the most important consumption and is not affected by the low-speed outer impeller, while the latter is affected by the former. In the laminar regime, the product of *Re* times N_P is constant and defined as power constant K_P which is a critical parameter for the power analysis. A clear relationship between power constant K_P and speed ratio R_N has also been demonstrated. There is finally a relationship between the speed ratio and the threshold of the transitional regime: the higher the speed ratio is, the lower the threshold becomes.
Mixing time investigations in coaxial mixers with turbine and anchor showed that the co-rotating mode is more effective than counter-rotating mode due to its better axial circulation. However, the ability to break segregated regions with shear effect is weaker in the co-rotating mode than in the counter one. Some results showed that mixing time in the co-rotating mode will increase along with the speed ratio and for the counter-rotating mode the mixing performance is more efficient at high speed ratio.

In the 1990's, a wide impeller named Maxblend™ was designed by SHI Mechanical & Equipment and showed excellent capabilities for operating in a wide range of fluid viscosities. The Maxblend mixer paddle is able to provide flow with axial circulation where the fluid goes upward at the tank wall and downward along the shaft. The results indicated that Maxblend has a uniform shear rate distribution compared with blade turbine impellers. In 2007, Louis Fradette et al. carried out a comprehensive investigation on the mixing characteristics of Maxblend and

confirmed that Maxblend impeller is very efficient for the mixing of viscous fluids based on short mixing time and low power consumption.

Recently, a new type of coaxial mixer named Superblend^{TM} has been proposed by SHI Mechanical & Equipment. It is formed from a combination of a Maxblend impeller and a helical ribbon. It has been proposed as a promising technology for viscous fluid mixing with large viscosity variation. In 2009, Farhat et al. firstly explored the power consumption and mixing time of Superblend using a new definition of rotational speed.

In this work, pushing further and deeper the investigation by Farhat et al., the objective is to quantify the effect of operating parameters (speed ratio and rotating mode) on the power consumption and mixing time of the Superblend mixer.

3.3 Experimental methods

Figure 3.1 shows the configuration of the Superblend (SB) studied in this work. It consists of an inner impeller (Maxblend, MB) and an outer impeller (helical ribbon, HR) driven with two separated motors. The diameter of Maxblend^{TM} is D_i = 0.2 m (D_i / T = 0.53, T = 0.38 m) and the specifics of the helical ribbon are shown in Table 3.1. The tank is a transparent cylinder with conical bottom. The liquid height is H = 0.44 m, and the liquid volume of the tank is approximately 40 L.

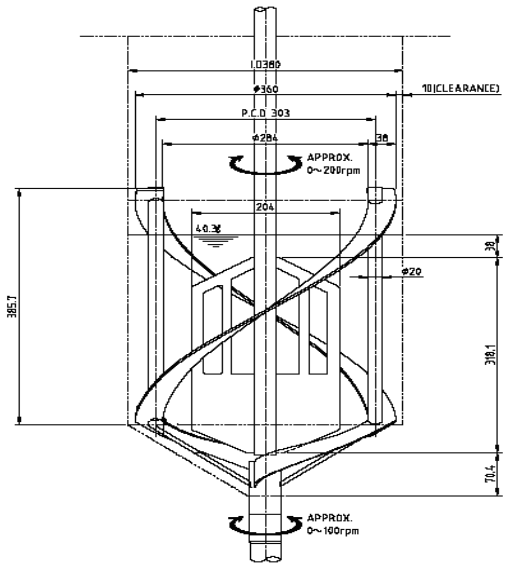

Figure 3.1: Configuration of the Superblend mixer.

Table 3.1: Geometrical variables of the helical ribbon impeller

n_b	D_o [m]	D_i / D_o	c / T	p / D_o	L [m]	w [m]	h [m]	D_s / T
2	0.36	0.56	0.08	1	0.54	0.03	0.38	0.07

where n_b is the number of blades, D_o the diameter of helical ribbon, c the clearance between the ribbon and tank wall, T the tank diameter, p the pitch, L the blade length, w the blade width, h the height of helical ribbon, and D_s the shaft diameter.

A series of glucose-water solutions with different concentrations were prepared and used as Newtonian fluids. All the viscosity measurements were taken with a Bohlin Rheometer. Temperature of the tank is closely monitored because these solutions tend to change viscosity quickly with temperature.

The experiments were run at speed ratios of 1, 2, 4, 6, and 8. The two rotating modes (co- and counter-) were used at all ratios. Co-rotation corresponds to upward pumping of the helical ribbon at the wall while the counter-rotation sees the fluid going downward at the tank wall.
The power consumption was determined by means of a torque meter mounted on the shaft of each impeller with a range of 0-20 N-m for the Maxblend and 0-100 N-m for the helical ribbon, respectively. Error on the torque measurement is 1% full scale, as per the manufacturer's specification.

The corrected torque value M_c was calculated by subtracting the residual torque from each measurement:

$$M_c = M_m - M_r \tag{3.1}$$

where, M_m is the measured torque and M_r the residual torque, in N-m, respectively. M_r is determined by measuring the torque at various speeds with the tank empty and the impellers on the shafts. It ranged from 0.3 - 0.6 N-m for the Maxblend and 0.1 - 0.5 N-m for the helical ribbon.

The power consumption is calculated with

$$P = M_c 2\pi N \tag{3.2}$$

Here, N is the rotational speed of the single impeller in s^{-1}.

In coaxial mixers, the coexistence of two impellers results in the ambiguous definition of N. Previously, either outer impeller's or inner impeller's parameters was chosen as the characteristic parameters. Taking speed ratio and operating mode into account, Foucault et al. (2005) expressed the characteristic speeds as $N_{co\text{-}rotating} = N_i - N_o$ and $N_{counter\text{-}rotating} = N_i + N_o$. In addition, the inner impeller's diameter was used as the characteristic diameter due to the finding that the power number of the inner impeller is independent of the speed ratio. These new correlations allow the unique power curves to be obtained. However, this approach can only be applied when the speed ratio is above 10. Given that the speed ratios in this work are all below 10, a correlation proposed by Farhat et al. with its applicability for the Superblend was adopted as the characteristic speed in this paper.

$$N' = \frac{(N_i D_i + N_0 D_0)}{D_i} \tag{3.3}$$

where, N_i *and* N_o are the rotational speeds of the inner impeller (Maxblend) and the outer impeller (helical ribbon), respectively.

Therefore, the power number N_P', Reynolds number Re' and power constant K_P' were expressed based on equation (3.3)

$$\mathrm{N_P}' = \frac{\mathrm{P}}{\rho \mathrm{N}'^3 \mathrm{D}_\mathrm{i}^5} \tag{3.4}$$

$$Re' = \frac{\rho N' D_i^2}{\mu} \tag{3.5}$$

$$K_P' = Re' \times N_p' \tag{3.6}$$

Mixing time was measured by means of a decolorization method based on a fast acid-base indicator reaction. 100 ml of pH indicator solution (0.08 wt % purple Bromocresol) is added to the fluid in the tank to visually differentiate between acidic (yellow, pH < 5.2) and alkaline (red, pH > 6.8) conditions. 10 ml of alkaline solution (NaOH) is poured into the tank and make the fluid appears red. At t = 0, 15 ml of acidic solution (HCl) is injected between the shaft and the wall on the liquid surface, while a video camera starts recording. A mixing evolution curve is

obtained after image analysis of the recording. From this curve, the mixing time is easily evaluated. In the present work, the time spent for reaching 95% of the complete decolorization state was chosen as the macro mixing time. This technique has been proven to be highly repeatable with low variability. No mixing time experiments are shown in the results for a speed ratio of 1 since these conditions only provided unmixed fluid and infinite mixing times.

3.4 Results and discussion

3.4.1 Overall Flow Pattern

The flow field being very complex in such a mixer, observation of the overall flow helps understand the mixing performance results. The flow field was observed by decolorization and tracer particles with density similar to the fluid (spray painted HDPE particles of 2 mm). Figure 3.2 respectively presents the flow field generated by each impeller alone (A), the expected flow field when both impellers are working (B), and the observed flow field from the experiments (C). The left side of Figure 3.2 A shows the flow field when the helical ribbon is pumping downward at the wall; the reverse direction simply generates the opposite flow field with all arrows reversed (typical operation of a helical ribbon). The right side of the same figure illustrates the flow field generally obtained with the Maxblend impeller showing a large circulation loop that is characteristic of this impeller.

Figure 3.2 B presents the expectations from the flow fields presented in Figure 3.2 A. On the left side of Figure 3.2 B, when impellers are in counter rotation i.e. when the helical ribbon is pumping downward, the expectations were so that the fluid would be going down along the shaft (Maxblend pumping) and the wall (helical ribbon pumping). Obviously, this requires a well balanced pumping between the two impellers so the fluid can go up in the gap between the two. The arrows indicate this expectation. On the right side of the same figure is represented the expectations for the co-rotation case i.e. when the helical ribbon is pumping upward at the wall. In this case, the collaboration of the two impellers is expected since both generate a flow that is very similar and should simply add to each other's effect.

Figure 3.2 C presents the observed flow field from the experiments conducted in the lab with the helical ribbon pumping downward. The left side of the figure is obviously similar to Figure 3.2 A

left i.e. that the flow field is largely dominated by the helical ribbon and the Maxblend is not influencing the flow field, at least apparently. The right side shows a flow field similar to the expectations (Fig. 3.2 B, right) but with the difference that again the helical ribbon is largely dominant.

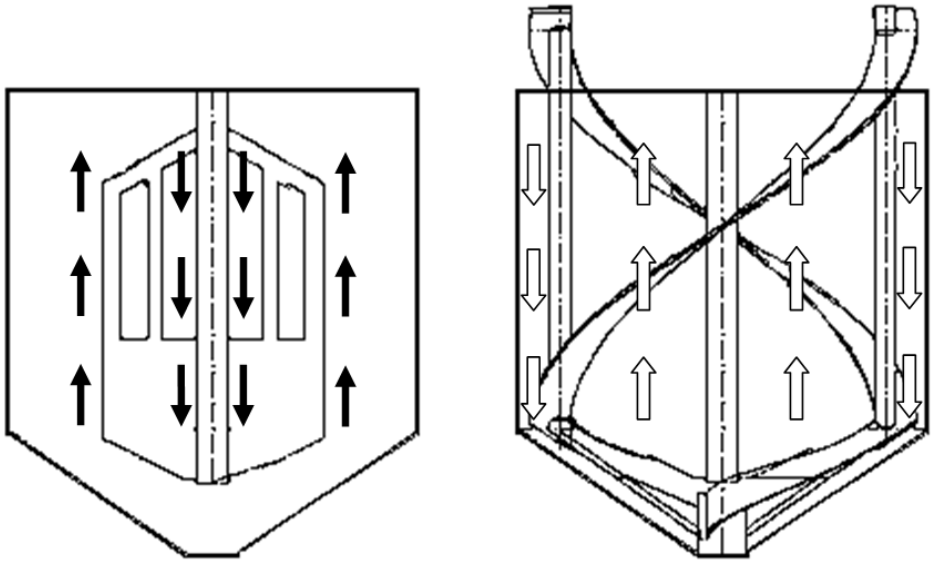

Figure 3.2 A: Expected flow field from the individual impellers in the Superblend

Left: Maxblend; Right: helical ribbon pumping downward.

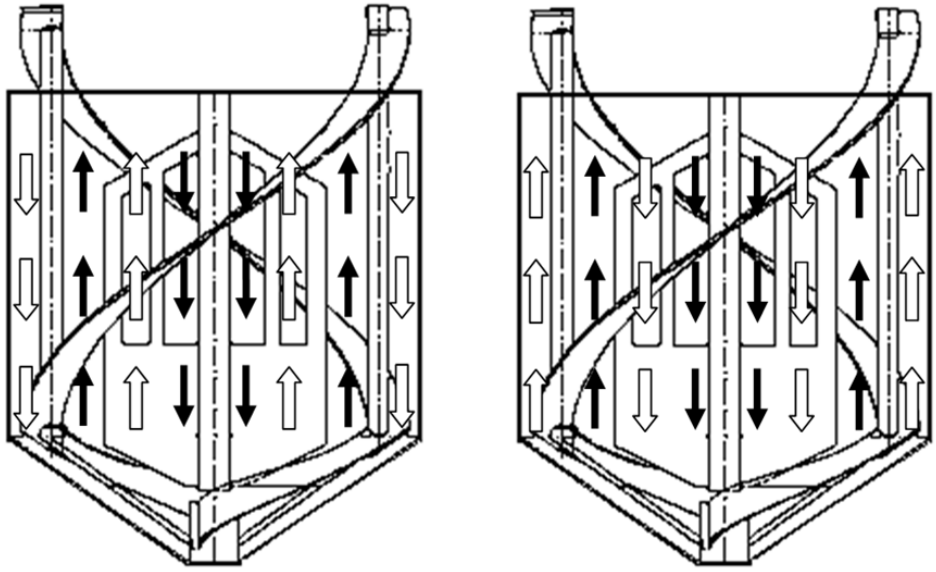

Figure 3.2 B: Expected flow field generated in the Superblend

Left: helical ribbon pumping downward; Right: helical ribbon pumping upward.

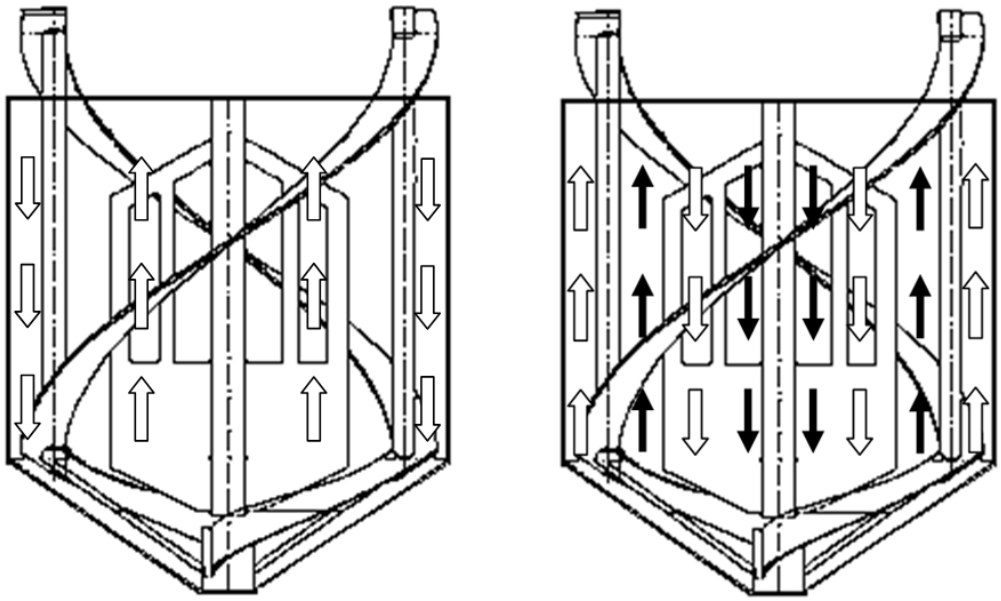

Figure 3.2 C: Observed flow field generated in the Superblend

Left: helical ribbon pumping downward; Right: helical ribbon pumping upward.

3.4.2 Mixing Time

The effect of operating parameters on the mixing time is shown in Figure 3.3 where four speed ratios and the two rotating modes are presented. In the laminar regime ($Re' < 10$), the smaller speed ratios were the most efficient i.e. generated the smallest mixing time. The rotating mode does not appear to have much effect on the results. In this regime, the flow in the tank dominated by viscosity and is relatively slow. In the transitional regime ($10 < Re' < 100$), mixing performance improves with a reduction of an order of magnitude in mixing time. In this flow regime, higher speed ratio brings more shearing and pumping effect to the flow which is positive to the mixing. As a result, the higher speed ratio leads to slightly lower dimensionless mixing times. In the turbulent regime, we could hardly see the influence of speed ratio on the mixing time, except for $R_N = 2$ in co-rotating mode (helical ribbon pumping upward at the wall) where the dimensionless mixing time is remarkably higher than other R_N due to the presence of a constantly unmixed island close to the liquid surface.

Additionally, it must be noted that the shape of the mixing time curves are very similar to the ones generally obtained with helical ribbons with two plateaus and a transition zone. This confirms the observed flow field presented above.

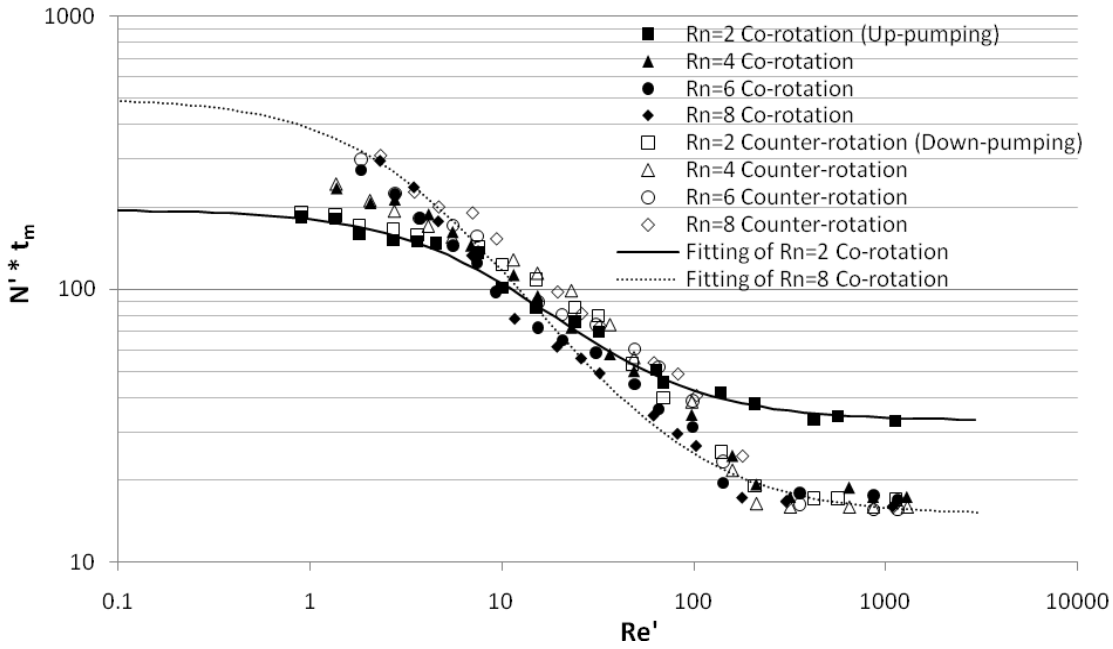

Figure 3.3: Influence of operation parameters on dimensionless mixing time.

In order to have a quantitative view of mixing time behaviour, all the curves in Figure 3.3 have been fitted by the following equation:

$$\frac{\Theta - \Theta_\infty}{\Theta_0 - \Theta_\infty} = \frac{1}{1 + \lambda Re'^{1/a}} \tag{3.7}$$

Here, Θ is the dimensionless mixing time ($N' * t_m$), Θ_0 is the plateau value at low Reynolds number, Θ_∞ is the plateau value at large Reynolds number, $1/\lambda$ represents the onset Re value for the transition from the low Re' plateau towards the high Re' plateau, a is the slope of the dependence of Θ on Re' in the transition region. Figure 3.3 presents two of the fitted data series to illustrate the goodness of fit obtained with the equation.

Table 3.2 presents the fitted parameters for all the data series of Figure 3.3. Θ_0 values clearly show that the smaller speed ratios are more effective in the laminar regime; values at $R_N = 2$ are always 2.5 times smaller than at $R_N = 8$ and this is observed in both rotating modes. The values of

Θ_∞ are all similar except for the one at the lowest speed ratio which is twice as large as the others. In this mode and conditions, the ribbon flow is clearly fighting the Maxblend flow and no apparent collaboration exists. The low speed of the Maxblend does not indeed allow for good pumping and the resulting performance is obviously the worst observed. Remember that the performance in the turbulent regime is expected to be very similar between the various modes and the longer time obtained here really reflects a shift in performance. From the observation of λ values, we can conclude that the two rotating modes and four speed ratio do not show clear differences in terms of this parameter which means that the onset of the transition zone is very similar for those operating conditions. Additionally, a values quantify the slope of the transition zone and are here almost constant for all conditions used; it can be concluded that the shift in flow regime always operate at the same rate.

Table 3.2: Fitted parameters of equation (3.7)

Curves	Θ_0	Θ_∞	$1/\lambda$	a
R_N =2 Co-rotation (helical ribbon pumping up)	195	33	10	1.1
R_N =4 Co-rotation	270	17	20	1.1
R_N =6 Co-rotation	410	17	5	1.1
R_N =8 Co-rotation	500	15	10	1.1
R_N =2 Counter-rotation (helical ribbon pumping down)	200	17	4	1.2
R_N =4 Counter-rotation	300	16	5	1.1
R_N =6 Counter-rotation	430	16	4	1
R_N =8 Counter-rotation	550	15	4	1

Based on mixing time results, the optimal operating conditions are to use low speed ratio with viscous fluids (Low *Re'*) and to increase the speed ratio with lower viscosity fluids.

3.4.3 Power Consumption of the Superblend

Figure 3.4a and b respectively show the power curves obtained for five speed ratios in both rotational modes: up- and down-pumping of the helical ribbon. In contradiction with the work by Farhat et al, a spread of the power curves is observed. This difference originates from the very low speed ratios investigated. While Farhat et al concentrated on ratios of 4 to 8, the deviations observed here come from the lowest speed ratios of 1 and 2. This spread is also an indication of a change in the work done by the mixer in these conditions. The mixing time experiments presented above clearly showed that the lowest speed ratios did not provide good mixing performance especially at transition and turbulent regimes.

Here, it is shown that the low speed ratios are the most power consuming conditions with the power curves consistently located above the group of curves obtained at values of R_N above 4. A difference in the total power can also be detected between the two modes: the power consumed in the co-rotational mode (upward pumping of the helical ribbon) consistently yields lower power values than in the counter one. In the turbulent regime, the position of the curves in the spread is completely reversed: the highest speed ratios are at the top and the lowest ones show lower power consumption. This comment is true for both operation modes at $Re' > 10$.

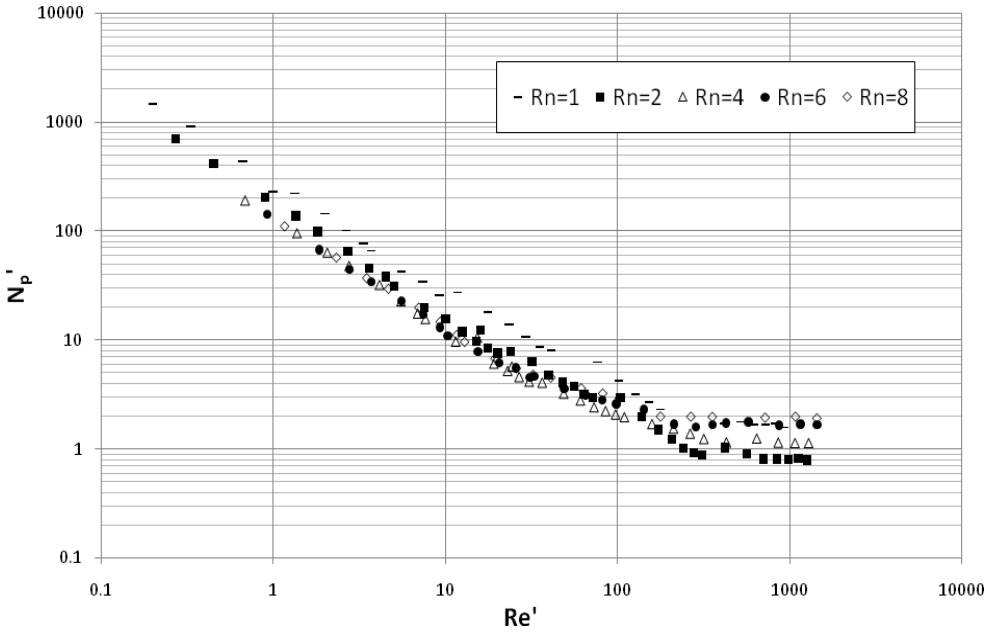

(a)

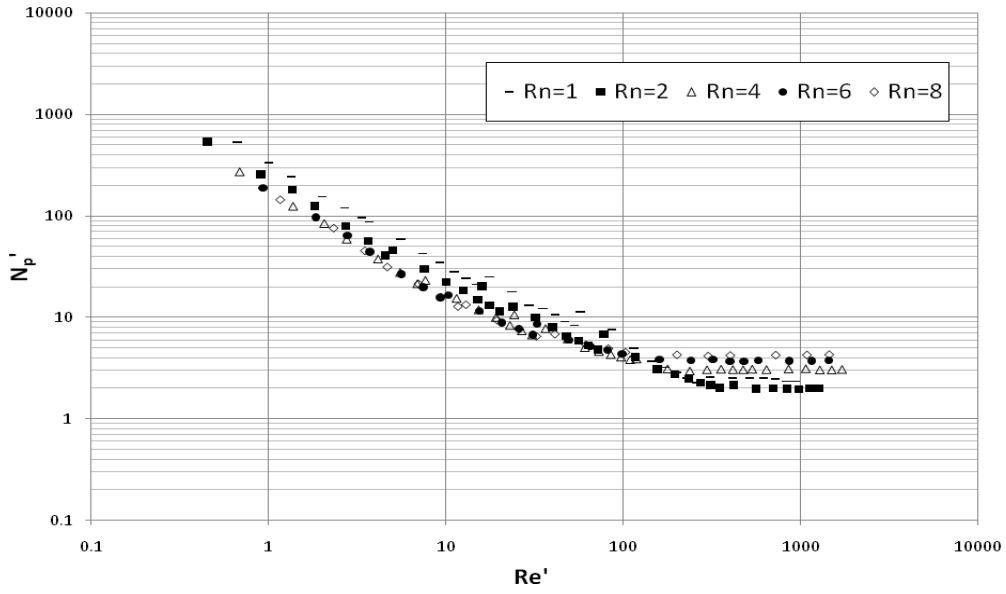

(b)

Figure 3.4: Experimental results obtained under different speed ratios and rotating modes: (a) up-pumping of the helical ribbon and co-rotation of the Maxblend; (b) down-pumping of the helical ribbon and counter-rotation of the Maxblend.

3.4.4 Power Split

It is very convenient to generate single power curves for dual- (and eventually multiple-) shafts mixers in order to study their power consumption behavior. For a better understanding of the collaboration/fighting between the impellers, the influence of the operating conditions and rotating modes on the power consumption for each individual impeller can bring interesting information. They show the power curves for the helical ribbon and the Maxblend impellers in both rotational modes: up-pumping of the helical ribbon and co-rotation of the Maxblend; down-pumping of the helical ribbon with counter-rotation of the Maxblend.

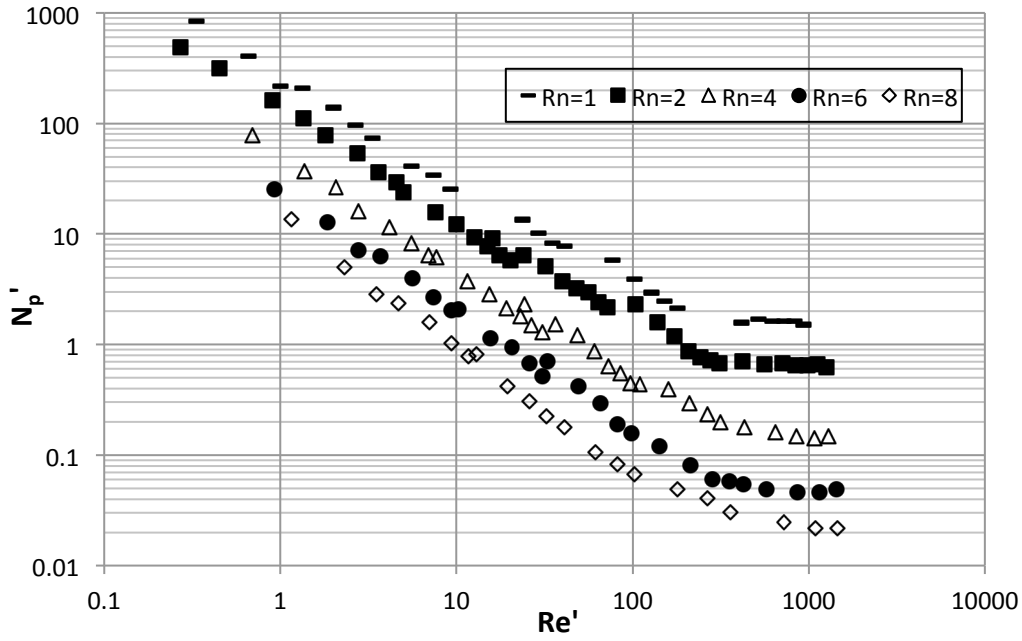

(a)

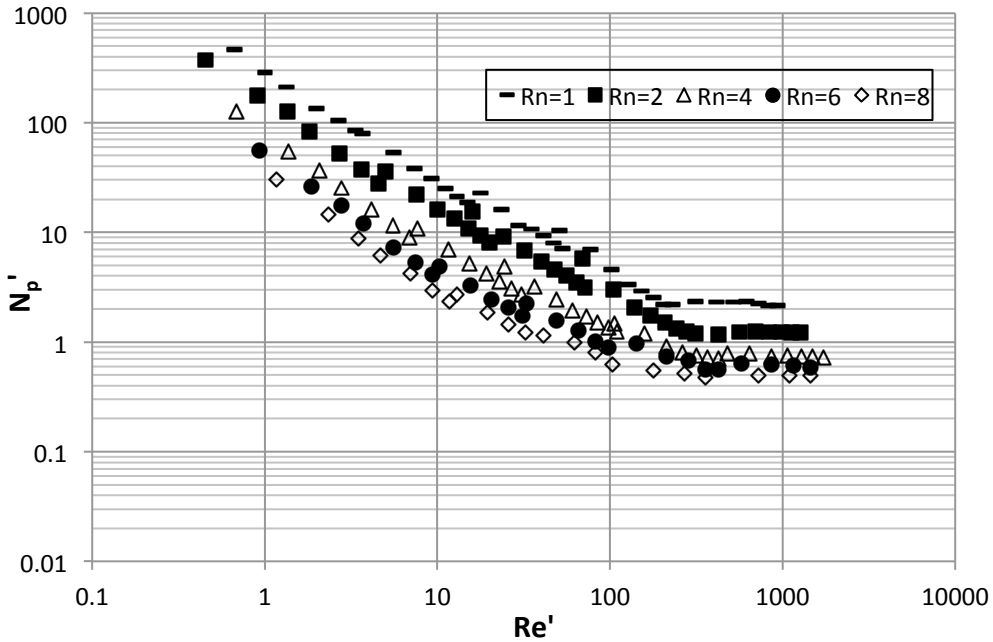

(b)

Figure 3.5: Power curves of the helical ribbon: (a) up-pumping of the helical ribbon and co-rotation of the Maxblend; (b) down-pumping of the helical ribbon and counter-rotation of the Maxblend.

The power curves from the helical ribbon have a completely different shape than the one obtained for the combined power curve of the Superblend (Figure 3.4 a and b). On both graphs, in the laminar and the transitional regimes, the curves of R_N =1 are on the top and the power numbers drop with the increase in speed ratio because of the growing interaction between the impellers. On both graphs, the curves of R_N =1 and 2 are approximately at the same position. This is an additional indication that the rotating mode does not influence the power at low R_Ns. When the impellers are co-rotating with a speed ratio equals or above 4, the power numbers of the helical ribbon drop with the larger amplitude than that in the counter-rotating mode. In co-rotating mode, it is also clear that the turbulent regime starts at higher *Re'* as the speed ratio increases. In counter-rotating mode, however, the curves of R_N = 2, 4, 6 and 8 almost overlap in the turbulent regime which means Maxblend impeller does not influence the power at higher R_N and that the interaction between the impellers is very low.

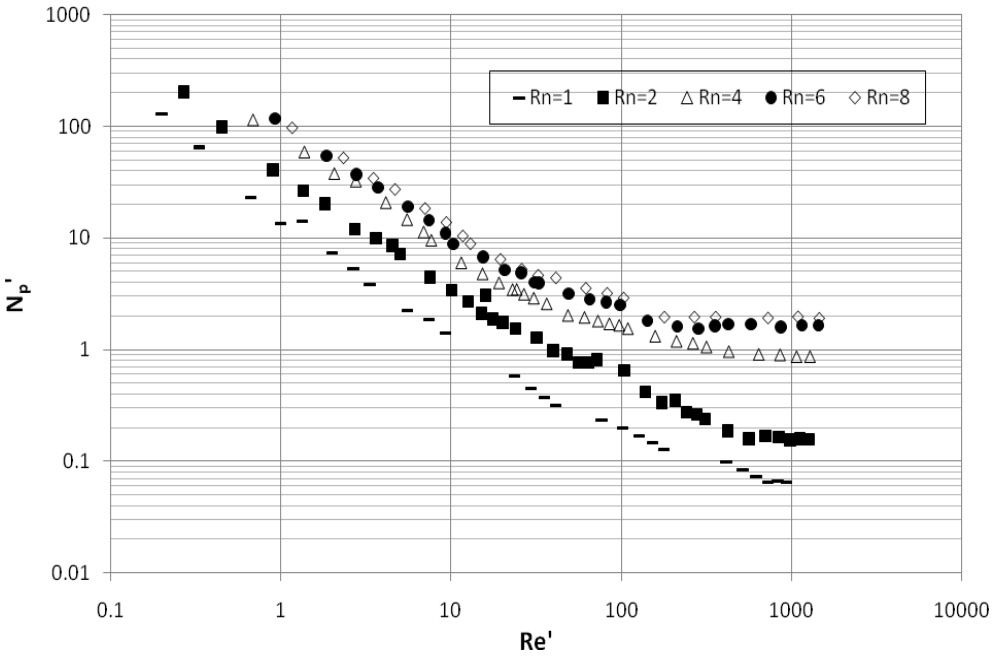

(a)

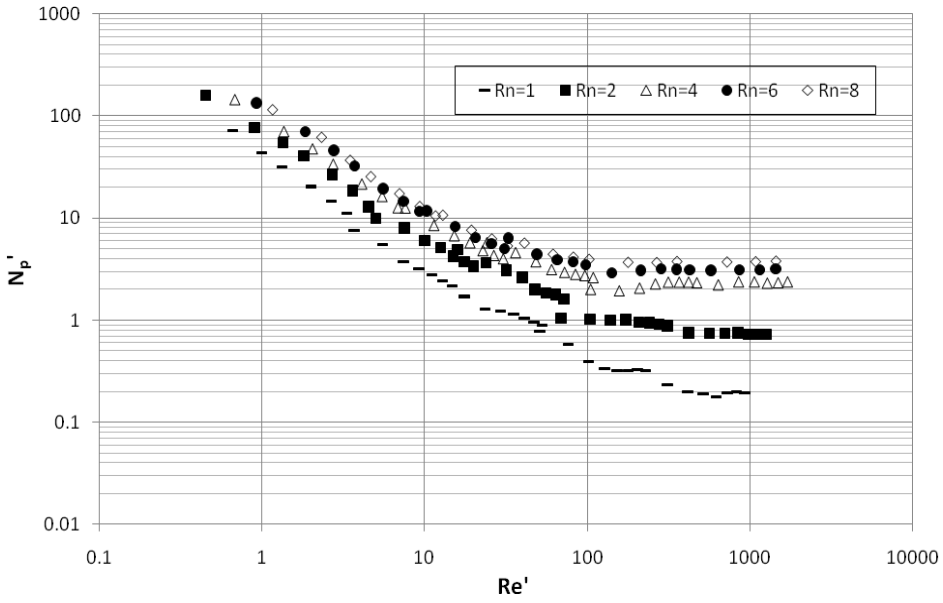

(b)

Figure 3.6: Power curves of the Maxblend impeller: (a) up-pumping of the helical ribbon and co-rotation of the Maxblend; (b) down-pumping of the helical ribbon and counter-rotation of the Maxblend.

In Figure 3.6a, two groups of curves are seen. Speed ratios of 1 and 2 form a first group at lower power values with a larger difference with the second group in the turbulent regime. The second group of curves is formed by speed ratios above 4. This group lays at slightly higher power values than for ratios of 1 and 2 in the laminar regime but at least five times higher values in the turbulent regime. These two situations are easily explained by the observations made above: at lower speed ratios, the helical ribbon is clearly leading the flow and the Maxblend simply acts as a rotating baffle. When the Maxblend impeller reaches a certain speed ($R_N \geq 4$) its pumping starts interacting with the helical ribbon. The power then increases for the Maxblend and lowers for the helical ribbon (Figure 3.5). In the counter-rotating mode (helical ribbon pumping down), all the power curves are getting closer in the laminar and transitional regimes and it has been said above that this mode is largely dominated by the helical ribbon flow with relatively less impact from the Maxblend.

Pushing further the investigation of the power consumption, Figure 3.7 presents the power consumed by the Maxblend impeller to the total power of the Superblend in the laminar regime.

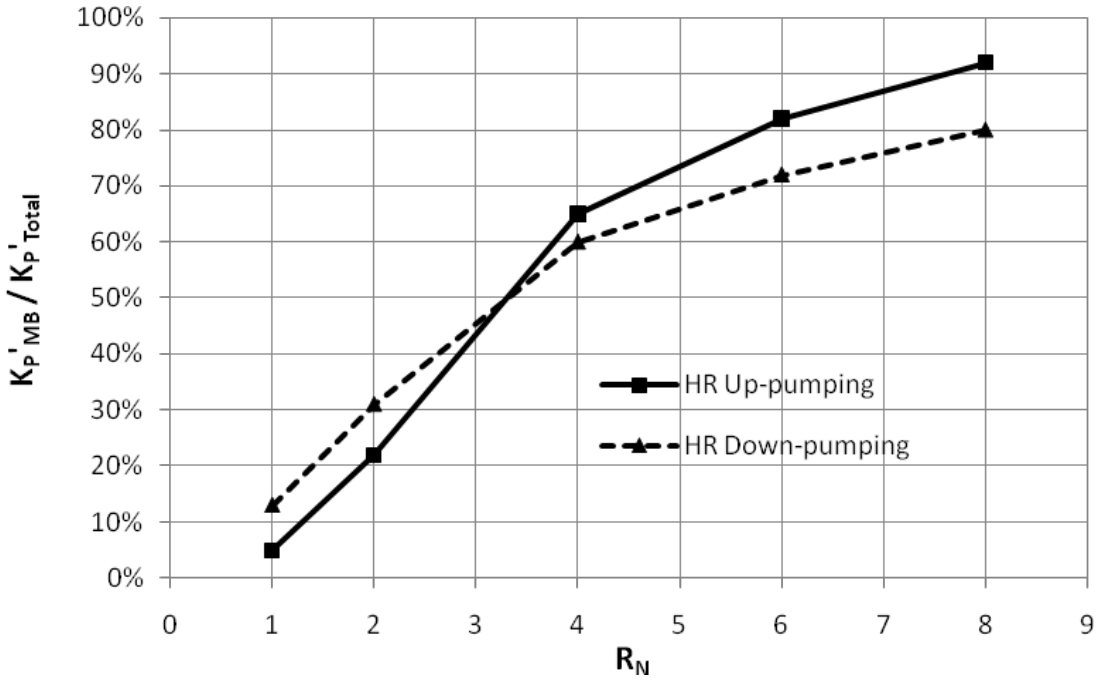

Figure 3.7: Maxblend power consumption to the total power expensed.

Previously published papers on multi-shaft mixers typically present the inner impeller as the largest power consumer with sometimes an effect on the power consumption of the outer impeller. In Figure 3.7, the Maxblend contributes to 50% of the power consumption or more only at $R_N \geq$ 3.3 for both modes; a clear indication that the Maxblend does not dominate the power at all speed ratios and the helical ribbon contributes more to the power consumption below this critical R_N. It has been discussed above that with the helical ribbon pumping downward at the wall, the Maxblend counteracts the pumping effect and lots of turbulence is generated with not much effect on the mixing performance (Figure 3.3, higher *Re'*). This is also easily seen in Figure 3.5 b where the power curve of the helical ribbon rapidly levels off at higher speed ratios indicating the transition towards the turbulent regime. At low R_N, the upward pumping of the helical ribbon goes along with the loop generated by the Maxblend and the power consumption of this latter remains low while a real collaboration exists between the two. Mixing time results in Figure 3.3 also indicate these beneficial conditions with the smallest values of mixing times at low R_N. In the case of down-pumping, the power expensed by the Maxblend is higher below that critical R_N than that in the case of up-pumping and lower above that critical R_N. This trend in the curve

simply indicates that the fight between the agitators weakens the power consumption of the helical ribbon below this critical R_N and that the fight weakens the power of the Maxblend above this critical R_N. Again, this should be seen as a waste when Θ_0 values from Table 3.2 are compared: the down-pumping mode at high R_N generates the longest mixing times of all conditions studied.

To push even further the analysis of the power consumption in the Superblend mixer, Figure 3.8 presents the K_P values of the individual impellers and their sum.

At low speed ratio (R_N = 1), the Maxblend consumes two times more power when the helical ribbon is down-pumping than that in up-pumping mode. Considering the fact that the power consumed by the helical ribbon is roughly the same in both modes at this R_N and that the mixing times are also very similar, it is clear that operation should favor the up-pumping mode. As the R_N is increasing, the helical ribbon exhibits descending power consumption in both modes while the Maxblend power consumption grows stably. It's noticed that there are two crossover points for both modes and they both locate at R_N = 3.3. This is again an indication that the inner impeller does not always act as the largest power consumer at all speed ratios. As another conclusion, operation should favor the up-pumping mode to make use of the least power since mixing times are similar.

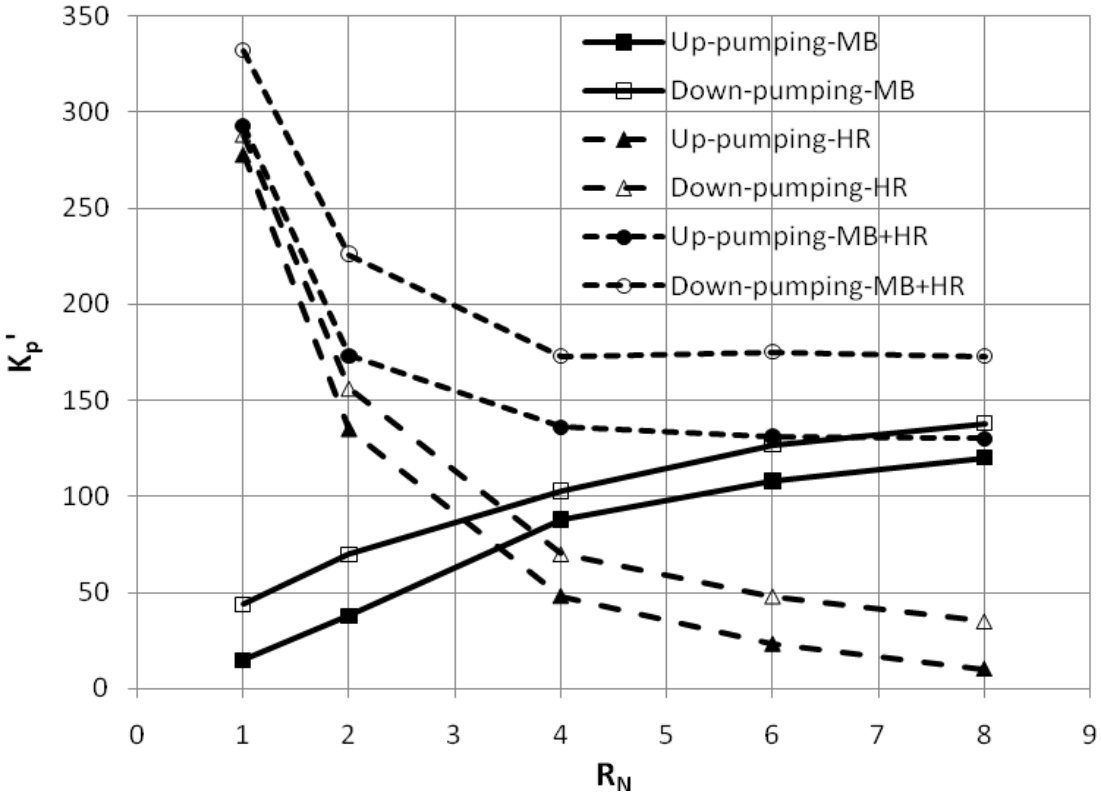

Figure 3.8: Influence of speed ratio and rotating mode on K_P.

Finally, the sum of the power consumption clearly indicates that the down-pumping mode consumes more power than the up-pumping one. With the same trend, they both go down along with the increase of the speed ratio till $R_N = 4$, where a stable status is obtained for the sum of the power consumption. Again, knowing that the mixing times are not largely affected by the rotational mode, the up-pumping is much more efficient in terms of energy consumption.

3.5 Conclusion

In addition to the work by Farhat et al, a complete experimental investigation of the Superblend mixer with Newtonian fluids allowed for the description of the overall flow field, the mixing time determination in a wide range of speed ratios, and a thorough analysis of the power consumption for both impellers individually and for the overall power consumption. Some of the results differed from the Farhat et al.'s research and a series of new findings have been pointed out. The impact of the helical ribbon, by opposition to the use of an anchor in a coaxial configuration, was clearly demonstrated. The results indicate that a proper pumping combination for the two

agitators must be determined based on the viscosity of the fluid in order to obtain the best mixing conditions. Based on the mixing time results, the optimal operating conditions are to use a low speed ratio with viscous fluids and to increase the speed ratio with lower viscosity fluids. Finally, it appears that the conclusions drawn from a different coaxial mixer involving a turbine and an anchor remain valid: the co-rotation of the agitators is the best compromise for low power consumption and short mixing times.

3.6 Acknowledgement

The authors wish to acknowledge the support from the National Science and Engineering Research Council of Canada (NSERC) for the financial support of this research.

3.7 Reference

BAKKER, A. and GATES, L. E. (1995). Properly Choose Mechanical Agitators for Viscous Liquids. *Chem. Eng. Prog.*, 91(12), 25-34.

BONNOT, S., CABARET, F. FRADETTE, L. and TANGUY, P. A. (2007). Characterization of Mixing Patterns in a Coaxial Mixer. *Chem. Eng. Res. Des.*, 85(A8), 1129-1135.

BRITO-DE LA FUENTE, E., CHOPLIN, L. and TANGUY P. A. (1997). Mixing with Helical Ribbon Impellers: Effect of Highly Shear Thinning Behaviour and Impeller Geometry. *Trans IChemE*., 75(A), 45-52.

CABARET, F., BONNOT, S., FRADETTE, L. and TANGUY, P. A. (2007). Mixing Time Analysis Using Colorimetric Methods and Image Processing. *Ind. Eng. Chem. Res.*, 46(14), 5032-5042.

CHAVAN, V. V. (1983). Close-clearance Helical Impeller: A Physical Model for Newtonian Liquids at Low Reynolds Numbers, *AIChE J*., 29(2), 177.

DIEULOT, J. Y., DELAPLACE, G., GUERIN, R., BRIENNE, J. P., LEULIET, J. C. (2002). Laminar Mixing Performances of A Stirred Tank Equipped with Helical Ribbon Agitator Subjected to Steady and Unsteady Rotational Speed. *Trans IChemE*., 80(A), 335-344.

ESPINOSA-SOLARES, T., BRITO-DE LA FUENTE, E., TECANTE, A., TANGUY, P. A. (2001). Flow Patterns in Rheologically Evolving Model Fluids Produced by Hybrid Dual Mixing Systems. *Chem. Eng. Technol*., 24(9), 913-918.

FARHAT, M., FRADETTE, L., HORIGUCHI, H., YATOMI, R. and TANGUY, P. A. (2009). Experimental Investigation of Superblend Coaxial Mixer. *J. Chem. Eng. Jpn.*, 42(11), 797-803.

FARHAT, M., FRADETTE, L., TANGUY, P. A. (2008). Revisiting the performance of a coaxial mixer. *Ind. Eng. Chem. Res.*, 47(10), 3562-3567.

FARHAT, M., RIVERA, C., FRADETTE, L., HENICHE, M. and TANGUY, P. A. (2007). Numerical and Experimental Study of Dual-shaft Coaxial Mixer with Viscous Fluids. *Ind. Eng. Chem. Res.*, 46(14), 5021-5031.

FOUCAULT, S., ASCANIO, G. and TANGUY, P. A. (2004). Coaxial mixer hydrodynamics with Newtonian and Non-Newtonian fluids. *Chem. Eng. Technol.*, 27(3), 324-329.

FOUCAULT, S., ASCANIO, G. and TANGUY, P. A. (2005). Power characteristics in coaxial mixing: Newtonian and Non-Newtonian fluids. *Ind. Eng. Chem. Res.*, 44, 5036-5043.

FOUCAULT, S., ASCANIO, G. and TANGUY, P. A. (2006). Mixing times in coaxial mixers with Newtonian and non-Newtonian fluids. *Ind. Eng. Chem. Res.*, 45(1), 352-359.

FRADETTE, L., THOME, G., TANGUY, P. A. and TAKENAKA, K. (2007). Power and Mixing Time Study Involving A Maxblend Impeller with Viscous Newtonian and Non-Newtonian Fluids. *Chem. Eng. Res. Des.*, 85(A11), 1514-1523.

IRANSHAHI, A., DEVALS, C., HENICHE, M., FRADETTE, L., TANGUY, P. A. and TAKENAKA, K. (2007). Hydrodynamics Characterization of the Maxblend Impeller. *Chem. Eng. Sci.*, 62, 3641-3653.

KOHLER, S. and HEMMERLE, W. (2003). Analysis of the power characteristic of a coaxial agitator with varied diameter and speed ratio inner and outer mixing device. *11th European Conference on Mixing*, Bamberg, 14-17.

KURATSU, M., YATOMI, R. and SATO, H. (1995). Design of Versatile Reactors. *Chem. Equipment.*, 8, 86-92.

PAUL, E. L., ATIEMO-OBENG, V. A., KRESTA, S. (2004). Handbook of Industrial Mixing: Science and Practice. John Wiley & Sons, Inc., Hoboken, New Jersey.

RIVERA, C., FOUCAULT, S., HENICHE, M., ESPINOSA-SOLARES, T. and TANGUY, P. A. (2006). Mixing Analysis in a Coaxial Mixer. *Chem Eng Sci*., 61(9), 2895–2907.

RUDOLPH, L., SCHAFER, M., ATIEMO-OBENG V. and KRAUME, M. (2007). Experimental and numerical analysis of power consumption for mixing of high viscosity fluids with a co-axial mixer. *Chem. Eng. Res. Des.*, 85(A5), 568-575.

TAKENAKA, K., YATOMI, R., MORINAGA, S. and TANGUY, P. A. (2006). Comparison of Solid-mixing Performance Between A Pitched Blade Turbine and the Maxblend Impeller. *Proceedings of the 12th European Conference on Mixing,* Bologna, Italy.

TANGUY, P. A., THIBAULT, F., BRITO-DE LA FUENTE, E., ESPINOSA-SOLARES, T. and TECANTE, A. (1997). Mixing performance induced by coaxial flat blade-helical ribbon impellers rotating at different speeds. *Chem. Eng. Sci.*, 52(11), 1733-1741.

TANGUY, P. A. and THIBAULT, F. (2002). Power consumption in the turbulent regime for a coaxial mixer. *Can. J. Chem. Eng.*, 80(4), 601-603.

THIBAULT, F. and TANGUY, P. A. (2002). Power-draw analysis of coaxial mixer with Newtonian and non-Newtonian fluids in the laminar regime. *Chem. Eng. Sci.*, 57, 3861-3872.

CHAPTER 4: ARTICLE 2: ANALYSIS OF POWER CONSUMPTION IN MULTI-SHAFT MIXERS

Article history: Submitted 4 April 2011, Accepted 8 September 2011, Published online 8 September 2011, Industrial & Engineering Chemistry Research.

Authors: Xiao Wang, Maya Farhat, Louis Fradette and Philippe A. Tanguy

4.1 Abstract

New definitions of the Reynolds and power numbers proposed by Farhat, Fradette and Tanguy (2008) for coaxial mixers were discussed and extended to some other types of multi-shaft mixers not considered previously. The results confirmed that these new correlations are also applicable for the dual shaft mixers configurations and the Superblend mixer. This universal applicability allowed the authors to experimentally investigate and compare the power consumption and the mixing time in the coaxial, the dual shaft, and the Superblend mixers based on uniform criteria. It was found that the Mixel TT-Anchor combination is the most power-efficient combination, while the Superblend mixer requires the most power. Besides, a general approach was introduced to predict the power constant of these multi-shaft mixers. Finally, the limitations of the new correlations were pointed out through the extension study of their applicability in Superblend and rotor stator-Paravisc dual shaft mixer.

4.2 Introduction

The quality of mixing in industrial reactors depends on various factors among others the vessel volume, the physical properties of the ingredients, and the evolution of the rheology in the bulk. One flexible equipment proposed to cope with complex rheology is the multi-shaft mixer, which typically combines two or more impellers in a single vessel. This approach has seen rapid acceptance due to its flexibility dealing with widely varying viscosity conditions. A thorough literature review on coaxial mixers, a particular case of multi-shaft mixers, can be found in the

work of Farhat et al. Based on the compilation of previous studies, Farhat et al. introduced new definitions for the Reynolds number and the power number in terms of impeller characteristic diameter and speed. These resulting power correlations were shown to be applicable for the coaxial mixer combining an anchor and either a radial impeller (Rushton turbine) or an axial impeller (Mixel TT). With respect to other types of multi-shaft mixers, several innovative studies have been carried out, based for instance on dual shaft configurations or Superblend mixer. The design and the optimization of multi-shaft mixers are at present mainly based on empirical knowledge mostly because the specific investigations on such mixers are fairly new but also due to the controversy about what should be used as their characteristic parameters, owing to their inherent hydrodynamic complexity.

The present work aims at analysing the power consumption of multi-shaft mixers and introducing a general approach to predict the power constant of multi-shaft mixers. This work is presented in three parts:

1) Discussion and extension of the new correlations proposed by Farhat et al.[1] to some mixing configurations not considered in the first instance;

2) Comparison and analysis of the power consumption, the mixing time and the mixing energy of three types of mixers operating in similar conditions;

3) Assessment of the applicability of the newly proposed correlations.

4.3 Materials and methods

In this specific case, the tank diameter was 0.38 m, the slow-speed peripheral agitator was an anchor of 0.36 m in diameter and the high-speed shaft could either be fitted with a Rushton turbine or a Mixel TT impeller of 0.2 m in diameter. Both shafts were connected to torque meters. This mixer was operated in both co- and counter-rotating modes of the impellers. While the rotating direction does not have an impact on the hydrodynamics for the radial turbine Rushton turbine, it induces up or down pumping conditions for the axial turbine Mixel TT.

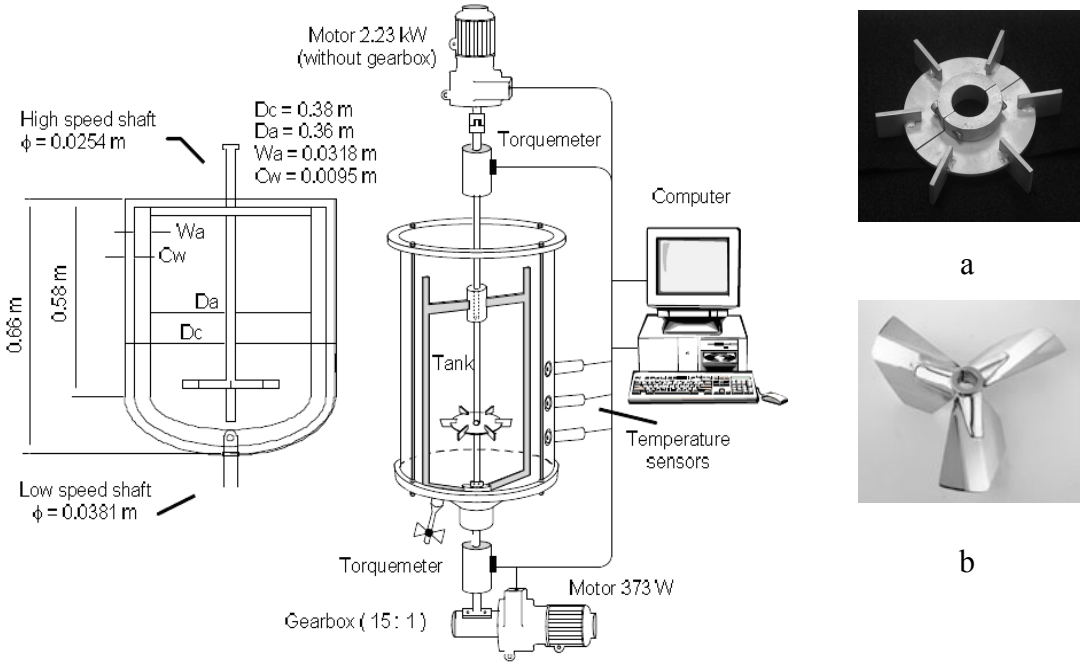

Figure 4.1: Coaxial mixer used in the work of Farhat et al.: (a) Rushton turbine; (b) Mixel TT

The second mixer was a 50 L dual shaft mixer as presented in the work of Barar Pour et al. (Figure 4.2). It consisted of a tank of 0.4 m in diameter fitted with a slow-speed scraping Paravisc impeller of 0.34 m in diameter (Figure 4.2a). Here again, torque was measured on both shafts. Two configurations were studied by changing the high-speed off-centered impeller. The first impeller was a Deflo disperser of 0.08m in diameter (Figure 4.2b) and the second Mixel TT of 0.09 m in diameter (Figure 4.1b). This mixer was operated only in the co-rotating mode i.e. the impellers are moving in the same direction.

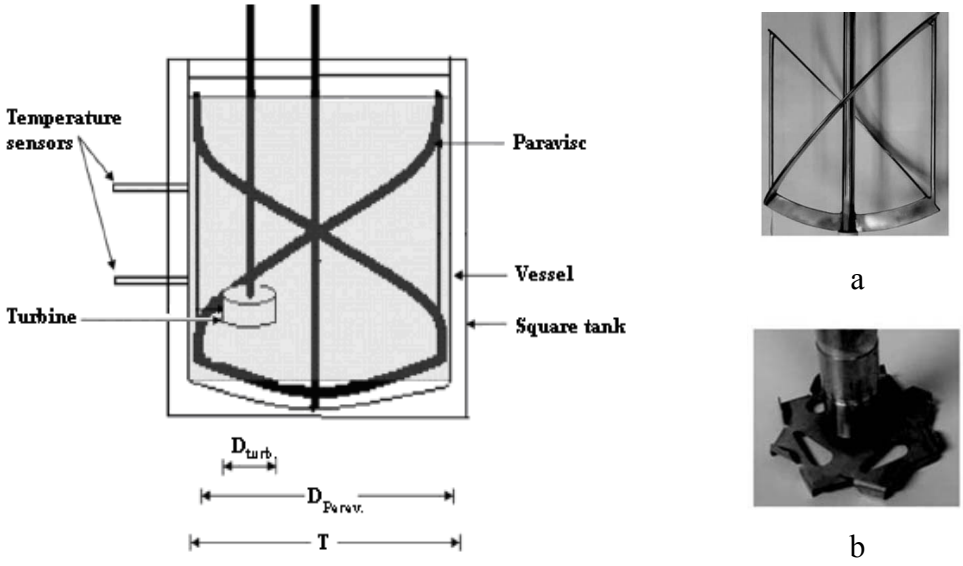

Figure 4.2: Dual shaft mixer used in the work of Barar Pour et al.:

(a) Paravisc-type impeller; (b) Deflo disperser

The third mixer was a 40 L Superblend mixer as shown in Figure 4.3.

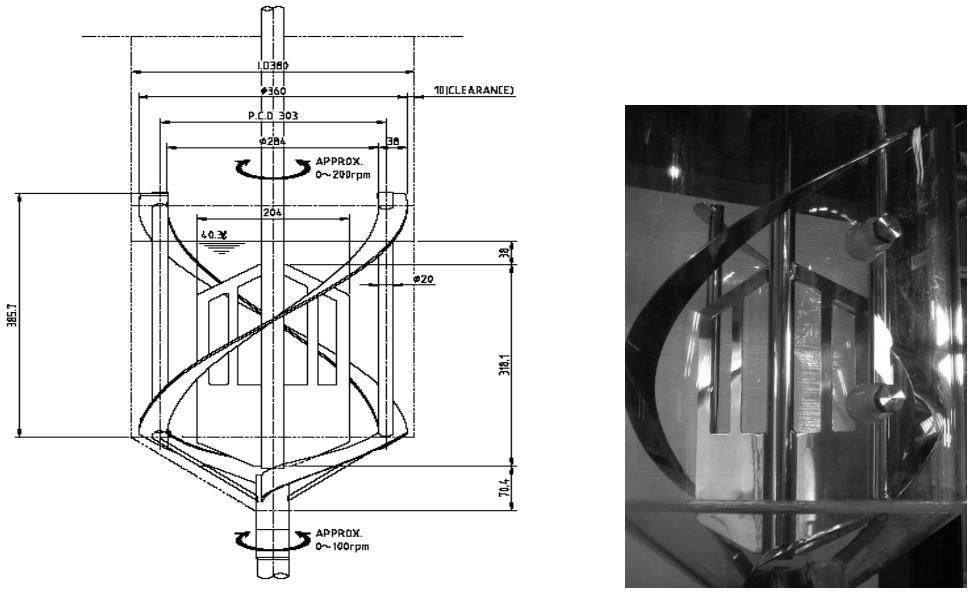

Figure 4.3: Superblend coaxial mixer experimental setup

The tank was a 0.38 m polycarbonate cylinder fitted with a conical bottom. The overall liquid height was 0.44 m. The Superblend mixer is composed of a low-speed helical ribbon at the periphery (diameter of 0.36 m) and a high-speed Maxblend impeller in the center (diameter of 0.2 m). Two independent motors are used to drive the agitators so that both agitators can be rotated co- and counter-clockwise. In our setup the power dissipated in the fluid could be measured by means of torque meters fitted on both shafts.

In all the experiments, the power input for each impeller was determined from the mechanical torque and the speed measurements as $P = M2\pi N$, where N is the shaft rotational speed and M the corrected torque (i.e. after having subtracted the residual torque measured without fluid). Aqueous solutions of corn syrup were used as the working fluids. The rheological properties of the Newtonian fluids were determined using a Bohlin viscometer. The viscosities ranged from 0.1 to 200 Pa.s. The fluid viscosity measurements as well as the mixing experiments were performed at room temperature (≈22°C). The effect of temperature was accounted for by correcting the viscosity appropriately.

Mixing time was measured by means of a decolourization technique based on a fast acid-base reaction. An aqueous solution of 0.08% bromocresol purple was firstly poured into the fluid as an indicator. At a pH lower than 5.2, the fluid appears yellow and it turns purple at a pH higher than 6.8. As a typical procedure, 10 ml of 10 N NaOH was firstly put into the tank, which made the fluid purple. Then, 10 ml of 10 N HCl mixed with the working fluid to avoid viscosity variation was poured into the tank. This addition was made only after a homogeneous purple color is obtained in the tank. Starting at the addition of HCL, the entire color-changing process was recorded by a video camera and subsequently an image processing technique developed by Cabaret et al. was used to quantitatively determine the color evolution from which a macro mixing time can be obtained.

4.4 Results

4.4.1 Discussion on Power Correlation

A number of studies have tried to characterize the power consumption of coaxial mixers by proposing different correlations with characteristic parameters. In Farhat et al., new definitions of

characteristic speed *N*, Reynolds number *Re* and power number *Np* were introduced as shown below. Using the combination of an anchor and Rushton turbines with four different diameters, and an anchor and a singe Mixel TT, they demonstrated that the power consumption obtained using these definitions could yield a single power curve regardless of the speed ratio, rotating mode and the high-speed impeller diameter.

$$N = \frac{(N_i D_i + N_0 D_0)}{D_i} \tag{4.1}$$

$$Re = \frac{\rho(N_i D_i + N_0 D_0) D_i}{\mu} \tag{4.2}$$

$$N_P = \frac{P}{\rho(N_i D_i + N_0 D_0)^3 D_i^2} \tag{4.3}$$

The above definitions are based on a weighing of the impeller tip speeds. Due to the fact that the high-speed impeller is dominant in the overall power consumption, using its diameter as the characteristic diameter is in agreement with the work of Foucault et al. Since both agitators induce fluid flow, the contribution from each must be taken into account. In the co-rotating mode, they create circulation in the same direction, while in the counter-rotating mode, the discharge flows oppose each other. The maximum velocity generated by each agitator is always located at its tip and becomes almost zero close to the tank wall. Initially it is expected that the velocity in the 'antagonistic' region (in between the impellers) will be almost zero due to the counteraction of the impellers. Nevertheless, Figure 4.4 illustrates that these flow patterns show the addition of the speeds, not only in the co-rotating mode but also in the counter-rotating mode. Consequently, the total flow is almost equivalent in both rotating modes. This reality is reflected in the newly proposed correlations where the tip speeds are summed up for both rotating modes. Since the characteristic speed in both rotating modes is the same and the flow pattern is similar, it does not come as a surprise that the total power values are approximately the same at the same Reynolds number.

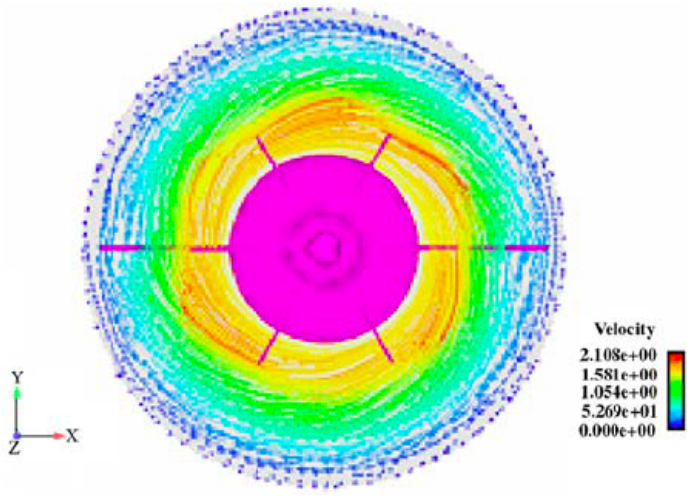

(a) co-rotating mode

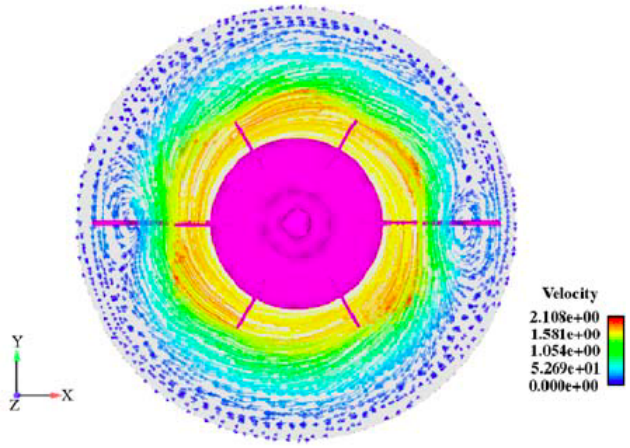

(b) counter-rotating mode

Figure 4.4: Flow patterns (tangential velocity, m/s) for the Rushton-Anchor configuration, plane XY is at Z = 0.2 m (Rivera et al.)

4.4.2 Extensions of the Applicability of the Power Correlations

In order to further assess the applicability of the newly proposed correlation, we verified its applicability to dual shaft mixers and the Superblend mixer. In Figure 4.5a, the power curves of the Deflo-Paravisc dual shaft mixer in co-rotating mode are shown using the definitions ($N_{co\text{-}rotating} = N_i - N_o$, $Re = \rho(N_i - N_o)D_i^2/\mu$) presented by Foucault et al.

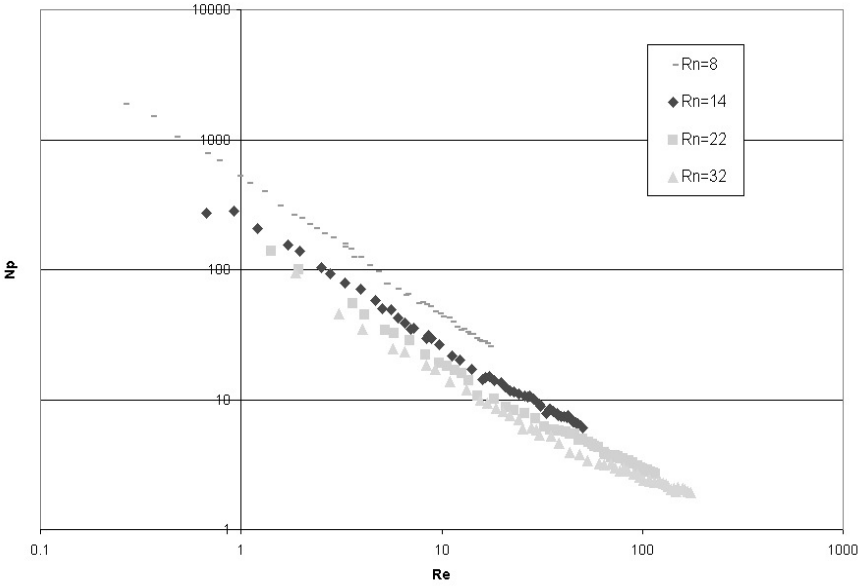

(a) using the correlations from the work of Foucault et al. (2005)

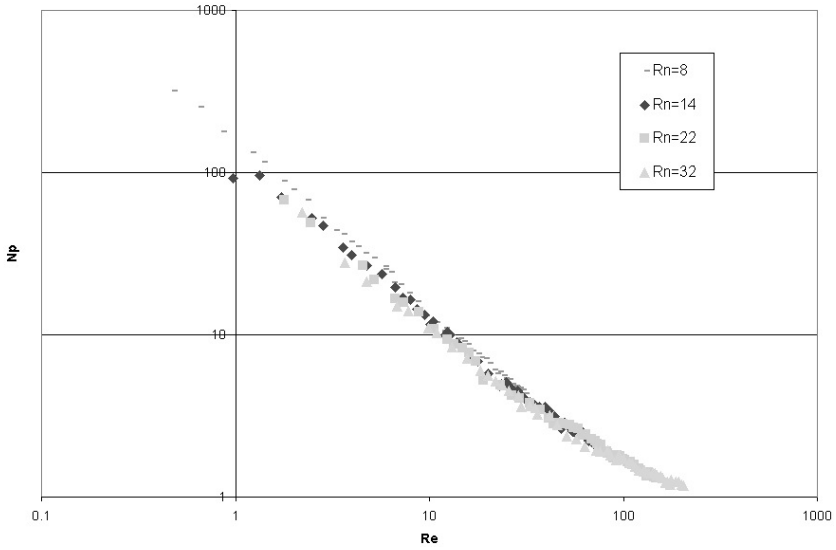

(b) using the new correlations

Figure 4.5: Power curve for the Deflo-Paravisc dual shaft

(a) using the correlations from the work of Foucault et al.; (b) using the new correlations

We can clearly see that the equations of Foucault et al. are not applicable to this dual shaft mixer, because the power consumption at each speed ratio still presents an independent curve. However, the power curves collapse onto a single curve that is independent of the various speed ratios when

using equation 2 and 3 as shown in Figure 4.5b. Very similar results were obtained for the Mixel TT-Paravisc dual shaft mixer in co-rotating mode as shown in Figure 4.6.

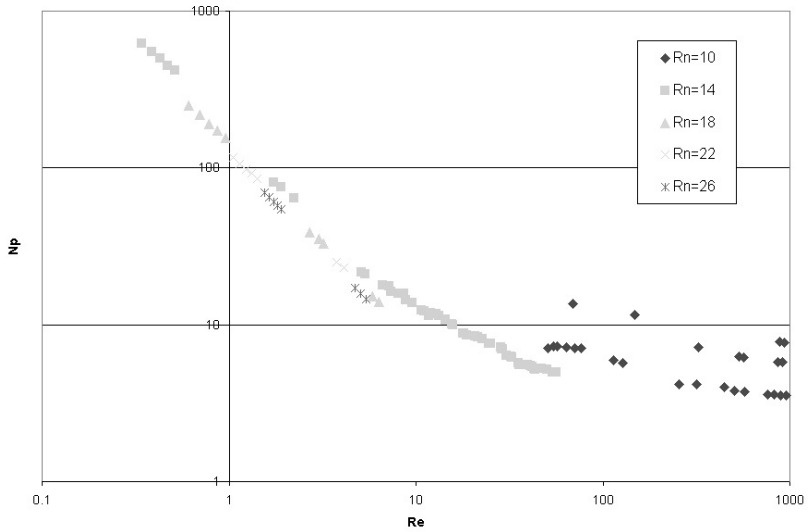

(a) using the correlations from the work of Foucault et al. (2005)

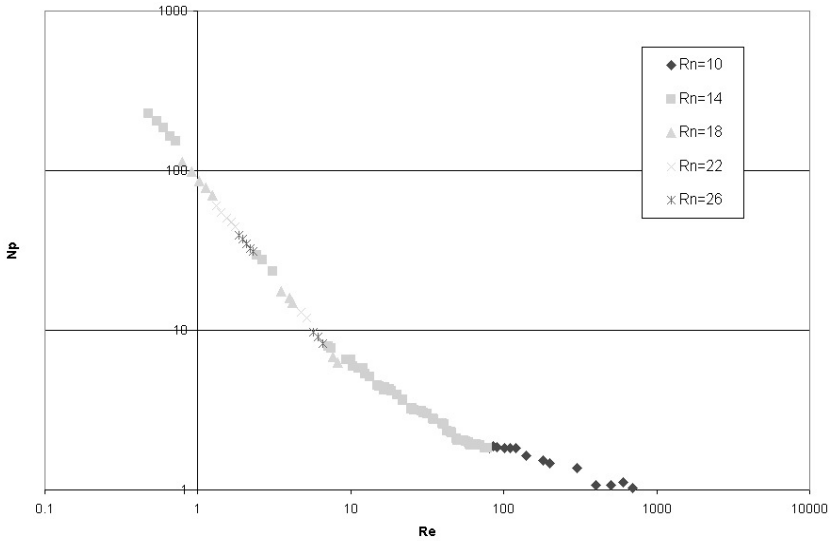

(b) using the new correlations

Figure 4.6: Power curve for the Mixel TT-Paravisc dual shaft

(a) using the correlations from the work of Foucault et al.; (b) using the new correlations

Taking advantage of the new correlations, a single power curve for the Superblend mixer regardless of speed ratio was obtained as shown in Figure 4.7. In addition, the rotating mode did not have to be explicitly included in the power number calculations.

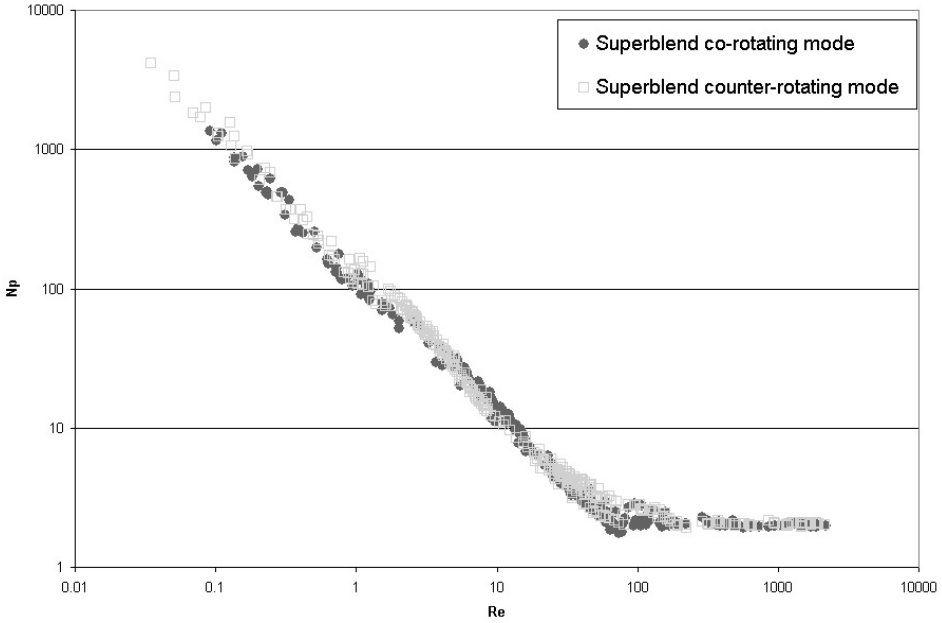

Figure 4.7: Power curve for the Superblend using the new correlations (Farhat et al.)

4.4.3 Performance Comparison

Obtaining single power curves for many different multi-shaft mixers makes it possible to compare the different mixers based on this 'universal' Reynolds number. The following sections aim at comparing the various geometries of mixers and determine, on a unified basis, which geometry has the most to offer in terms of power constant and mixing time.

4.4.3.1 Power Constant

Derived from equations 4.2 and 4.3, the definition of power constant in this work is shown as below,

$$K_P = Re \times N_P = \frac{P}{\rho(N_i D_i + N_0 D_0)^2 D_i} \tag{4.4}$$

Table 4.1 shows the power constants for all the three mixers in co-rotating mode. It shows that the coaxial mixer consisting of the Mixel TT-Anchor combination has the lowest power constant

(45), while the Superblend consumes the most power in the laminar regime (130). Meanwhile, as another proof of the power-efficient effect of Mixel TT, the power constant of Mixel TT-Paravisc (60) is remarkably lower than that of Delfo-Paravisc (110).

Table 4.1: The comparison of K_P for multi-shaft mixers

Multi-shaft mixers	K_P of high-speed impeller	K_P of low-speed impeller	K_P of multi-shaft mixer
Coaxial Rushton-Anchor (L-L)	70	170	70
Coaxial Mixel TT-Anchor (L-L)	45	170	45
Dual shaft Deflo-Paravisc (L-H)	65	368	110
Dual shaft Mixel TT-Paravisc (L-H)	45	368	60
Superblend (H-H)	200	370	130

The fact that the Mixel TT-anchor system was more efficient can be explained by the axial pumping effect of the Mixel TT (axial turbine). This pumping is far superior to the one generated by the Rushton turbine (radial turbine). On the other hand, the Mixel TT- Paravisc dual shaft mixer is less power-efficient than the Mixel TT- anchor coaxial mixer. This can be explained by the existence of more effective impeller interactions or less counteraction between the Mixel TT and the anchor compared to that between the Mixel TT and the Deflo with the Paravisc. In all these regimes, the Superblend is the most power consuming mixer. Again, this does not come as a surprise since the Maxblend is bulkier than any of the turbines used.

We also compared the power constant of the high-speed impellers to the one of the multi-shaft systems when they are at high speed ratio (R_N >10) in Table 1 as well. The K_P values for the individual impellers composing the multi-shaft mixers are listed along with the K_P value of the multi-shaft mixer itself. Three cases can be seen: 1) both impellers have fairly low K_P (case Low-Low i.e. L-L); 2) both impellers have high K_P (Superblend, case High-High i.e. H-H); 3) the high-speed impeller with low K_P and the low speed impeller with high K_P (Dual shaft with RT/TT + Paravisc, case Low-High i.e. L-H).

In the L-L case, the first observation is that the K_P of the Rushton or the Mixel TT alone equals that of the multi-shaft system. This behaviour can be explained by the fact that the high-speed impeller plays the dominant role in the power consumption of the coaxial system, especially at high speed ratio. Indeed, the low speed impeller mostly acts as a rotating baffle in that mode of operation. Moreover, in this work the low speed impeller is an anchor well known for its lack of axial pumping. Therefore, its impact on the overall hydrodynamics is minimal and explains why the high-speed impeller alone is representative of the overall power consumption. Based on this result, we can easily predict the K_P of any coaxial mixer of that type (L-L), operating at high speed ratio, as the K_P value of the high-speed impeller. The simple calculation can be used when changing the type of high-speed turbine for example and where the geometry of the mixer remains the same.

In the case of Low-High, the overall power consumption is not as much dominated by the high-speed impellers only. In these configurations, the low speed impeller is a Paravisc type and it contributes to the overall hydrodynamics, much more than an anchor can do. This results in a dual-shaft power constant that is higher than that of the high-speed impeller and lower than that of the low-speed impeller (Paravisc - Deflo: $65 < 110 < 368$; Paravisc - Mixel TT: $45 < 60 < 368$. In these configurations, the K_P of the dual shaft system is close to the one of the high speed impeller but always above. This can easily be interpreted as if the high-speed impeller is still dominant in the power consumption; the dominance is not as overwhelming as in the coaxial mixers. Hence, an intermediate K_P value is obtained. This intermediate value cannot be predicted from our results.

The case of the Superblend (H-H) is somehow puzzling at first look. The K_P of the Superblend is lower than that of the individual impellers ($200 > 130 < 370$). The Superblend is a coaxial mixer that possesses a high-speed impeller with high K_P combined to the contribution from the helical ribbon also with a high K_P. When the helical ribbon is static and the K_P of the Maxblend is obtained, the ribbon acts like a baffle that increases the K_P of the Maxblend. The opposite is also true when the K_P of the ribbon is obtained with the Maxblend being static in the tank: its K_P rose compared to a ribbon alone in a tank. When the helical ribbon is rotating along with the Maxblend, the interaction between the two tends to lower the overall power consumption. There

is no doubt that the Maxblend is dominating the power consumption in this condition and the K_P of Superblend should be close to 200, which is K_P of Maxblend. Being different from other coaxial mixers, however, the gap between those two impellers is so small that the effect of power saving produced by helical ribbon leads the K_P of Superblend to a much lower value. The behavior of the K_P value could also indicate an optimum operating speed ratio. This optimum has not been found, however.

4.4.3.2 Mixing time

Figure 4.8 presents the dimensionless mixing time $N \times t_m$ (t_m, mixing time) for all the three mixers in different configurations and rotating modes as a function of the Reynolds number calculated from Equation 4.2. It clearly shows that the Superblend mixer either in the co-rotating mode or in the counter-rotating mode requires much less time to reach complete mixing at the same Re value as other mixers. The coaxial mixer with both Rushton-Anchor and Mixel-anchor configurations in co-rotating mode is always more efficient than that in counter-rotating mode. The dual shaft mixer performs the worst in terms of mixing time.

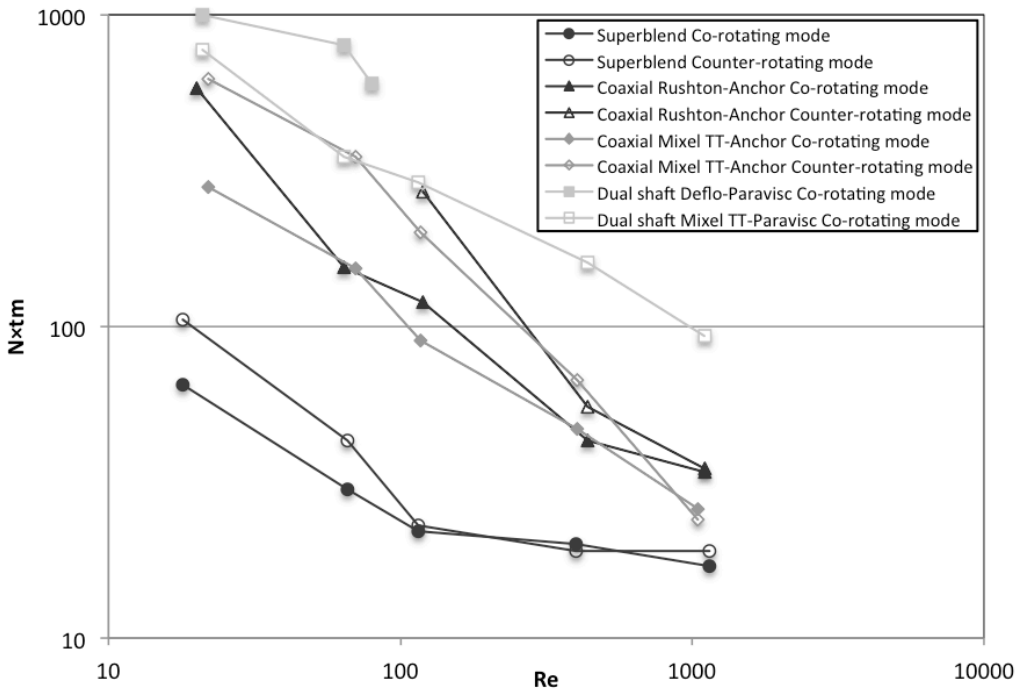

Figure 4.8: Dimensionless mixing time comparisons for all mixers

The uniform shear and efficiency of the Maxblend impeller has already been highlighted in a series of articles. This combination of Maxblend impeller and double helical ribbon is proposed to be very efficient in deep laminar regime mixing since both impellers have good pumping capacities with highly viscous fluids. The coaxial mixer in both configurations performs better than the dual shaft mixer. This result can be explained from the perspective of the diameter of the agitators. It is well known that the mixing performance can be affected by the diameter ratio of the impeller to the tank in the laminar regime. Herein, diameter ratio of the high-speed impeller to the tank in the coaxial mixer is about 0.5 and that of the dual shaft mixers just reaches 0.2. The introduction of a high-speed impeller into the dual shaft system is aiming at breaking the vortex, disperse and help to form a full circulation in the tank. Finally, as expected, the co-rotating mode is more efficient than the counter-rotating mode for all mixers, which is also supported by a number of previous studies.

4.4.3.3 Mixing energy

Aiming to assess the mixing efficiency of each mixer considering both the energy consumption and mixing time, the performance of these mixers are compared again in Figure 4.9 in terms of the dimensionless mixing energy, $E_{mix} = N_P \times N \times t_m$, where we can clearly see the superiority of the Superblend mixer. Although this combination consumes more energy in comparison with other mixers as shown in Table 1, its overwhelming performance on mixing time allow it to be the most efficient mixer in terms of mixing energy. In mixing efficiency comparison, the coaxial mixers with Rushton-Anchor and Mixel-anchor configurations are following the Superblend, and dual shaft Deflo-Paravisc mixer is still the worst. However, it is surprising that Mixel TT-Paravisc dual shaft becomes more efficient than the Rushton-Anchor coaxial mixer in counter-rotating mode when both power consumption and mixing time are taken into account.

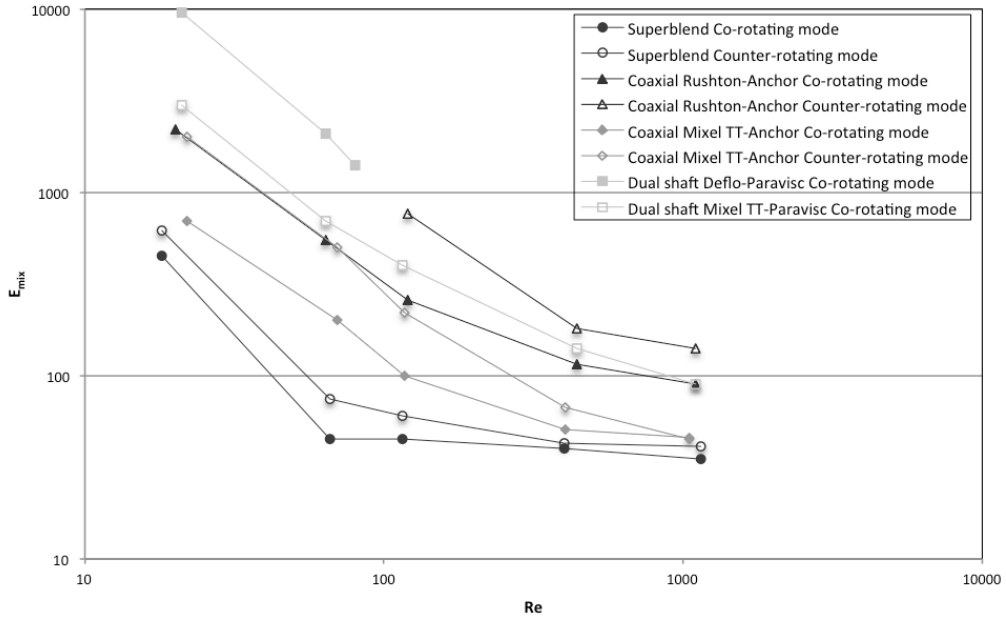

Figure 4.9: Dimensionless mixing energy comparisons for all mixers

On the other hand, Figure 4.9 does not only allow comparing the different mixers, it also allows comparing co- and counter-rotating modes. The performance of the co-rotating mode is, once again, superior to the counter-rotating mode for all tested configurations. As the power demands of different types of mixers are quite different, mixing energy allows us to compare their mixing performance taking both the effects of the power consumption and the mixing time into account.

4.4.3.4 Limitations of the New Power Correlations

We extended the assessment of the applicability of the new correlations to a dual shaft mixer provided with an off-centered rotor-stator (VMI-Rayneri, France). The rotor-stator is characterized by a strong dissipating capacity but a rather poor pumping contribution. Figure 4.10 shows the power curves for the Rotor Stator-Paravisc dual shaft mixer using the new correlations. In this figure, instead of a single curve, different power curves were obtained at different speed ratios, which means the speed ratio still has influence on the power curve, which cannot be universalized by the new correlations.

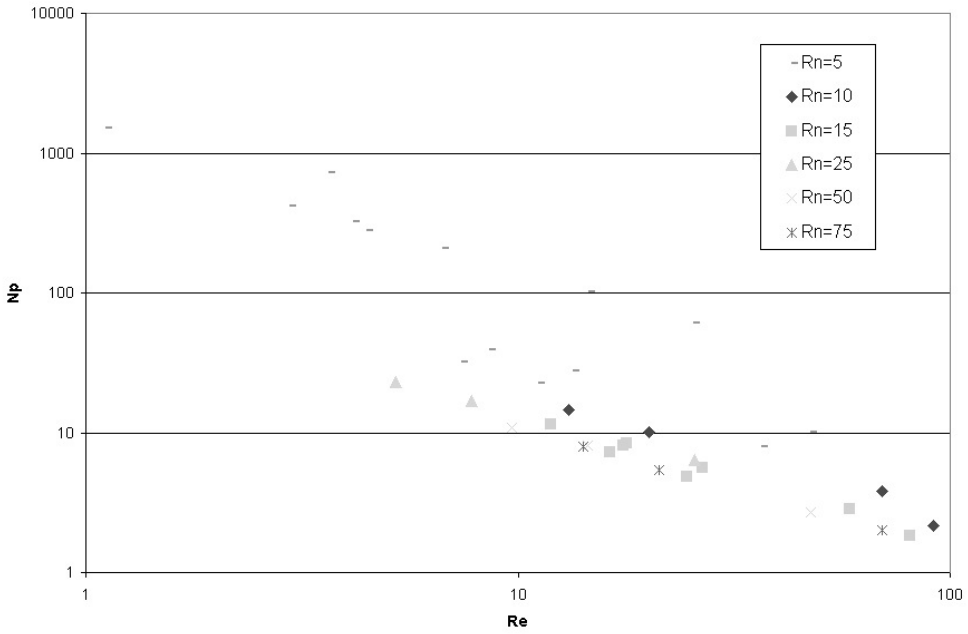

Figure 4.10: Power curve for the Rotor Stator-Paravisc dual shaft using the new correlations

This finding is consistent with the conclusion proposed by Wang et al. They carried out the investigation of the effect of speed ratio on the power consumption of the Superblend mixer specifically at very low speed ratio (R_N= 1-8, while R_N >8 in the work of Farhat et al.) and failed to attain a single curve for all speed ratios and modes as shown in Figure 4.11. Indeed, this figure presents the strong effect of speed ratio and rotating mode on the power consumption. It also shows that the helical ribbon is taking a non-negligible role in the power consumption at low speed ratio.

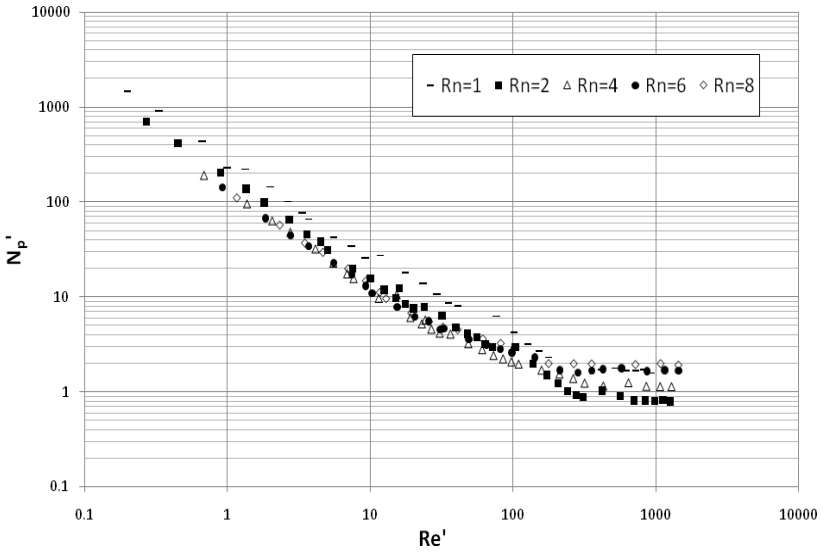

(a) co-rotatng mode

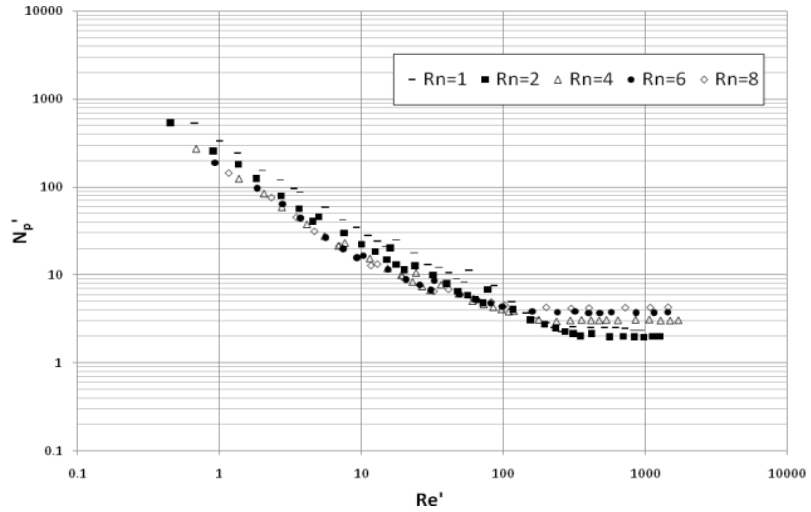

(b) counter-rotating mode

Figure 4.11: Power curves of Superblend mixer using the new correlations (N_P' and *Re'* are equivalent with N_P and *Re* presented in this work): (a) co-rotating mode; (b) counter-rotating mode. (Wang et al., 2012)

Based on the peculiar cases above, it can be concluded that the new correlations are applicable when the high-speed impeller is the largest contributor to the fluid circulation in the tank. The quantitative evaluation of this contribution can be done according to published work, specifically using the proposed Momentum Number. The important aspect is that this hydrodynamically-

dominating impeller also dominates the power consumption. More specifically, the rotor-stator discharge as a jet flow through stator teeth is the main dissipation mechanisms. This can hardly bring any axial pumping to the dual shaft system. The domination in the power consumption is determined not only by the configuration of each impeller, but also by the speed ratio between them. The higher the speed ratio is, the higher the domination is. Since the previous results of coaxial mixers were also focused on high speed ratio, we can notice that as for Rotor Stator-Paravisc dual shaft mixer or coaxial mixers at low speed ratio, the lack of pumping from high-speed impeller and the power contribution from the low-speed impeller causes the failure of the applicability of the new power correlations in such mixing systems.

4.5 Conclusion

The first objective of this work was to discuss and extend the investigation of the applicability of the new correlations proposed by Farhat et al. It was found that these correlations are well suited for dual shaft mixers and the Superblend. The second objective was to compare the power consumption, the mixing time and the mixing energy of different mixers and introduce a general approach to predict the power constant of multi-shaft mixers. The results showed that the Superblend mixer requires more power than all the other mixers, while the Mixel TT-Anchor combination is the most power-efficient. On the other hand, the Superblend shows an excellent mixing efficiency in terms of mixing time and mixing energy outperforming both coaxial and dual shaft mixers. As another conclusion, the possibility of predicting the power constant of multi-shaft mixers was based on two assumptions: the speed ratio must be high enough to allow the high-speed impeller to dominate the power consumption and the interaction must be weak enough to avoid the interference from the low-speed impeller. Finally, the limitations of the new correlations were discussed through the extension application on Superblend at low speed ratios and rotor stator-Paravisc dual shaft mixer.

4.6 Acknowledgement

The support of NSERC and the research consortium on Non-Newtonian Innovative Mixing Technologies is gratefully acknowledged.

4.7 Reference

BARAR POUR, S.; FRADETTE, L. and TANGUY, P. A. (2007). Laminar and slurry blending characteristics of a dual shaft impeller system. *Chem. Eng. Res. Des.*, *85* (A9), 1305-1313.

BONNOT, S., CABARET, F. FRADETTE, L. and TANGUY, P. A. (2007). Characterization of Mixing Patterns in a Coaxial Mixer. *Chem. Eng. Res. Des.*, 85(A8), 1129-1135.

CABARET, F., BONNOT, S., FRADETTE, L. and TANGUY, P. A. (2007). Mixing Time Analysis Using Colorimetric Methods and Image Processing. *Ind. Eng. Chem. Res.*, 46(14), 5032-5042.

CABARET, F., RIVERA, C., FRADETTE, L., HENICHE, M. and TANGUY, P. A. (2007). Hydrodynamics performance of a dual shaft mixer with viscous Newtonian liquids. *Chem. Eng. Res. Des.*, *85* (A5), 583-590.

FARHAT, M., FRADETTE, L., HORIGUCHI, H., YATOMI, R. and TANGUY, P. A. (2009). Experimental Investigation of Superblend Coaxial Mixer. *J. Chem. Eng. Jpn.*, 42(11), 797-803.

FARHAT, M., FRADETTE, L., TANGUY, P. A. (2008). Revisiting the performance of a coaxial mixer. *Ind. Eng. Chem. Res.*, 47(10), 3562-3567.

FARHAT, M., RIVERA, C., FRADETTE, L., HENICHE, M. and TANGUY, P. A. (2007). Numerical and Experimental Study of Dual-shaft Coaxial Mixer with Viscous Fluids. *Ind. Eng. Chem. Res.*, 46(14), 5021-5031.

FOUCAULT, S., ASCANIO, G. and TANGUY, P. A. (2004). Coaxial mixer hydrodynamics with Newtonian and Non-Newtonian fluids. *Chem. Eng. Technol.*, 27(3), 324-329.

FOUCAULT, S., ASCANIO, G. and TANGUY, P. A. (2005). Power characteristics in coaxial mixing: Newtonian and Non-Newtonian fluids. *Ind. Eng. Chem. Res.*, 44, 5036-5043.

FOUCAULT, S., ASCANIO, G. and TANGUY, P. A. (2006). Mixing times in coaxial mixers with Newtonian and non-Newtonian fluids. *Ind. Eng. Chem. Res.*, 45(1), 352-359.

FRADETTE, L., THOME, G., TANGUY, P. A. and TAKENAKA, K. (2007). Power and Mixing Time Study Involving A Maxblend Impeller with Viscous Newtonian and Non-Newtonian Fluids. *Chem. Eng. Res. Des.*, 85(A11), 1514-1523.

KHOPKAR, A., FRADETTE, L. and TANGUY, P. A. (2007). Hydrodynamics of a dual shaft mixer with Newtonian and non-Newtonian fluids. *Chem. Eng. Res. Des.*, *85*, 863-871.

KOHLER, S. and HEMMERLE, W. (2003). Analysis of the power characteristic of a coaxial agitator with varied diameter and speed ratio inner and outer mixing device. *11th European Conference on Mixing*, Bamberg, 14-17.

KURATSU, M., NISHIMI, H., YATOMI, R., SATO, H. and MISHIMA, M. (1994). Mixing Reactor "Superblend" applied to wide range of viscosity. *Sumitomo Heavy Industries Technical Review*, *42* (124), 82-85.

MACHADO, M. B., NUNHEZ, J. R., NOBES, D. and Kresta, S. M. (2012). Impeller Characterization and Selection: Balancing Efficient Hydrodynamics with Process Mixing Requirements. *AIChE J.*, *58* (8), 2573-2588.

RIVERA, C., FOUCAULT, S., HENICHE, M., ESPINOSA-SOLARES, T. and TANGUY, P.A. (2006). Mixing Analysis in a Coaxial Mixer. *Chem Eng Sci*., 61(9), 2895–2907.

TAKENAKA, K., YATOMI, R., MORINAGA, S. and TANGUY, P. A. (2006). Comparison of Solid-mixing Performance Between A Pitched Blade Turbine and the Maxblend Impeller. *Proceedings of the 12th European Conference on Mixing,* Bologna, Italy.

THIBAULT, F. and TANGUY, P. A. (2002). Power-draw analysis of coaxial mixer with Newtonian and non Newtonian fluids in the laminar regime. *Chem. Eng. Sci.*, 57, 3861-3872.

WANG, X., FRADETTE, L., TAKENAKA, K. and TANGUY, P. A. (2012). Effect of operating parameters on the mixing performance of the Superblend coaxial mixer. *Ind. Eng. Chem. Res.*, *51* (4), 1826-1833.

YAO, W., MISHIMA, M. and TAKAHASHI, K. (2001). Numerical Investigation on Dispersive Mixing Characteristics of Maxblend and Double Helical Ribbons. *Chem. Eng. J.*, *84*, 565–571.

YATOMI, R., TAKENAKA, K., MORINAGA, S., TAKAHASHI, K. and TANGUY, P.A. (2006). Large Paddle Impeller for Enhancing Surface Aeration: Application to Polymerization Reactor with Liquid Level Change. *Proceedings of the 12th European Conference on Mixing*, Bologna, Italy.

CHAPTER 5: ARTICLE 3: EXTENDED CHARACTERIZATION OF THE SUPERBLEND™ COAXIAL MIXER WITH SHEAR-THINNING FLUIDS

Article history: Submitted March 17, 2014, Industrial & Engineering Chemistry Research.

Authors: Xiao Wang, Inci Ayranci, Louis Fradette and Philippe A. Tanguy

5.1 Abstract

The mixing performance of a Superblend™ coaxial mixer was studied with both Newtonian and non-Newtonian fluids. The inner impeller of the Superblend is a Maxblend™ impeller and the outer impeller is a helical ribbon, which enable mixing in both laminar and transitional regimes. Such a design offers promising mixing efficiency in both laminar and transitional flow regimes. Torque meters mounted on each shaft combined with a decolorization-image-processing technique were utilized in order to quantify the influence of the operating conditions such as speed ratio, rotating mode, and rheological behavior of the fluid on the power consumption and Metzner-Otto constant of the impellers, the mixing evolution, the mixing time, and the mixing energy. Results showed that the operating parameters strongly influence the mixing performance of the Superblend mixer. The mixing performance with non-Newtonian fluids is significantly different from the one observed with Newtonian fluid. The analysis of all the results allows the derivation of the optimal operation for Superblend with complex fluids.

5.2 Introduction

Fluid mixing with complex rheological behaviours has been a challenge to the mixing community for many years. With new formulated products involving less solvents and higher solid loading, the non-Newtonian characteristics are enhanced, making the mixing challenges more pronounced. A series of complex mixers have begun to emerge to cope with this situation such as coaxial, dual shaft and Maxblend mixers. Their design as well as their operation in

industry is still mainly based on experimental results with viscous Newtonian fluids with the assumption that Newtonian fluid results can be extrapolated to the non-Newtonian fluid cases. As shown in the literature, this assumption is unfortunately misleading.

Referring to the coaxial mixers, Tanguy and Thibault (1997) pointed out that the dispersion and segregation-breaking capabilities of the inner impeller (a Rushton turbine) are enhanced with shear-thinning fluids. Thibault et al. (2002) and Tanguy et al. (2002) found that the power constant K_P of the outer impeller (an anchor) increases with an increase on the speed ratio for the Newtonian fluid and the shear-thinning fluids, and it decreases when the power-law index decreases. Rivera et al. (2006) concluded that although the power consumption of shear-thinning fluid is lower than that of Newtonian fluid, the mixing time with shear-thinning fluid is longer than that with Newtonian fluid attributed to the existence of an axial velocity reduction and a large low viscosity zone with shear-thinning fluid. With regard to the dual shaft mixers, Khopkar et al. (2007) observed that an off-centered inner impeller (a rotor-stator) has no influence on the Metzner-Otto constant, K_S, of the outer impeller (a Paravisc) regardless of the fluid rheology. Moreover, the effect of power-law index n on the K_S of rotor-stator is obvious, but not at all on that of Paravisc. In fact, the conclusions on K_S are still to be demonstrated. Some researchers such as Brito-De La Fuente et al. (1997) reported that n indeed has an influence on the K_S of a helical ribbon, while others such as Bao et al. (2011) reported that it has no impact on the K_S of the outer impeller (an anchor) at all. For the Maxblend mixer, Fradette et al. (2007) highlighted that for the shear-thinning fluids the threshold for transition between each hydrodynamic regime is surprisingly different, and the increase of the off-bottom clearance reduces the K_S of the Maxblend impeller. Guntzburger et al. (2013) introduced the decolorization method for the pumping evaluation of the Maxblend mixer and proposed an equation featured by the slope of the mixing curve to express the global pumping effect from the comprehensive behaviour of the axial, radial and tangential flows rather than the simple integration of the single flows. They noted that the pumping capacity with shear-thinning fluid decreases noticeably due to the 'pathological mixing situation' emerged at low Reynolds number (Re < 80), and even the segregation phenomenon occurs when Re < 10. The method of pumping evaluation is still to be extended to other mixers.

As an improved design of the Maxblend mixer, the Superblend coaxial mixer was developed for highly viscous mixing. Farhat et al. (2009) studied its mixing performance with viscous Newtonian fluids at high speed ratios ($R_N > 10$). Wang et al. (2012) extended this study into low speed ratio ($R_N < 10$) and discussed the power performance of each impeller individually. In order to have a complete picture of the mixing efficiency of this mixer, the aim of the present work is to experimentally characterize and compare the mixing performance of the Superblend using both Newtonian and non-Newtonian shear-thinning fluids in terms of mixing evolution, mixing time, power consumption, Metzner-Otto constant and mixing energy.

5.3 Setup and Materials

As shown in Figure 5.1, the Superblend coaxial mixer is characterized by a combination of a Maxblend impeller and a helical ribbon. Figure 1 also provides the dimensions of the setup used in all the experiments. In our mixing equipment, the tank diameter T is 0.38 m and the liquid height H is 0.44 m, which make the liquid volume approximately 40L. The diameter of the Maxblend mixer D_i is 0.2m ($D_i / T = 0.53$), and the diameter of the helical ribbon D_o is 0.36 m ($D_o / T = 0.95$).

Speed ratio R_N and rotating mode are two important operating parameters in the coaxial mixers. R_N is the rotational speed ratio of the Maxblend to the helical ribbon. The Superblend can be operated in two modes: co- and counter-rotation. The individual Maxblend impeller generates down-pumping flow in the central part of the tank and up-pumping flow near the wall, and the flow pattern remains the same in both rotating directions. Therefore, the Maxblend impeller rotates in the same direction in both modes. In the co-rotating mode, the helical ribbon produces up-pumping flow near the wall and down-pumping flow in the central part of the tank, which enhances the similar flow pattern produced by the Maxblend impeller. In the counter-rotating mode, the helical ribbon produces down-pumping flow near the wall and up-pumping flow in the central part of the tank, which conflicts with the flow pattern produced by the Maxblend impeller. In that operating mode, the flow pattern generated by the helical ribbon overwhelms the one generated by the Maxblend impeller. This hydrodynamic conflict has been extensively discussed by Wang et al. (2012). Attributed to the significant impact of the helical ribbon on the flow pattern, Wang et al. (2012) also proposed to define the operating mode in the Superblend by the

pumping direction of the helical ribbon: up-pumping mode when the helical ribbon produces up-pumping flow near the wall; down-pumping mode when the helical ribbon produces down-pumping flow near the wall.

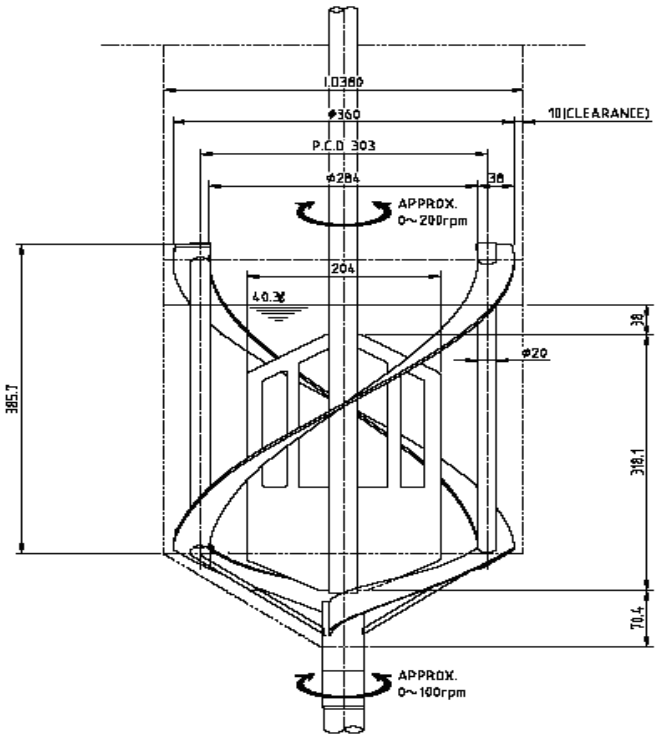

Figure 5.1: Configuration and dimensions of Superblend mixer

Glucose solutions with different concentrations were used as Newtonian fluids. The viscosities ranged from 0.1Pa.s to 39 Pa.s. The most common fluids used to model industrial non-Newtonian fluids are Xanthan gum and Carboxymethylcellulose **(**CMC) solutions. The mixing time measurements were done by decolorization method which requires a transparent solution. Xanthan gum solution is not transparent; therefore, it was not used in this study. CMC solution is transparent; therefore, those were chosen as the model fluid. CMC solutions follow shear-thinning behavior. The shear-thinning fluids prepared in this work strictly follow the power-law, which can be described as

$$\mu_a = k\dot{\gamma}^{n-1} \tag{5.1}$$

where μ_a represents the apparent viscosity in Pa.s, $\dot{\gamma}$ the shear rate in 1/s, k the consistency index and n the power-law index. CMC solutions were composed of CMC powder, water and glucose

solutions. The K values of the CMC solutions were varied by varying the glucose solution concentration. Table 5.1 shows the properties of the liquids.

Table 5.1: Rheological properties of the studied shear-thinning fluids

n	k	ρ [kg/m^3]
0.7	2.9	1100
0.7	0.24	1000
0.6	3.51	1100
0.6	0.89	1000
0.5	4	1100
0.5	1.8	1000

Due to the complexity of fluid mixing with elasticity, the appearance of elasticity is avoided in the preparation of shear-thinning fluids by measuring elastic modulus *G'*. Results showed that the elasticity was assumed to be negligible when the CMC concentration was below 2 wt%. All the rheological measurements were carried out with an AR2000 rheometer in a rheology laboratory. Because of the sensitivity of viscous fluids to the temperature, a thermometer was used to monitor the temperature variation during the measurements and ensure consistency between the measurements.

5.4 Methodology

By means of the torque meter mounted on each shaft, the power consumption of each single impeller can be calculated as

$$P = M_c 2\pi N \tag{5.2}$$

where M_c is the effective torque corrected by subtracting the residual torque from the measurement during the experiments with the fluids. The residual torque is measured with the

tank empty and accounts for the torque caused by all the other contributors but the fluid in the system.

The power number N_P, Reynolds number Re and the power constant K_P of each impeller for Newtonian and shear-thinning fluids can be determined by the standard equations below,

$$N_P = \frac{P}{\rho N^3 D^5} \tag{5.3}$$

$$Re = \frac{\rho N D^2}{\mu}, Re_\eta = \frac{\rho N^{2-n} D^2}{k} \tag{5.4}$$

$$K_P = N_P \times Re \quad , \; K_P(n) = N_P \times Re_\eta \tag{5.5}$$

For consistency with previous work with Newtonian fluids, the correlation proposed by Farhat et al. (2008) is applied as the characteristic rotational speed of the Superblend mixer:

$$N' = \frac{(N_i D_i + N_0 D_0)}{D_i} \tag{5.6}$$

Using the diameter of the Maxblend impeller as the characteristic diameter, the characteristic power number and Reynolds number for the Superblend mixer for Newtonian and shear-thinning fluids are defined as

$$N_P{}' = \frac{P}{\rho N'^3 D_i^5} \tag{5.7}$$

$$Re' = \frac{\rho N' D_i^2}{\mu}, Re'_\eta = \frac{\rho N'^{2-n} D_i^2}{k} \tag{5.8}$$

Mixing time in the present work was measured using a decolorization technique based on a fast acid-base reaction (Cabaret et al, 2007). Initially, a certain amount of pH indicator solution (0.08 wt% purple Bromocresol) was poured into the fluid to visually observe the evolution between acidic (yellow, $pH < 5.2$) and alkaline (purple, $pH > 6.8$) fluids. As the second step, 10 ml of NaOH solution was added and well mixed, which makes the fluid purple. The acid was prepared by premixing 15 ml of the HCl solution with the fluid in the tank to avoid density/viscosity variations. A video camera recorded the color variation at the same time as the HCl solution was injected between the shaft and the tank wall at the liquid surface. Based on the video a mixing curve illustrating the color evolution can be generated by using an image processing code. Using

this mixing curve the macro mixing time can be determined by finding the time needed to reach 95% of the complete decolorization state.

5.5 Results & Discussion

5.5.1 Mixing Evolution

Wang et al. (2012) showed that the helical ribbon generates bottom-to-top flow in the central part of the tank in the down-pumping mode with Newtonian fluid. This flow can overwhelm the down-pumping flow generated by the Maxblend impeller in this region and form a flow pattern that is dominated by the helical ribbon in the whole tank. This behavior is referred to as hydrodynamic conflict in the rest of this paper. To better observe this unexpected phenomenon, the order of acid-base input was reversed, namely putting acid first and then pouring base. Visually, purple is an easier color to detect on yellow than vice versa. In this case, the color will change from yellow to purple so the purple mixed portion can be clearly differentiated from the unmixed portion with the bright yellow background. However, the evolution from purple to yellow is used for other experiments when the aim is to detect the purple unmixed portion in yellow mixed fluid.

As shown in Figure 5.2a, the color of Newtonian fluid starts from bright yellow (photo1). After turning both impellers on and pouring the base solution, the purple color first appears at the central grids of the Maxblend impeller (photo 2) where the shear effect is proven to be very strong. Due to the fact that the fluid viscosity is very high and the diffusion phenomenon is weak, we can clearly see the helical ribbon pumping up the mixed fluid layer by layer in the central part of the tank. This is also a convincing evidence to prove that the down-pumping capacity of the Maxblend impeller in this mode is completely overwhelmed by the up-pumping capacity of the helical ribbon. Afterwards, the mixed fluid is involved into a top-to-bottom circulation generated by the helical ribbon along the tank wall. Therefore, the fluid keeps being pumped through the high shear region and mixed until all the fluid in the tank turns purple (photo 4). Referring to the last zone that gets mixed (photo 3), and comparing it with the configuration of Superblend we notice that the last well-mixed area is exactly the gap between the helical ribbon and the Maxblend impeller, which illustrates that both shear and pumping effects are found poor in this

zone. As a summary of the mixing process, in down-pumping mode with Newtonian fluids the mixing starts and mainly occurs at the central grids of the Maxblend impeller, while the helical ribbon acts like a powerful pump that consistently transports the fluid throughout the tank with a top-to-bottom pumping near the tank wall and bottom-to-top pumping along the shaft.

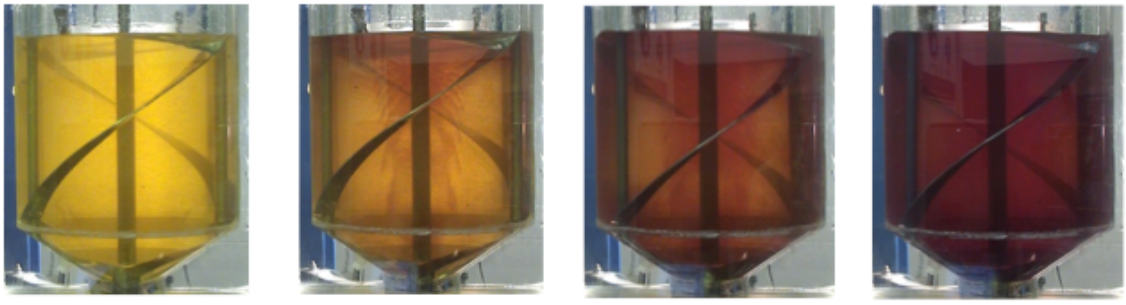

1 2 3 4

(a) Newtonian fluid

1 2 3

(b) Shear-thinning fluid

Figure 5.2: Decolorization images of mixing evolution in down-pumping mode

For shear-thinning fluid mixing in the down-pumping mode, however, the situation is surprisingly simple: mixing occurs at the top edge and the central grids of the Maxblend impeller and spreads to the whole tank with the circulation dominated by the helical ribbon. Being different from the Newtonian fluid mixing, the high shear region enlarges to the top edge of the Maxblend impeller with shear-thinning fluid. Put another way, the dispersion capacity of the

Maxblend impeller is enhanced with shear-thinning fluid. This finding is consistent with what Tanguy and Thibault (1997) have reported for a mixer composed of a helical ribbon and a Rushton turbine. Due to the viscosity drop under the shear effect, the top edge becomes capable of mixing the less viscous fluid. As a conclusion, although the direction of the flow circulation remains the same, rheological behavior enables the mixing process with shear-thinning fluid to be distinct from that with Newtonian fluid.

To investigate whether the mixing process of shear-thinning fluid in the up-pumping mode is also different from that of Newtonian fluid, we made a comparison in Figure 5.3. Figure 5.3a illustrates that the high shear region for the shear-thinning fluid in the up-pumping mode moves down to the lower half of the Maxblend impeller instead of the upper half. Herein, the fluid rheology again plays an important role in the distribution of the high shear region. Two conclusions can be drawn by comparing the locations of the high shear region in two modes. First, the high shear region is at the edge of the Maxblend impeller. This is not surprising since the Maxblend impeller is the high shear disperser component of the Superblend mixer. Second, the particular location of the high shear region depends on the rotating mode. In the down-pumping mode it is at the top edge of the Maxblend impeller and in the up-pumping mode it is at the bottom edge of the Maxblend impeller.

Figure 5.3b shows the Newtonian fluid mixing in up-pumping mode. The decolorization, therefore mixing, occurs everywhere in the entire tank simultaneously. This is an indication that in this rotating mode the shear is well-distributed throughout the tank. This is an evidence that supports the agreement widely approved by many researchers that co-rotating mode (up-pumping mode in this work) of the coaxial mixers is more efficient for Newtonian fluid mixing.

While the generation of high shear throughout the vessel is a significant advantage of the up-pumping mode, there is a drawback regardless of the rheology. The last mixed region is always located near the liquid surface, and it takes a while to disappear. Figure 5.3a and b (photo 3) shows this last mixed region which has different shapes for the two liquids. This region appears larger in the Newtonian fluid. This phenomenon is mainly caused by the weak interaction or even counteraction between those two impellers at the liquid surface.

The effect of speed ratio on the mixing process was also studied and the results showed that speed ratio does not have influence on mixing evolution. Above all, it is concluded that both the rotating mode and the fluid rheology have significant influences on the distribution of high shear region and the mixing process.

1 2 3

(a) Shear-thinning fluid

1 2 3

(b) Newtonian fluid

Figure 5.3: Decolorization images of mixing evolution with two fluids in up-pumping mode

Taking advantage of the decolorization technique, we made an attempt to investigate the mixing behaviors in various operating conditions based on the mixing curves. We collated the curves for each condition and found that the speed ratio has no influence on the mixing evolution in the tank. So far, the speed ratio does not impact either mixing process or mixing curve. It is not a

surprise because technically the same mixing processes generate the same mixing curves. The slope of the mixing curve is defined as the slope value of the linear portion of the mixing curve in the range of the percentage of the well-mixed fluid between 20% and 80%. In Figure 4 the mixing curves for all the operating conditions at N_i = 80 rpm and N_o = 10 rpm are presented. The data for up-pumping mode, which are represented in solid marks, show that the slopes of the mixing curves of the shear-thinning fluids are consistent regardless of the power-law index. A comparison between the Newtonian and shear-thinning fluid showed that the slope of the shear-thing fluid is 20% lower than the Newtonian fluid.

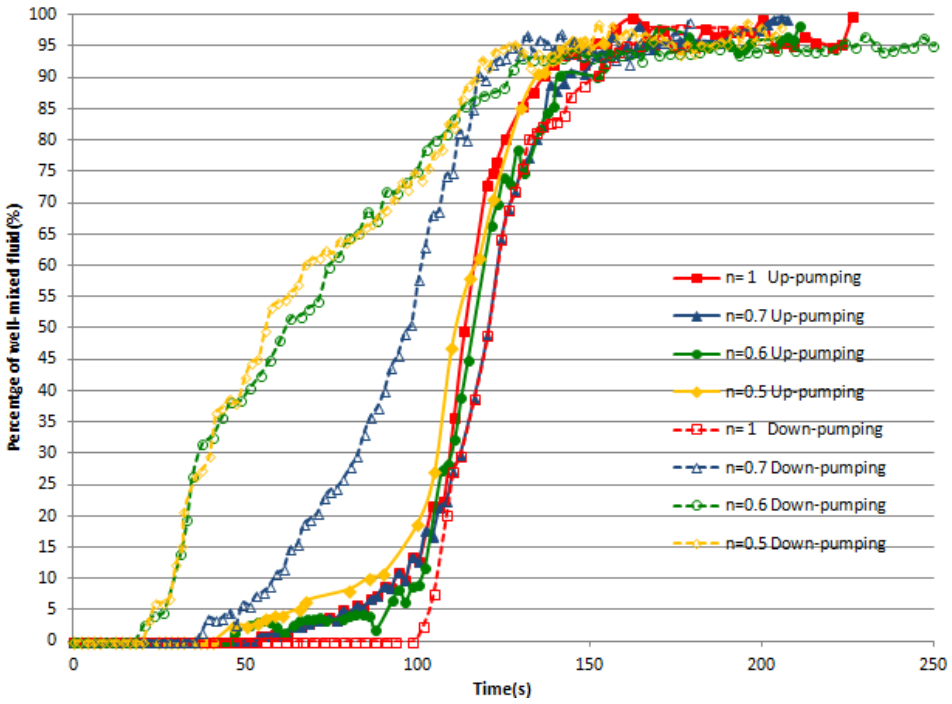

Figure 5.4: Mixing curves for all the operating conditions at N_i = 80 rpm and N_o = 10 rpm

In Figure 5.4 the data for down-pumping mode, which are represented in open marks, show that the slope of the mixing curves become different from the ones in the up-pumping mode except for Newtonian fluid. Therefore, we can conclude that the rotating mode has no effect on the mixing evolution observed with a Newtonian fluid, which is consistent with the result reported by Wang et al. (2012). Among different power-law index fluids the slopes are almost the same for n = 0.5 and n = 0.6; however, they are 50% lower than that for n = 0.7. Comparing slopes of the Newtonian and shear-thing fluids we see that the slopes of the shear thinning fluids are lower. Referring to the fluid with weak shear-thinning effect as n = 0.7, the slope decreases by 33%

compared to that in up-pumping mode. As the shear-thinning effect becomes stronger at n = 0.6 and 0.5, the slope decreases by 62% and 67% compared to that in the up-pumping mode, respectively. In addition, the trend of the curves changes from accelerating growth to decelerating growth. Namely, the mixing accomplishment increases faster and faster in up-pumping mode with all kinds of fluids, but more and more slowly in down-pumping mode with stronger shear-thinning fluids. Guntzburger et al. (2013) correlated the mixing curve and global pumping capacity, and proved that the higher the slope of the mixing curve, the stronger the pumping capacity of the mixing system. They also pointed out that the pumping capacity with shear-thinning fluid is weaker than that with Newtonian fluid in a Maxblend mixer. Taking advantage of their observations, we can conclude with our results that the pumping capacity with shear-thinning fluid is also weaker than that with Newtonian fluid in the Superblend mixer. The power-law index has no influence on the pumping capacity of the Superblend mixer in the up-pumping mode, but it does in the down-pumping mode: as the shear-thinning effect becomes strong, the pumping capacity decreases by up to 67% compared to that in the up-pumping mode, and by up to 72% compared to that with Newtonian fluid.

Guntzburger et al. (2013) pointed out that in a Maxblend mixer the shear-thinning effect causes a viscosity gap between the fluid in the impeller region and the rest of the tank. This effect weakens the pumping capacity of the impeller. In the Superblend mixer, there is a helical ribbon in addition to a Maxblend impeller. In the up-pumping mode the pumping generated by the helical ribbon eliminates the viscosity gap, and therefore the impact of the shear-thinning effect on pumping. In down-pumping mode, however, instead of elimination, the hydrodynamic conflict between impellers enlarges the impact of the shear-thinning effect on pumping. As the shear-thinning effect becomes stronger, the pumping capacity decline becomes more dramatic.

5.5.2 Mixing Time

As discussed in Wang et al. (2012), rather than the rotating mode, speed ratio has a strong effect on the dimensionless mixing time $N't_m$ (t_m is mixing time in seconds) with viscous Newtonian fluid. In this work, a similar investigation was carried out with shear-thinning fluids. We can see from Figure 5.5 that there is a clear influence of the rotating mode and the speed ratio on the dimensionless mixing time.

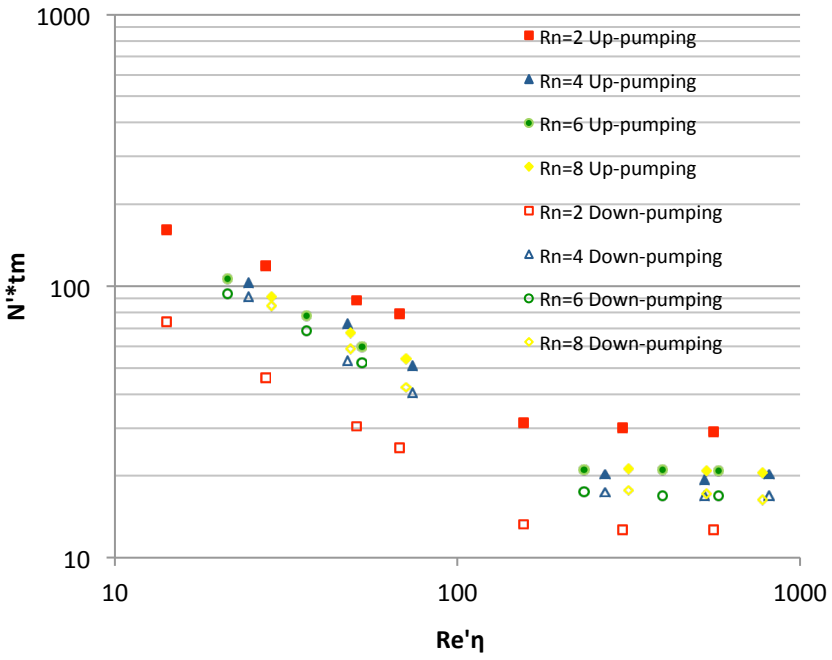
1000
100
10
N'*tm
10
100
1000
Re'η
Rn=2 Up-pumping
Rn=4 Up-pumping
Rn=6 Up-pumping
Rn=8 Up-pumping
Rn=2 Down-pumping
Rn=4 Down-pumping
Rn=6 Down-pumping
Rn=8 Down-pumping

$n = 0.7$

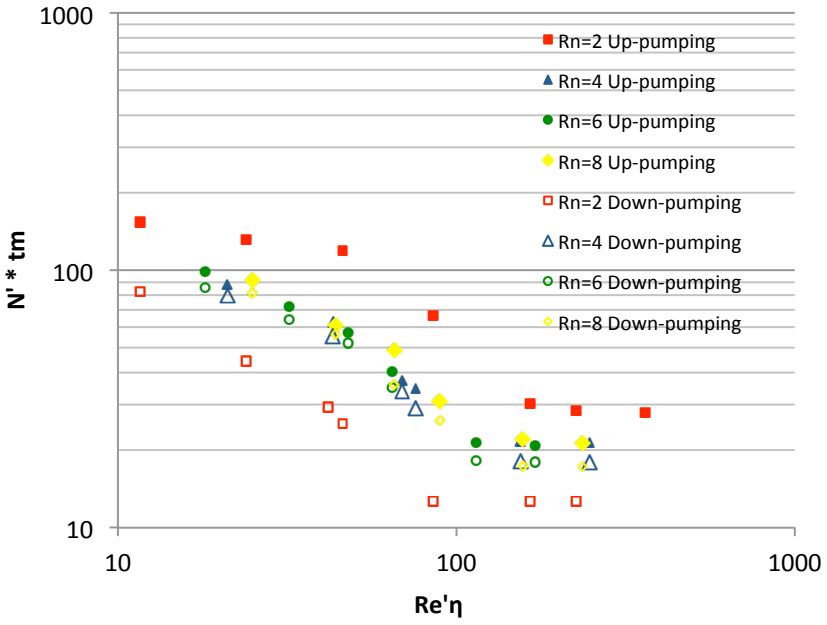
1000
100
10
N' * tm
10
100
1000
Re'η
Rn=2 Up-pumping
Rn=4 Up-pumping
Rn=6 Up-pumping
Rn=8 Up-pumping
Rn=2 Down-pumping
Rn=4 Down-pumping
Rn=6 Down-pumping
Rn=8 Down-pumping

$n = 0.6$

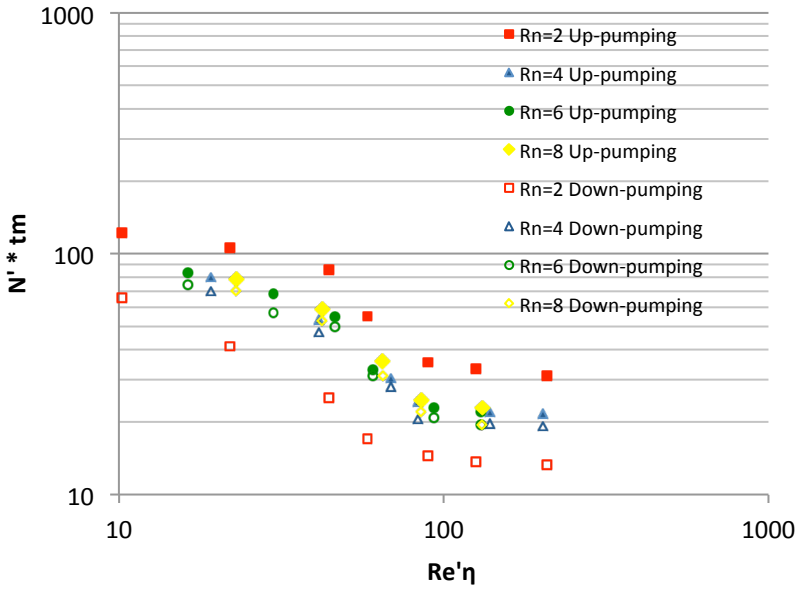

$n = 0.5$

Figure 5.5: Influence of speed ratio and rotating mode on dimensionless mixing time

The analysis of the dimensionless mixing time yields two main results: firstly, in contrast with the same performance observed in both rotating modes with Newtonian fluids, the down-pumping mode is more efficient than the up-pumping mode with the shear-thinning fluids regardless of the speed ratio. We can also see this fact directly from the mixing curves in Figure 5.4. Even though the pumping capacity in the down-pumping mode is weaker than in the up-pumping mode with shear-thinning fluid, the hydrodynamic conflict between the two impellers brings more drastic shear for mixing, which is also augments the viscosity difference. The stronger shear and the decreased viscosity overcome the weakness of the pumping and lead to a shorter dimensionless time. Secondly, $R_N = 2$ is a particular case for both rotating modes. At this speed ratio, the down-pumping mode is the most efficient operating condition, where the contribution of pumping from the helical ribbon is the most; while the up-pumping mode is the least efficient one, which is attributed to the last mixed region near the liquid surface. As the speed ratio reaches 4 and above, the speed ratio presents no influence on the dimensionless mixing time.

As a conclusion, from a hydrodynamics perspective, besides the findings of Guntzburger et al. (2013) which demonstrated that the pumping effect of the impeller has great influence on the

performance of the mixing time, we can see from this case that the mixing process (location of the high shear region and the existence of the last mixed region) also plays important role in the evaluation of the mixing performance.

Figure 5.6 shows the influence of the rheological behavior on the dimensionless mixing time. For shear-thinning fluids in early transitional regime ($10 < Re < 70$) where the viscosity effect still exists, the dimensionless mixing time decreases along with the power-law index. As discussed above, the increase of the power-law index has no effect on the pumping capacity in the up-pumping mode and even leads to the decrease of the pumping capacity in the down-pumping mode. Therefore, the decrease of the dimensionless mixing time is attributed to the larger viscosity drop, which is caused by the decrease of the power-law index. The faster viscosity drop speeds up the mixing process in the high shear region and results in the higher efficiency despite the reduced pumping capacity. At $Re > 500$ where the viscosity effect is weak, however, the dimensionless mixing time tends to be a constant value regardless of the power-law index and the rotating mode. In addition, this constant value is also lower in down-pumping mode. Compared with Newtonian fluid, we can see that at $10 < Re < 70$ the dimensionless mixing time with shear-thinning fluid is higher than that with Newtonian fluid in up-pumping mode and lower in down-pumping mode. As a conclusion, the up-pumping mode is good for Newtonian fluid mixing and down-pumping mode is recommended for shear-thinning fluid mixing.

up-pumping mode

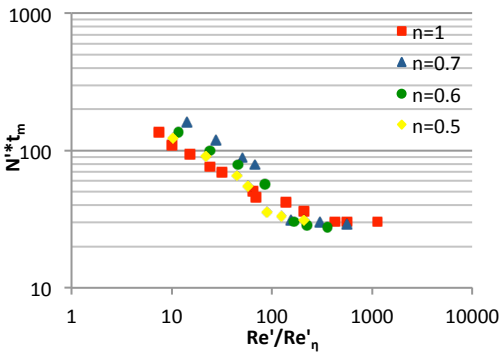

down-pumping mode

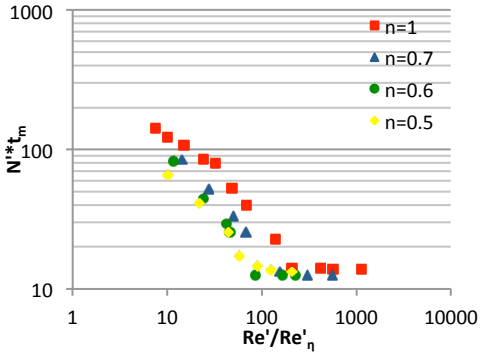

$R_N = 2$

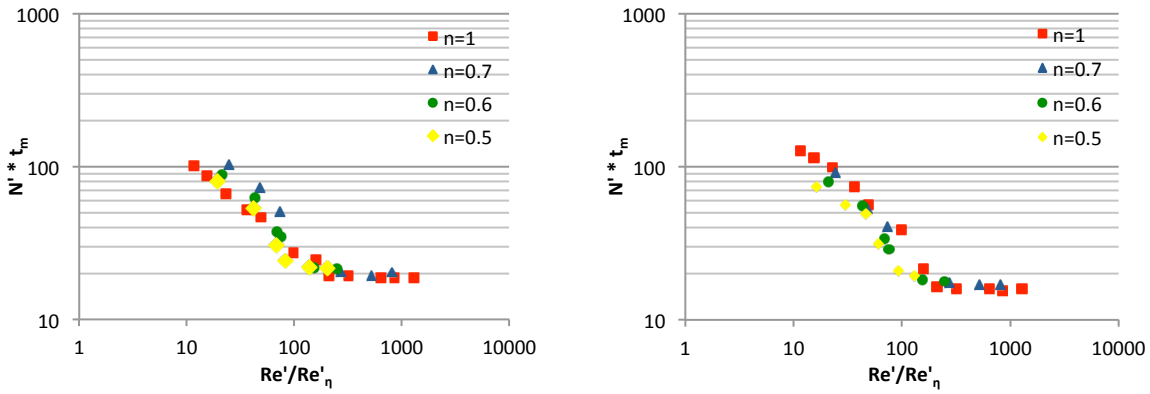

$R_N = 4$

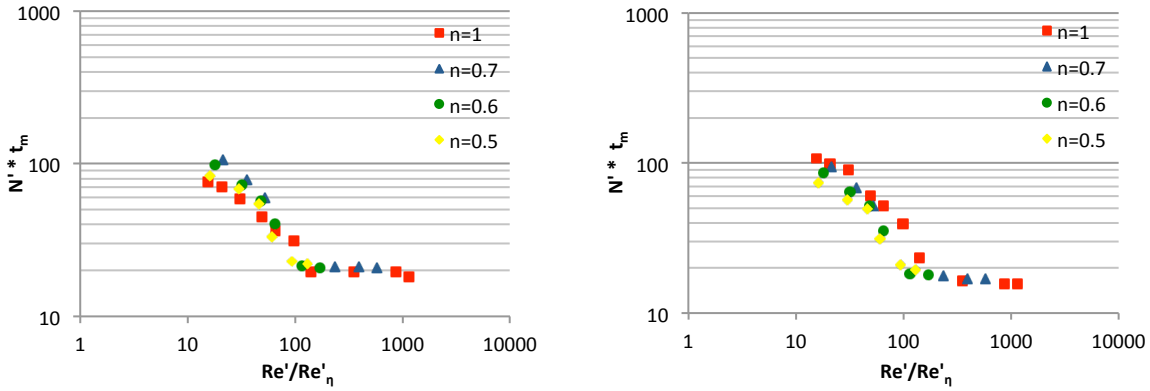

$R_N = 6$

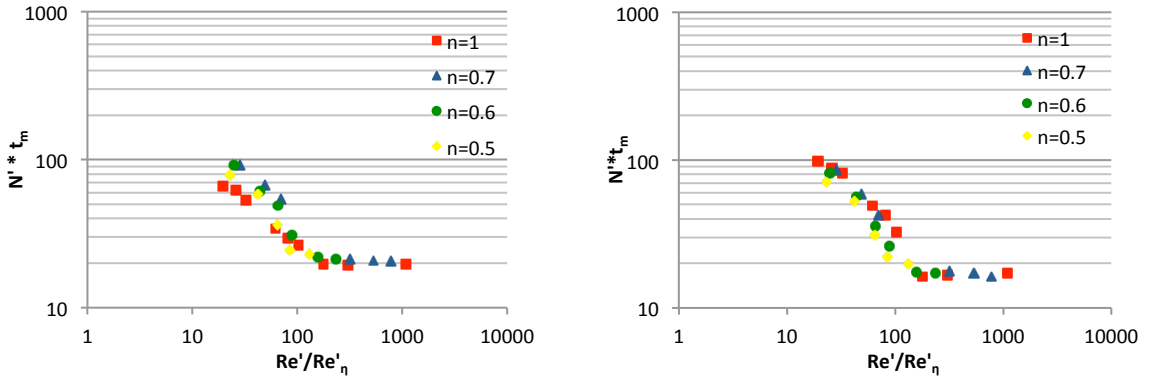

$R_N = 8$

Figure 5.6: Influence of rheological behavior on mixing time

5.5.3 Power Consumption

It can be seen in Figure 5.7 that the power consumption of the Superblend with shear-thinning fluid shows similar results as the ones with Newtonian fluid both in terms of rotating mode and the effect of speed ratio. First, the up-pumping mode is more power-efficient. Second, $R_N = 2$ consumes the most power regardless of rheological behavior and rotating mode in the early transitional regime ($10 < Re < 100$). When the speed ratio reaches or exceeds 4, the speed ratio does not affect the power consumption of the Superblend at all in early transitional regime; however, at $Re > 100$ the power consumption will increase along with the speed ratio. This speed ratio limit is consistent with the mixing time observations.

up-pumping mode

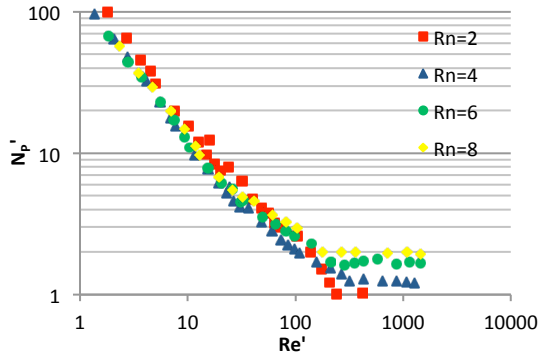

down-pumping mode

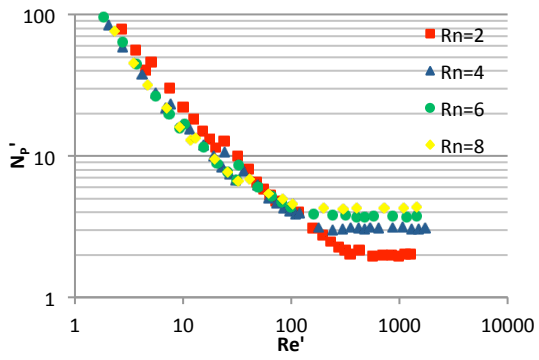

Newtonian fluid

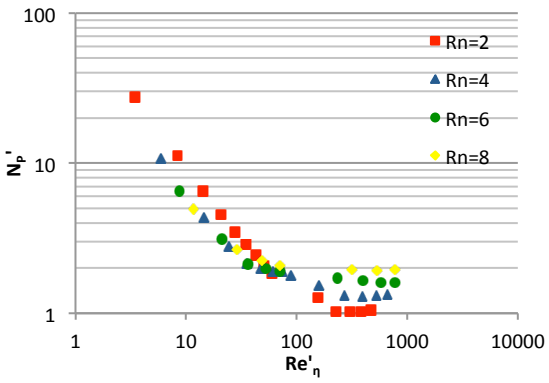

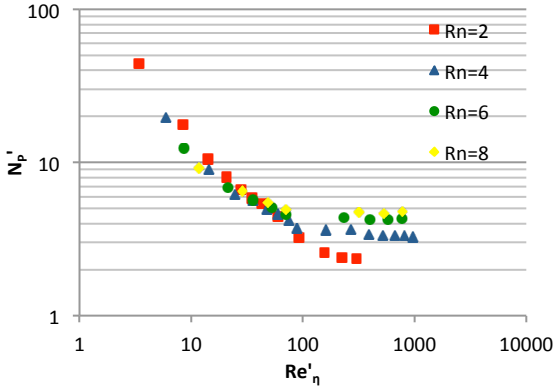

$n = 0.7$

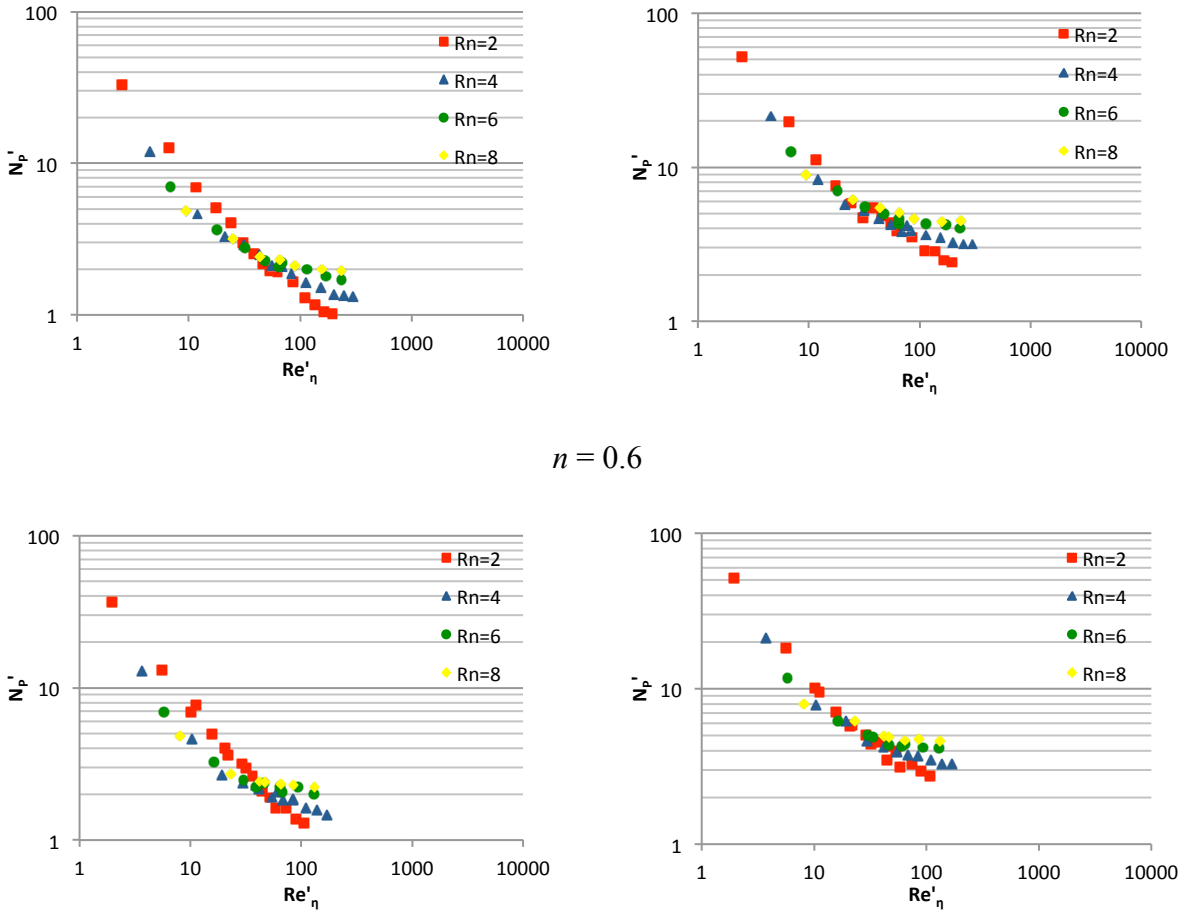

$n = 0.6$

$n = 0.5$

Figure 5.7: Effect of the speed ratio on the power consumption

The torque measurement on each impeller allowed us to calculate the power number of each impeller. As shown in Figure 5.8, the variation of K_P of each impeller with shear-thinning fluid is the same as for the Newtonian fluid. In figure 5.8a, regardless of the rheological behavior, the K_P of the helical ribbon decreases along with the increase of speed ratio in the up-pumping mode and the opposite in the down-pumping mode. The Maxblend impeller has a remarkable impact on the K_P of the helical ribbon. In the up-pumping mode, a higher speed ratio brings more power saving for the helical ribbon due to the fact that they are moving the fluid in the same direction. In the down-pumping mode, however, the higher speed ratio causes more hydrodynamic conflict between the two impellers, which leads to a higher K_P of the helical ribbon. In figure 5.8b, in the up-pumping mode the K_P of the Maxblend impeller increases along with the increase in speed

ratio, which means the helical ribbon also provides a power saving for the Maxblend impeller. The higher the speed ratio, the lower the power saving. When the speed ratio grows up to a certain value, the power saving from the helical ribbon completely vanishes and the K_P of the Maxblend impeller turns to the value of this latter alone. In the down-pumping mode the speed ratio does not affect the K_P of the Maxblend impeller any longer. Comparing the K_P of the Maxblend impeller alone, even though the K_P of the Maxblend impeller slightly increases when the helical ribbon is on regardless of speed ratio, the impact from the helical ribbon on the power consumption of the Maxblend impeller is still very weak. As agreed in the coaxial mixer literature, the high-speed impeller affects the power consumption of the low-speed impeller, while the latter does not have obvious influence on that of the former. In our work, we found the same conclusion in down-pumping mode only. It should be noted that the dimension of the Maxblend impeller in the Superblend mixer is much larger than any other high-speed impellers that have been studied by previous researchers. Therefore, due to the same pumping direction of the Maxblend impeller and the helical ribbon in up-pumping mode, the wall-scraping effect of the helical ribbon saves the power required by Maxblend impeller to move the fluid near the wall at low speed ratio. On the contrary, when it is down-pumping mode, the hydrodynamic conflict from the helical ribbon does not affect the power input of the Maxblend impeller significantly.

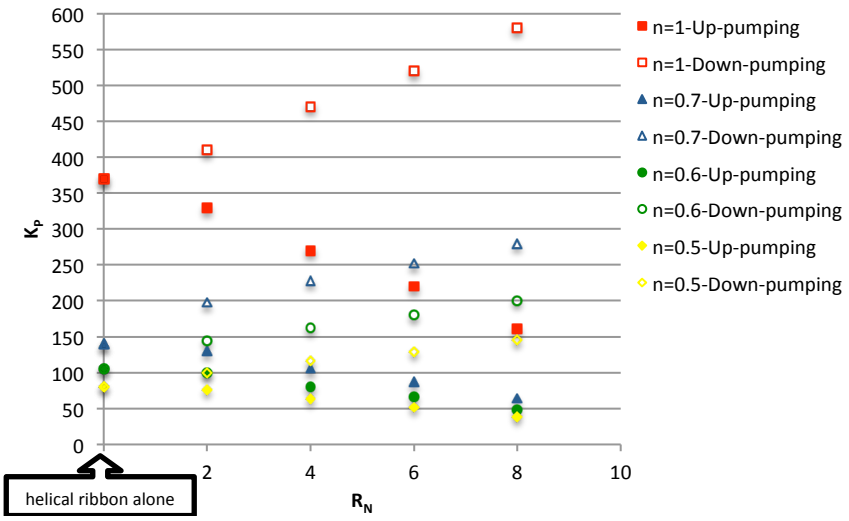

(a) helical ribbon

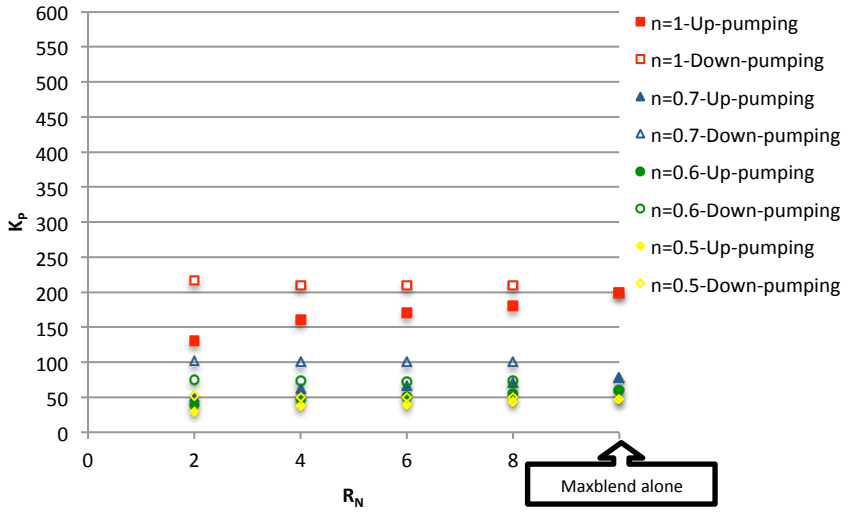

(b) Maxblend

Figure 5.8: The effect of speed ratio, rotating mode and power-law index on K_P

The effect of rheological behavior on the power consumption was also studied. Figure 5.9 and 5.10 show that as n decreases, the less power is needed. The effect of speed ratio on K_P can also be seen again. As a conclusion, the shear-thinning effect by now presents a positive factor in both the performance of the mixing time as well as the power consumption for the down-pumping mode.

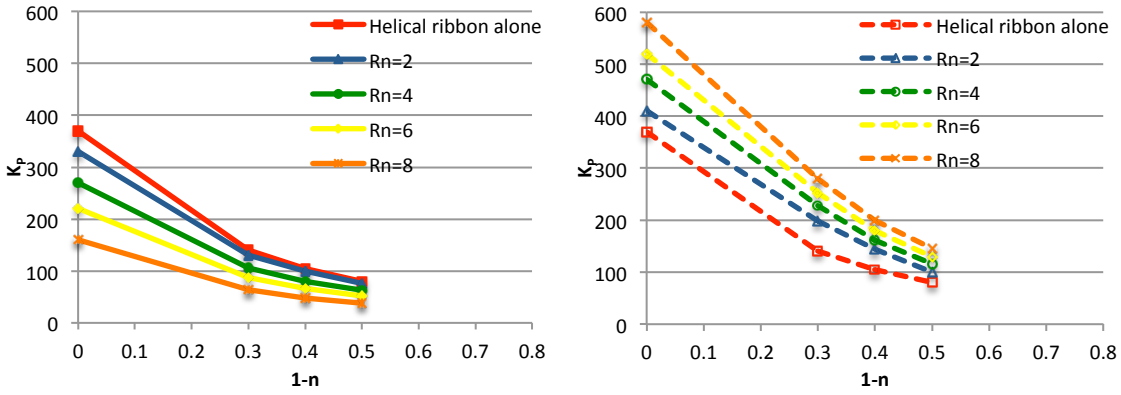

(a) up-Pumping mode (b) down-pumping mode

Figure 5.9: The effect of power-law index on K_P of the helical ribbon

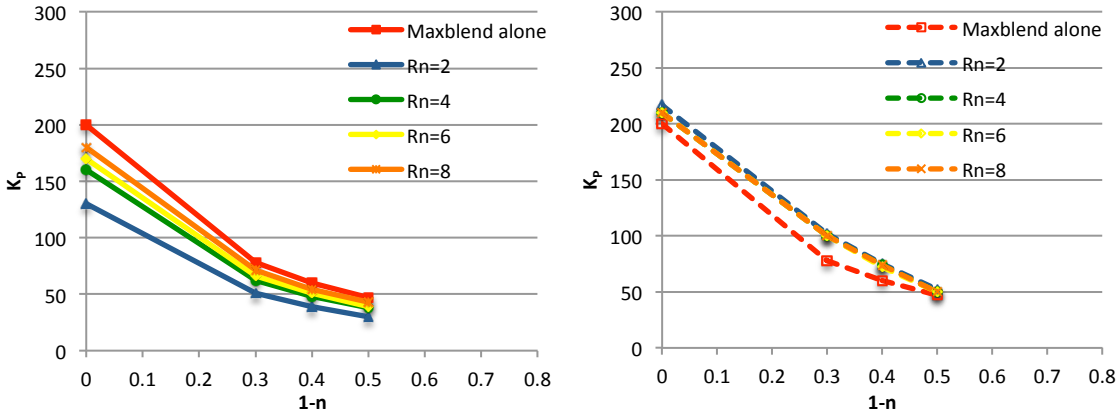

(a) up-Pumping mode (b) down-pumping mode

Figure 5.10: The effect of power-law index on K_P of the Maxblend impeller

Pointing at the effective rate-of-deformation with non-Newtonian fluid, Metzner and Otto (1957) proposed a correlation between average shear rate in mixer and the impeller speed as

$$\dot{\gamma}_{av} = K_S \times N \tag{5.9}$$

where *Ks* is a proportionality parameter Metzner constant. Rieger and Novak (1973) introduced an approach to calculate *Ks* by using power constant measurement in laminar regime as,

$$K_S = \left(\frac{K_P(R_N,n)}{K_P(R_N,n=1)}\right)^{\frac{1}{n-1}} \tag{5.10}$$

Figure 5.11 shows the evaluation of the impact of speed ratio, rotating mode and power-law index on *Ks* of each impeller in Superblend mixer. The first conclusion is that the rotation of one impeller affects the *Ks* of the other. As the Maxblend impeller starts rotating, the *Ks* of the helical ribbon in either mode decreases because of the interference of the flow field caused by the Maxblend impeller. On the other hand, as the helical ribbon starts rotating in up-pumping mode, the resulting interference is too weak to affect the *Ks* of the Maxblend impeller; but in down-pumping mode, the hydrodynamic conflict between impellers reduces the *Ks* of the Maxblend impeller remarkably. However, once two impellers are both on, the speed ratio does not affect *Ks* at all. This indicates the independence of *Ks* of one impeller to another in Superblend when two impellers are working.

As the second conclusion, it is obvious that as the power-law index *n* decreases, the *Ks* drops in the up-pumping mode but increases in the down-pumping mode. At a given impeller speed a lower *n* results in a faster viscosity decrease near the impeller region and a viscosity difference in the tank. In down-pumping mode, the conflict between impellers helps break the difference and the stronger shear-thinning effect makes breaking the difference easier, which leads to a higher *Ks*. In the up-pumping mode, however, since the pumping directions of the two impellers are the same, as the shear-thinning effect gets stronger, the resulting increase of the viscosity difference is able to lower the *Ks* value.

It can also be seen that the *Ks* in the up-pumping mode is always higher than that in the down-pumping mode regardless of rheological behavior. As a matter of fact, different rotating modes in coaxial mixer produce distinct flow fields. To some degree the change of rotating mode is equivalent to the change of geometry of the mixer. Since *Ks* largely depends on the geometry, its variation in different rotating modes is expected.

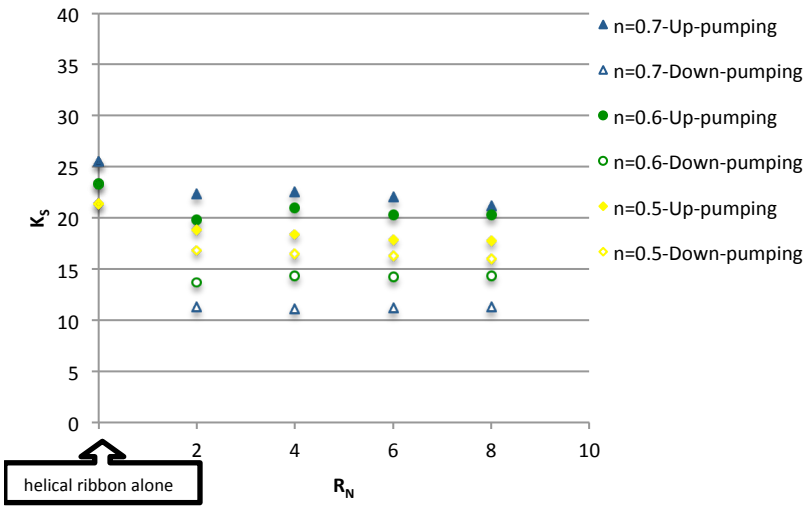

(a) helical ribbon

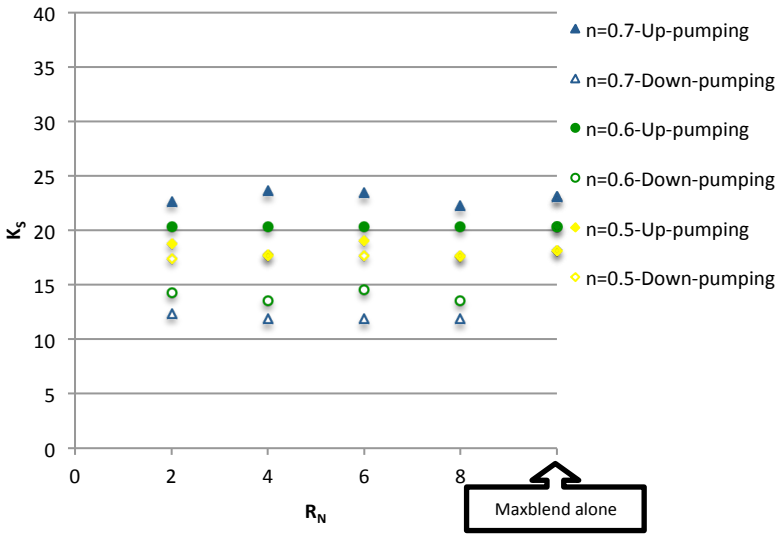

(b) Maxblend

Figure 5.11: The effect of speed ratio, rotating mode and power-law index on K_S

5.5.4 Mixing Energy

In order to assess the mixing performance based on comprehensive consideration of power consumption and mixing time, we extend this investigation to mixing energy. Mixing energy, E_{mix}, combines the performance of mixing time and power consumption together:

$$E_{mix} = N_P' \times N' t_m \tag{5.11}$$

Since the physical meaning of N_P' is the drag index that needed to be overcome in the mixing process and that of $N' t_m$ is the number of revolutions needed to complete the mixing, the mixing energy illustrates the energy required by the mixer system to complete the mixing. Therefore, the mixing energy is a good indicator to assess the mixing performance of Superblend regarding both mixing time and power consumption. The results are shown in Figure 5.12 and 5.13.

As we can see in Figure 5.12, in down-pumping mode, R_N = 2 becomes one of the most efficient conditions for all these fluids due to its high efficiency in mixing time. In contrast, even though R_N = 2 in up-pumping mode is the most power-efficient at Re > 100, the poor performance in mixing time makes it out of the competition of the least mixing energy. Referring to the influence of speed ratio and rotating mode on the mixing energy, it follows the trends in power

consumption of Superblend. Therefore, we can conclude from Figure 12 that in addition to $R_N = 2$ in the down-pumping mode, $R_N = 4$ in the up-pumping mode is also an optimal condition for a wide range of Reynolds number ($10 < Re < 1000$) in terms of mixing energy.

Figure 5.13 demonstrates that in the down-pumping mode the influence of power-law index on the mixing energy is very similar to that on mixing time: the mixing energy with the shear-thinning fluid is lower than the Newtonian fluid at $Re < 100$. In the up-pumping mode, however, the mixing time was lower for the Newtonian fluid at $Re < 100$, but the mixing energy is lower for the shear-thinning fluid. As a conclusion, rheological behavior of the fluid has significant influence on the mixing efficiency, and the shear-thinning fluid mixing in Superblend mixer exhibits its outstanding efficiency in both rotating modes in terms of mixing energy.

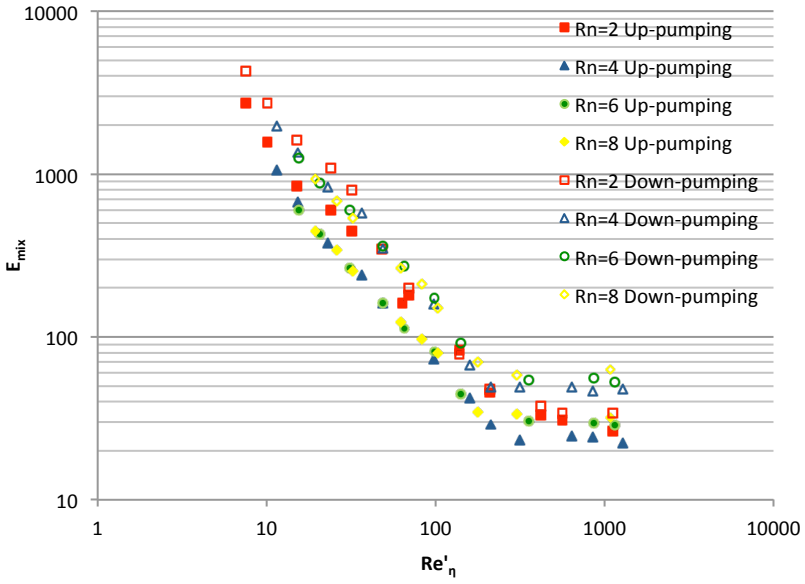

$n = 1$

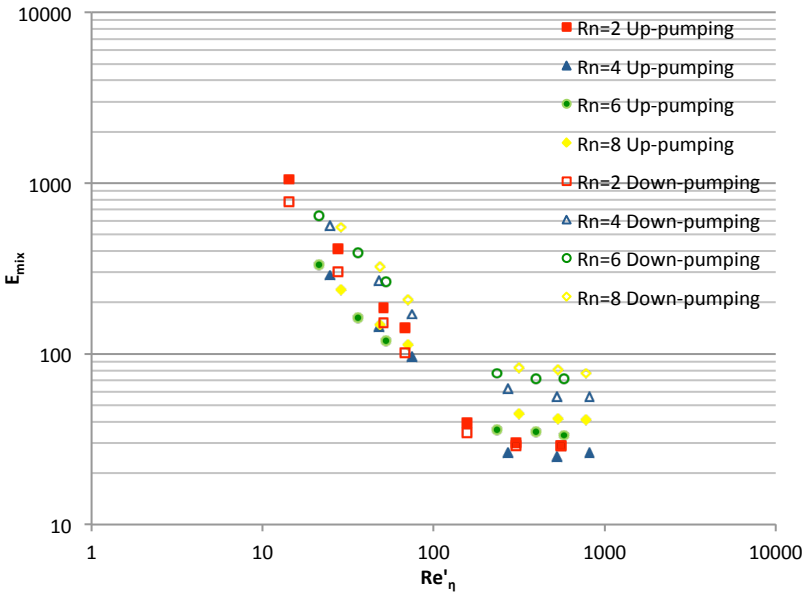
10000
1000
100
10
1
10
100
1000
10000
E_{mix}
Re'_{η}
Rn=2 Up-pumping
Rn=4 Up-pumping
Rn=6 Up-pumping
Rn=8 Up-pumping
Rn=2 Down-pumping
Rn=4 Down-pumping
Rn=6 Down-pumping
Rn=8 Down-pumping

$n = 0.7$

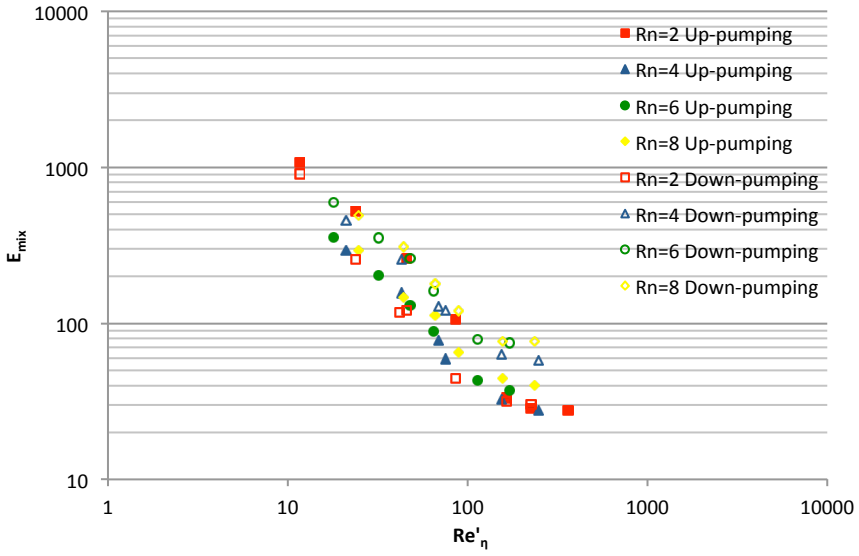
10000
1000
100
10
1
10
100
1000
10000
E_{mix}
Re'_{η}
Rn=2 Up-pumping
Rn=4 Up-pumping
Rn=6 Up-pumping
Rn=8 Up-pumping
Rn=2 Down-pumping
Rn=4 Down-pumping
Rn=6 Down-pumping
Rn=8 Down-pumping

$n = 0.6$

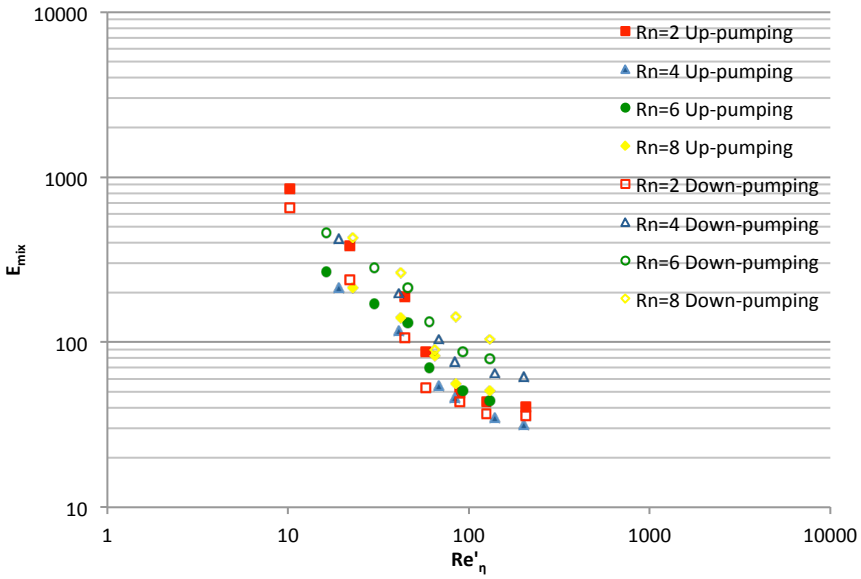

$n = 0.5$

Figure 5.12: Influence of speed ratio and rotating mode on mixing energy

up-pumping mode

down-pumping mode

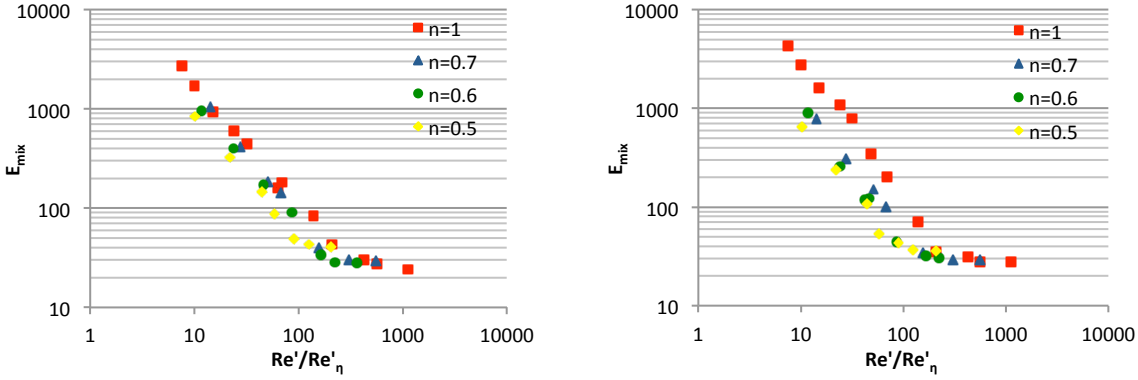

$R_N = 2$

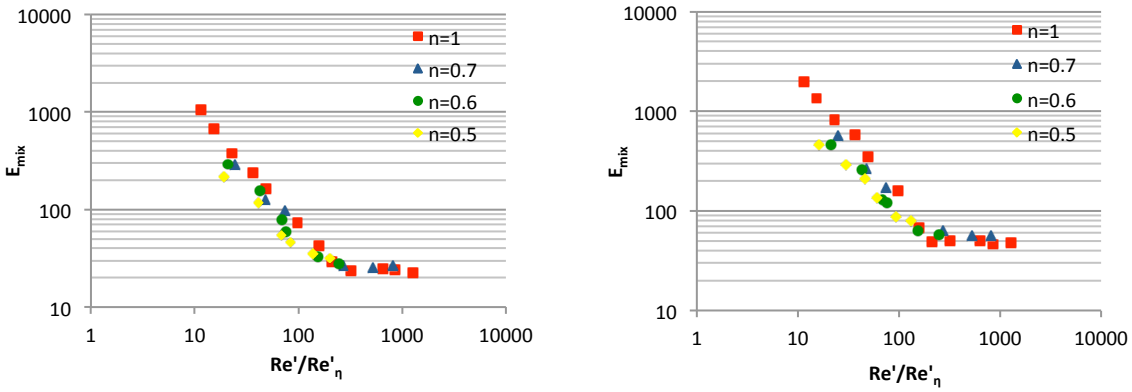

$R_N = 4$

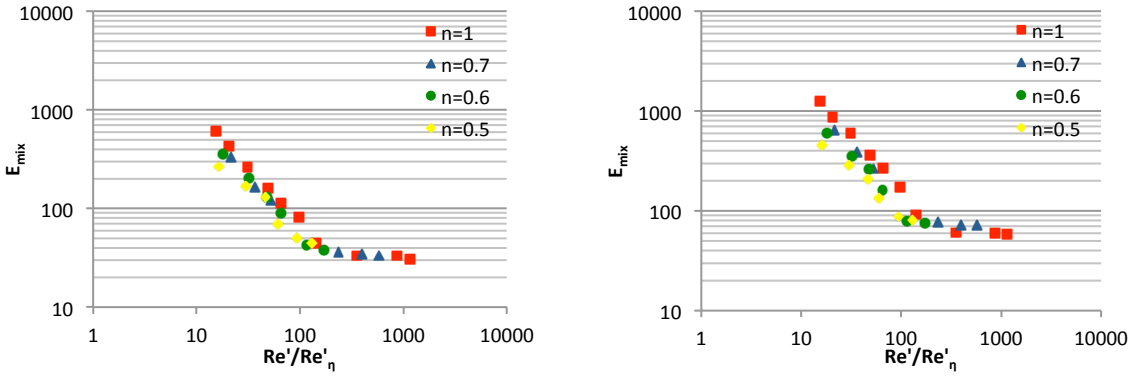

$R_N = 6$

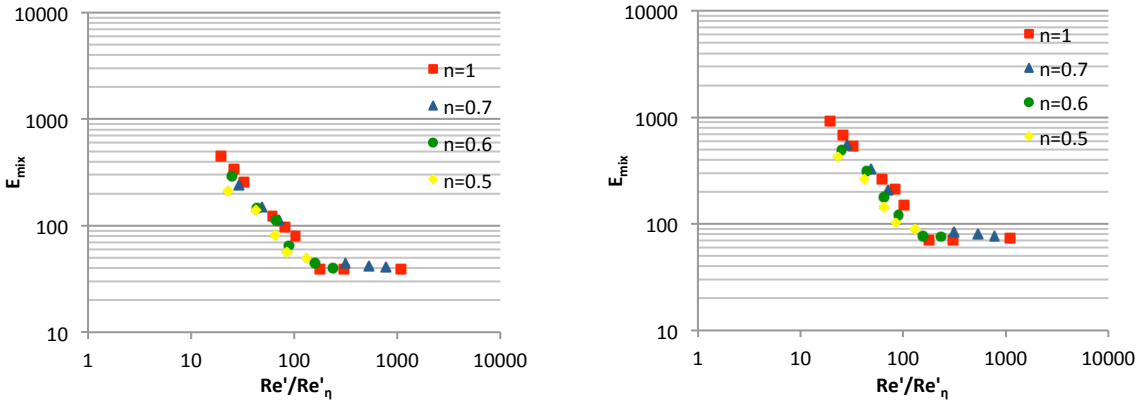

$R_N = 8$

Figure 5.13: Influence of rheological behavior on mixing energy

5.6 Conclusion

A thorough investigation of the mixing performance of the Superblend coaxial mixer with both Newtonian and non-Newtonian fluids was carried out in this work. Taking advantage of the decolorization-image-processing technique, the mixing efficiency in the tank was not only qualitatively but also quantitatively characterized in terms of mixing evolution and macro mixing time. The results illustrate that the rheological behavior of the fluid and the operating parameters of the Superblend have significant influences on the mixing evolution and mixing time, the power consumption of the Superblend mixer, and the power constant and Metzner-otto constant of each impeller. Among all the contributors, the hydrodynamic conflict between the flow patterns generated by the two impellers in the down-pumping mode and the shear-thinning effect are the most critical factors. Finally a comprehensive evaluation of the mixing performance of the Superblend mixer was discussed from the perspective of the mixing energy. Based on the comparison of the mixing energy, it is proven that the mixing efficiency of the Superblend mixer with shear-thinning fluid outperforms that with Newtonian fluid, and R_N = 2 in the down-pumping mode and R_N = 4 in the up-pumping mode are proposed as the optimal operating conditions for both Newtonian and non-Newtonian fluids in a wide range of Reynolds numbers (10<Re<1000).

5.7 Acknowledgement

The support of NSERC and the research consortium on Non-Newtonian Innovative Mixing Technologies is gratefully acknowledged.

5.8 Reference

BAO, Y., YANG, B., XIE, Y., GAO, Z., ZHANG, Z., LIU, T. and Gao, X. (2011). Power demand and mixing performance of coaxial mixers in non-Newtonian fluids. *J. Chem. Eng. Jpn.*, 44, 57-66.

BRITO-DE LA FUENTE, E., CHOPLIN, L. and TANGUY P. A. (1997). Mixing with helical ribbon impellers: Effect of highly shear thinning behavior and impeller geometry. *Chem. Eng. Res. Des.*, 75, 45-52.

CABARET, F., BONNOT, S., FRADETTE, L. and TANGUY, P. A. (2007). Mixing Time Analysis Using Colorimetric Methods and Image Processing. *Ind. Eng. Chem. Res.*, 46(14), 5032-5042.

FARHAT, M., FRADETTE, L. and TANGUY, P. A. (2008). Revisiting the performance of a coaxial mixer. *Ind. Eng. Chem. Res.*, 47(10), 3562-3567.

FARHAT, M., FRADETTE, L., HORIGUCHI, H., YATOMI, R. and TANGUY, P. A. (2009). Experimental Investigation of Superblend Coaxial Mixer. *J. Chem. Eng. Jpn.*, 42(11), 797-803.

FOUCAULT, S., ASCANIO, G. and TANGUY, P. A. (2004). Coaxial mixer hydrodynamics with Newtonian and Non-Newtonian fluids. *Chem. Eng. Technol.*, 27(3), 324-329.

FOUCAULT, S., ASCANIO, G. and TANGUY, P. A. (2005). Power characteristics in coaxial mixing: Newtonian and Non-Newtonian fluids. *Ind. Eng. Chem. Res.*, 44, 5036-5043.

FOUCAULT, S., ASCANIO, G. and TANGUY, P. A. (2006). Mixing times in coaxial mixers with Newtonian and non-Newtonian fluids. *Ind. Eng. Chem. Res.*, 45(1), 352-359.

FRADETTE, L., THOME, G., TANGUY, P. A. and TAKENAKA, K. (2007). Power and Mixing Time Study Involving A Maxblend Impeller with Viscous Newtonian and Non-Newtonian Fluids. *Chem. Eng. Res. Des.*, 85(A11), 1514-1523.

GUNTZBURGER, Y., FONTAINE, A., FRADETTE, L. and BERTRAND, F. (2013). An experimental method to evaluate global pumping in a mixing system: Application to the Maxblend™ for Newtonian and non-Newtonian fluids. *Chemical Engineering Journal*, 214, 394-406.

KHOPKAR, A., FRADETTE, L. and TANGUY, P. A. (2007). Hydrodynamics of a dual shaft mixer with Newtonian and non-Newtonian fluids. *Chem. Eng. Res. Des.*, *85*, 863-871.

KURATSU, M., NISHIMI, H., YATOMI, R., SATO, H. and MISHIMA, M. (1994). Mixing Reactor “Superblend” applied to wide range of viscosity. *Sumitomo Heavy Industries Technical Review.*, *42* (124), 82-85.

KURATSU, M., YATOMI, R. and SATO, H. (1995). Design of versatile reactors. *Chem. Equipment.*, 8, 86-92.

METZNER, A. B. and OTTO, R. E. (1957). Agitation of non-Newtonian fluids. *AIChE J.*, 3(1), 3-10.

PAUL, E. L., ATIEMO-OBENG, V. A., KRESTA, S. M. (2004). Handbook of industrial Mixing: Science and Practice. John Wiley & Sons, Inc., Hoboken, New Jersey.

RIEGER, F. and NOVAK, V. (1973). Power consumption of agitators in highly viscous non-Newtonian liquids. *Trans. IChemE.*, 51, 105-111.

RIVERA, C., FOUCAULT, S., HENICHE, M., ESPINOSA-SOLARES, T. and TANGUY, P.A. (2006). Mixing Analysis in a Coaxial Mixer. *Chem Eng Sci*., 61(9), 2895–2907.

TANGUY, P. A., THIBAULT, F., BRITO-DE LA FUENTE, E., ESPINOSA-SOLARES, T. and TECANTE, A. (1997). Mixing performance induced by coaxial flat blade-helical ribbon impellers rotating at different speeds. *Chem. Eng. Sci.*, 52(11), 1733-1741.

TANGUY, P. A. and THIBAULT, F. (2002). Power consumption in the turbulent regime for a coaxial mixer. *Can. J. Chem. Eng.*, 80(4), 601-603.

THIBAULT, F. and TANGUY, P. A. (2002). Power-draw analysis of coaxial mixer with Newtonian and non Newtonian fluids in the laminar regime. *Chem. Eng. Sci.*, 57, 3861-3872.

WANG, X., FRADETTE, L., TAKENAKA, K. and TANGUY, P. A. (2012). Effect of operating parameters on the mixing performance of the Superblend coaxial mixer. *Ind. Eng. Chem. Res.*, *51* (4), 1826-1833.

CHAPTER 6: ARTICLE 4: SOLIDS DISTRIBUTION IN A SUPERBLEND COAXIAL MIXER USING ELECTRICAL RESISTANCE TOMOGRAPHY CHARACTERIZATION

Article history: Submitted March 24, 2014, Chemical Engineering Journal

Authors: Xiao Wang, Inci Ayranci, Louis Fradette and Philippe A. Tanguy

6.1 Abstract

An experimental investigation on the solids distribution in a Superblend coaxial mixer with viscous Newtonian continuous phase was conducted. The homogenization speed (N_H) was introduced as the critical speed to reach homogeneity in solids distribution. A quantitative measurement of the homogenization speed and mixing time by means of electrical resistance tomography (ERT) was developed to characterize the mixing performance. Results indicate that the particle size and concentration, the speed of the helical ribbon, the rotating mode of the Superblend mixer and the viscosity of the continuous liquid have significant influence on the homogenization speed and the mixing time. Based on the comprehensive consideration of both mixing time and power consumption, the optimal operating conditions for homogeneous solids distribution are discussed.

6.2 Introduction

Solid liquid mixing is widely used in chemical processes such as crystallization, dissolution and leaching, adsorption and solid-catalyzed reactions, to name a few. The objective for these operations is to maximize the mass transfer between solid and the liquid. There are two conditions to accomplish this objective: utilization of the entire surface area offered by the solid and uniform distribution of the solids throughout the processing volume. The entire surface area of the solid can be used when the vessel is operated under complete off-bottom suspension

conditions. Since this has a significant importance for most process designs, numerous stirred tanks with various agitators have been designed and studied by researchers throughout the world for decades. Uniform distribution becomes very important for processes such as crystallization or catalytic reactions and for the production of some formulated products. Above 10 wt% solids concentrations a clear liquid layer may appear in the top part of the vessel, and the mixing time in that clear liquid volume can be 20 times longer than in the lower parts of the vessel (Bujalski et al., 1999). If this were to happen in a catalytic reaction system, important yield losses and unnecessary costs are inevitable. In crystallization, high saturation in certain parts of the vessel can cause poor results in crystal growth and final crystal shape and size. While these operations can be in low or high viscosity fluids, there are some operations that require a uniform solids distribution in high viscosity fluids. Production of toothpaste, gum, and putties are some examples of such processes. There are no studies in the literature that deal with solids distribution in viscous liquids. Solids distribution in high viscosity liquids is the focus of this article.

The conventional techniques for determining the solids distribution in a vessel are sampling, optical or electrical attenuation techniques. These techniques all have some drawbacks. In the sampling method only local measurements are made. Many samples in several locations must be taken to build the solids distribution on a plane or in axial direction. A sample that represents the local conditions at the sampling point is very difficult to obtain and repeat (Brown et al., 2004). Also, some part of the slurry is lost with each sample which can eventually reduce the amount of slurry in the tank and affect the results. The optical and electrical attenuation techniques are also limited in terms of the location of the measurements. These techniques provide the solids concentration data on a line across the vessel diameter, not for the entire plane (Barar Pour et al., 2007; Fajner et al., 1985; Ochieng et al., 2006). This does not allow for a representative measurement of degree of homogeneity in the tank. These drawbacks have been overcome by electrical resistance tomography (ERT). ERT is a non-intrusive technique, and the primary advantage of this technique is online signal capture and analysis and visualization on a whole plane without interfering with the flow field (Holden et al., 1998; Wang et al., 2000). Despite seminal work almost 20 years ago on solid-liquid applications (Mann et al, 1997), ERT has started to be really applied to solids distribution in stirred tanks recently, and the effect of geometrical and particle related parameters on the homogeneity of the slurries with Newtonian

fluids (water) was studied (Hosseini et al., 2010 and Tahvildarian et al., 2011). Hosseini et al. (2010) and Tahvildarian et al. (2011) concluded that homogeneity increases as the impeller speed is increased; however, further increases on the impeller speed above the homogenization speed is detrimental to the homogeneity; higher impeller speeds are required for larger particle diameters compared to smaller particles.

The presence of solids might have an effect on the mixing time which is an important parameter in defining the mixing efficiency. The general findings in the literature about the effect of presence of solids on the mixing time indicate an increase with increasing solids concentration. Raghav Rao and Joshi (1998) and Kraume (1992) stated that the mixing time increases with the addition of solids even at low solids concentrations, but Bujalski et al. (1999) and Micheletti et al. (2003) argued that the mixing time is not affected until high concentrations of solids (~10 wt%). It should be noted that both the ERT and the mixing time studies are limited low viscosity Newtonian fluids, and we expect very different results with high viscosity media.

In this work, electrical resistance tomography is utilized to quantitatively measure and analyze the solids distribution in viscous fluid in Superblend coaxial mixer. The Superblend mixer combines a helical ribbon and a Maxblend impeller. It has been reported by many researchers (Kuratsu et al., 1994, Farhat et al., 2009 and Wang et al., 2012) as a powerful technology for high viscosity fluid mixing. Aiming at exploring the application potential of the Superblend mixer at distributing solids in viscous liquids, a series of investigations on the influence of the particle size and concentration, the viscosity of the fluid, and the operating conditions of the coaxial mixer on the solids distribution were carried out.

6.3 Experimental methods

As shown in Figure 6.1, the Superblend mixer used in this study is composed of a transparent cylindrical tank with a diameter of $T = 0.38$ m with a conical bottom, and a combination of a helical ribbon ($D_{helical\ ribbon} = 0.36$ m, $D_{helical\ ribbon} / T = 0.95$) and a Maxblend impeller ($D_{Maxblend} = 0.2$ m, $D_{Maxblend} / T = 0.53$). The low-speed helical ribbon provides wall-scraping and pumping effects, while the high-speed Maxblend performs as a disperser and a pumping element. The volume of the solid-liquid mixture is kept constant as 40 L.

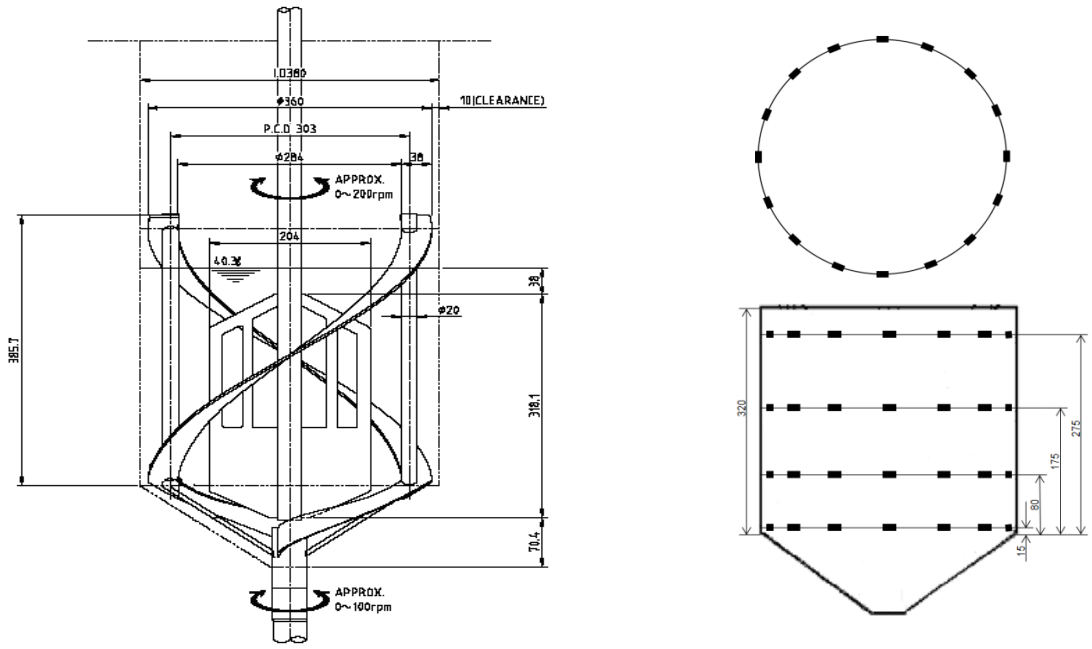

Figure 6.1: Superblend mixer and installation of electrodes

Coaxial mixers are different from single impeller mixers because of the synergistic or antagonistic effects of the impellers. Apart from the rotational speed, two specific parameters must be considered in a coaxial mixer namely the speed ratio between the impellers (in this work, we use the speed ratio of the inner impeller to the outer impeller $R_N = N_i / N_o$) and the rotating mode, i.e. clockwise or counter-clockwise. In the Superblend mixer, the rotation direction of the Maxblend impeller has no influence on the flow field it generates, the same direction of rotation is therefore applied for all the experiments. The definition of the rotating mode is based on the pumping direction generated by the helical ribbon: up-pumping mode when the helical ribbon rotates in the same direction as the Maxblend impeller and down-pumping mode when it rotates in opposition to the Maxblend impeller. In the up-pumping mode the impellers provide the same pumping pattern: upward flow near the wall and downward flow in the central part of the tank. In the down-pumping mode the helical ribbon produces a downwards flow near the wall and an upwards flow in the central part of the tank which counters the flow produced by the Maxblend impeller. Experimental work by Wang et al. (2012) has thoroughly described and analyzed this

pumping conflict and proved that the flow produced by helical ribbon eventually overwhelm the flow produced by the Maxblend impeller.

The properties of the particles and liquids are listed in Table 1. Spherical glass beads of 75 μm and 500μm at three solids concentrations - 10, 20 and 30 wt% - were used in the experiments. Glucose solutions with viscosities of 0.1Pa.s and 4 Pa.s were prepared and used as low viscosity and high viscosity liquids. All the viscosity measurements were taken with a Bohlin rheometer.

Particles smaller than 75 μm could not be used because of the impractical settling times (several days) with the viscosities tested. The viscosities also had to be adjusted based on the settling time of the particles. Since all the particles must completely settle on the bottom of the tank before each experiment, a reasonable settling time is necessary. The settling time of the particles was tested experimentally. For the particles of 500 μm, the settling time in the highly viscous liquid is not acceptable until the viscosity is reduced to 4 Pa.s, where complete settling takes eight hours at 30 wt%. For the particles of 75 μm, however, they cannot settle out in one day in 4 Pa.s liquid. An acceptable settling time is obtained when the viscosity is reduced to 0.1 Pa.s (eight hours at 30 wt%). Comparing the practical settling times and the estimated ones shown in Table 6.1, their consistency validates the applicability of Richardson-Zaki correlation (Richardson and Zaki, 1954) in the studied cases.

Table 6.1: Properties of solid and liquid

Material	Density (kg/m^3)	Size (μm)	Liquid Viscosity (Pa.s)	Liquid Density (kg/m^3)	Hindered settling velocity Vø* (m/hour) 30 wt% - 10 wt%	Estimated settling time** (hour) 30 wt% - 10 wt%
Spherical glass beads	2500	75	0.1	1200	0.057 - 0.113	7.7 - 3.9
			4	1300	0.0014 - 0.0026	310 - 170
		500	0.1	1200	2.5 - 5	0.2 - 0.1
			4	1300	0.059 - 0.116	7.5 - 3.8

*Calculated using Richardson-Zaki correlation (Richardson and Zaki, 1954)

**Settling distance (liquid height) is 0.44 m

Using the torque meter mounted on each shaft, the power consumption of each impeller and total power consumption of the Superblend mixer can be calculated using

$$P = 2\pi N M_c \tag{6.1}$$

$$P_{Superblend} = P_{Maxblend} + P_{helical\ ribbon} \tag{6.2}$$

where N is the rotational speed of the impeller in 1/s, and M_c the corrected torque in N·m. The torque measurement is corrected by subtracting the residual torque, which is caused by all the other contributors but the working material in the system. The residual torque is obtained by measuring the torque in empty tank at the studied speeds.

Homogenization speed N_H and mixing time t_H were evaluated by means of the ERT technique. The just suspended speed (N_{js}) is the most common parameter for complete off-bottom suspension in conventional mixers. It is defined as the impeller speed at which there are no particles remaining stationary at the bottom of the tank for more than one or two seconds (Zwietering, 1958). The N_{js} and complete off-bottom suspension can hardly be studied in the Superblend mixer because the off-bottom clearance of the helical ribbon is very small and acts like a bottom scraper for particles. Once the Superblend begins to rotate (even at N~0) the particles can easily move at the bottom without being suspended. The Zwietering criterion is not applicable in this geometry. Therefore, the Homogenization Speed N_H was proposed as an indicator of the uniform suspension. N_H is defined as the speed of the Maxblend impeller, $N_{Maxblend}$, required for the slurry to reach a homogeneous status at a given speed of the helical ribbon, $N_{helical\ ribbon}$. In this work, three $N_{helical\ ribbon}$ were studied: 10 rpm, 20 rpm and 30 rpm. The t_H is the time required to reach the homogeneous status at N_H.

The calculation of the Reynolds number of the liquid Re_{liquid} is based on the definition proposed by Farhat et al. (2008)

$$Re_{liquid} = \frac{\rho_{liquid} N' D^2_{Maxblend}}{\mu_{liquid}} \tag{6.3}$$

$$N' = \frac{N_{helical\ ribbon} \times D_{helical\ ribbon} + N_{Maxblend} \times D_{Maxblend}}{D_{Maxblend}} \tag{6.4}$$

The Reynolds numbers studied in this work correspond to early or late transitional regime.

The use of ERT allows visualization of multiphase flows based on the measurement of voltages at the periphery of a horizontal plane. As shown in Figure 6.1, 16 electrodes are uniformly placed around the tank, and all the electrodes are connected to a data acquisition system included in the ITS tomography P-2000 (Industrial Tomography Systems Plc, UK). A single ground electrode is installed at a short distance from the measurement electrodes to supply a common ground source. In order to monitor the distribution status of the particles throughout the tank, four planes of electrodes were installed at different vertical positions. The ITS system injects a current of 75 mA at a frequency of 4800 hz between a pair of adjacent electrodes and collects the voltage difference between other adjacent electrode pairs. The parameters including the current input and the frequency are optimized aiming at attaining the optimum signal-to-noise ratio. In order to enhance the signal-to-noise ratio by enlarging the conductivity gap between the non-conductive particles and continuous media, saturated NaCl solution was added and the electrical conductivity of the liquid was set around 600 μs/cm (Giguere et al., 2009). The particle diameters tested are large enough that the formation of agglomerates due to the presence of salt can be neglected. A single measurement contains 104 independent voltage measurements. The system then converts the voltage feedback to the tomograms of conductivity and solids concentration by utilizing a Linear Back Projection (LBP) image reconstruction algorithm. This algorithm is the simplest image reconstruction technique and is widely used in electrical tomography. The LBP algorithm provides fast processing time and allows for the realization of online monitoring and imaging of the multiphase flows. The drawback is that it provides a qualitative information. More advanced algorithms can be used to improve both the resolution and the quantitative capacity of the systems such as a generalized iterative algorithm (Giguere et al., 2008). This algorithm is however not implemented in the software and was not used in this work. With the purpose of characterizing the quantitative variation of the solids distribution, the resistivity analysis across the measurement planes was used. As the raw data, the average resistivity ρ is calculated with

$$R = \frac{V}{I} \tag{6.5}$$

$$\rho = \frac{R}{K} \tag{6.6}$$

where R is the resistance in Ω, V the averaged voltage in V, I the current input in A, K the geometrical parameter in 1/m. K is correlated with the geometries of the electrodes and the stirred tank.

Figure 6.2a shows the response of the resistivity on the homogeneity status of the particles on one plane. This is a representative graph for all four planes and all experimental conditions as the trend of the evolution of N_H measurements is similar in all cases. Once the impellers start rotating, some settled particles become suspended, and the amount of particles reaching the superior planes increases. Because the particles are non-conductive, the level of resistivity on each plane raises until a stable distribution is achieved. However, if the speed of the helical ribbon is fixed and the speed of Maxblend is increased, the particles will be redistributed and the resistivity on each plane will increase. When the speed of the Maxblend reaches a critical value, the resistivity ceases from increasing and keeps constant, despite further increases on the speed of the Maxblend. This critical speed is called the homogenization speed, N_H. Once the N_H is determined, the impellers are stopped to allow for the particles to settle out on the bottom. Then a new experiment is started at the pre-determined N_H to find the mixing time, t_H. Figure 6.2b shows the actual data that gives the curve of the resistivity evolution at N_H over time. The time at which the resistivity remains constant is called the t_H. The trend of the curve on this figure is specifically for the conditions investigated. The trend may vary for other cases, but the method to determine the t_H remains the same.

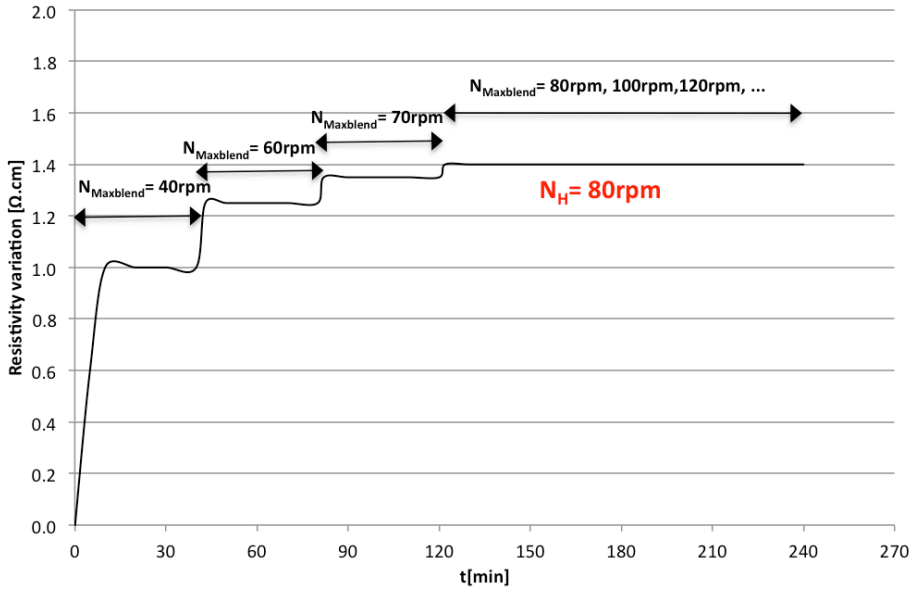

(a)

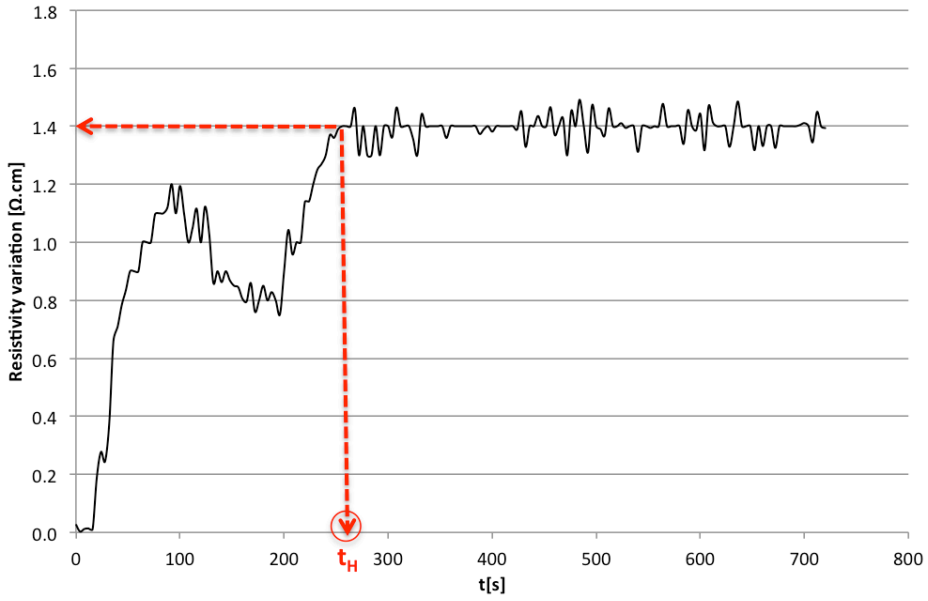

(b)

Figure 6.2: Resistivity evolution measured by ERT with 20 wt% particles of 500 µm in the liquid of 0.1Pa.s at $N_{helical\ ribbon}$ = 20 rpm: (a) response on the variation of solids distribution; (b) determination of t_H

6.4. Results and discussion

6.4.1 Homogenization speed

In this section first the distribution of 500 µm particles in 4 Pa.s and 0.1 Pa.s liquids, and then 75 µm particles in 0.1 Pa.s liquid will be given. This will be followed by the comparisons of the distribution of 500 µm particles in 4 and 0.1 Pa.s liquids and the two sizes of particles in 0.1 Pa.s liquid.

6.4.1.1 Distribution of 500 µm particles in 4 Pa.s liquid

With the 4 Pa.s viscosity liquid, the flow lies in the early transitional regime (Re_{liquid} = 17 - 33 at the studied speeds) where the viscosity factor plays an important role in the hydrodynamics. The coarse particles closely follow the orderly liquid flow without random movement and settling ($V\emptyset$ = 0.059 - 0.116 m/hour). As shown in Figure 6.3, in the up-pumping mode $N_{helical\ ribbon}$ has no impact on N_H for all solids concentrations. In the up-pumping mode although the higher $N_{helical\ ribbon}$ brings more pumping to the system, it does not produce shearing and dispersing effect or enhance the shearing and dispersing capacities of the Maxblend impeller. This is an evidence of the critical importance of the shearing and dispersing capacities of the Maxblend impeller for solids distribution, while the helical ribbon maintains the flow near the wall. In the down-pumping mode, however, N_H decreases as the speed of the helical ribbon increases. In this mode, the upward flow in the central part of the tank produced by the helical ribbon lifts the particles from the bulk flow and enhances the motion of the particles at the upper part of the tank. The advantage of the upward flow on the homogeneous solids distribution has been reported previously (Tahvildarian et al., 2011; Ozcan-Taskin et al., 2003). Besides, the hydrodynamic conflict with the Maxblend impeller enables the helical ribbon to shear the slurry and disperse the particles. The increase of $N_{helical\ ribbon}$ enhances the pumping, shearing and dispersing capacities of the Superblend mixer, and therefore reduces the required $N_{Maxblend}$ (or N_H).

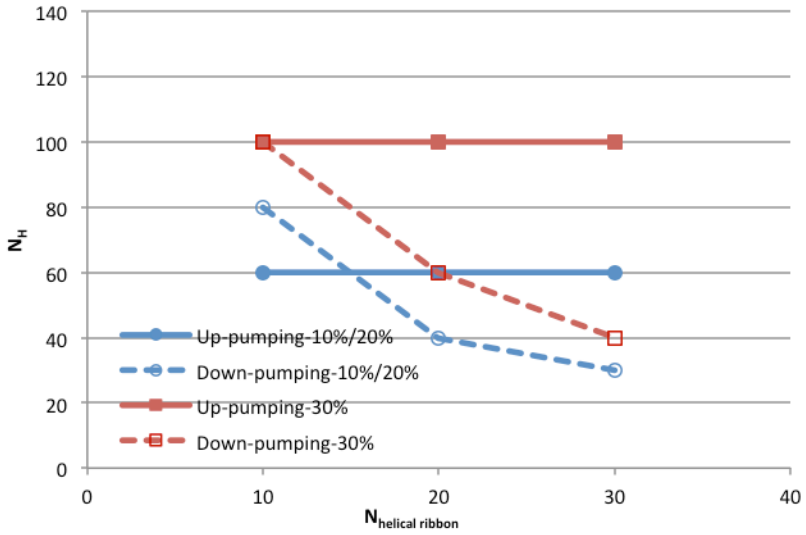

Figure 6.3: Effects of solids concentration, rotating mode, and the speed of the helical ribbon on the homogenization speed for 500 μm particles in 4 Pa.s liquid

The effect of the rotating mode on N_H is strongly conditioned by the speed of the helical ribbon. When $N_{helical\ ribbon}$ is at 10 rpm in the down-pumping mode, the upward flow produced by the helical ribbon and the shearing and dispersing capacities of the Maxblend impeller are all weakened due to the hydrodynamic conflict between the two impellers. As a result, the advantage of the upward flow does not exist and an equal or higher N_H is required in the down-pumping mode than in the up-pumping mode. When $N_{helical\ ribbon}$ is above 20 rpm in the down-pumping mode, however, both the upward flow produced by the helical ribbon and the hydrodynamic conflict with the Maxblend are enhanced, which considerably promote the solids distribution. Consequently, a lower N_H is required in the down-pumping mode than in the up-pumping mode.

The solids concentration has no influence on N_H in both rotating modes until it rises up to 30 wt%. When the solids concentration is low (20 wt% or below), even though the number of the particles and the apparent viscosity and density of the mixture increase along with the solids concentration, the pumping and dispersing capacities of the impellers are sufficient to accomplish the homogeneous solids distribution (Atiemo-Obeng et al., 2004). But when the solids concentration reaches a critical value of 30 wt%, the pumping and dispersing capacities of the impellers are not sufficient and higher N_H is required to achieve homogeneous solids distribution.

6.4.1.2 Distribution of 500µm particles in 0.1Pa.s liquid

When the viscosity of the liquid is decreased to 0.1 Pa.s the liquid flow lies in the late transitional regime (Farhat et al., 2009; Wang et al., 2012) (Re_{liquid} = 784 - 1232 at studied speeds). In this flow regime, the influence of the viscosity factor on the hydrodynamics is weakened, and the unsteady vortices and momentum convection start appearing on different scales. The coarse particles follow a random pattern with a hindered settling velocity of 2.5 - 5 m/hour. A certain level of shear force or high momentum convection must be produced by the impellers to suspend and distribute them. The results are as shown in Figure 6.4. In the up-pumping mode for the solids concentration of 10 wt% and 30 wt%, $N_{helical\ ribbon}$ has no influence on N_H; however, at 20 wt% N_H increases at $N_{helical\ ribbon}$ = 30 rpm. At $N_{helical\ ribbon}$ = 20 rpm, the particles can be homogeneously distributed at $N_{Maxblend}$ = 80 rpm (N_H). As $N_{Maxblend}$ remains constant and $N_{helical\ ribbon}$ increases to 30 rpm, the particles merely move along with the helical ribbon above the bottom plane of the electrodes without any axial suspension. This segregation phenomenon is shown in Figure 6.5. The lack of sufficient axial pumping is the primary reason for the segregation. The mixing performance of the Superblend mixer with viscous Newtonian fluid has been reported by Fahrat et al. (2009) and Wang et al. (2012). These single phase studies did not show any indication of a possible segregation region in early or late transitional regimes. This illustrates that the addition of particles leads to the segregation phenomenon. Taking the configuration of the Superblend into account, in the lower viscous liquid when the liquid flow carries particles to the bottom portion of the helical ribbon blades, some particles are deviated from the bulk flow and entrapped in the interspaces of the bottom portion of the helical ribbon blades most probably because of the low pressure zone produced locally by the helical ribbon. The entrapped particles and the blades form a blocking layer, which dramatically reduces the pumping capacity of the Superblend mixer. In the high viscosity liquid the particles strictly follow the liquid flow and pass through the bottom portion of the helical ribbon blades with no interference. Therefore, the blocking layer does not form in that case. To overcome this blocking layer problem, either a higher $N_{Maxblend}$ is required which provides more pumping or a lower $N_{helical\ ribbon}$ is required to avoid the formation of the blocking layer.

As a conclusion, in the up-pumping mode the helical ribbon in high-speed rotation results in a restraining effect to the solids distribution in low viscosity liquid. This effect does not appear at

10 or 30 wt% at $N_{helical\ ribbon}$ = 30 rpm because at 10 wt% there is not enough particles to help with the blocking effect, and at 30 wt% there are too many particles, and therefore too many particle-particle collisions that allow the particles to go through blocking blades of the helical ribbon. In the down-pumping mode N_H decreases as $N_{helical\ ribbon}$ increases. It proves that the flow generated by the helical ribbon promotes the solids distribution, which is consistent with the result in high viscosity liquid for the same particles.

The effect of the rotating mode on N_H at a given $N_{helical\ ribbon}$ was also studied. At $N_{helical\ ribbon}$ = 10 rpm and 20 rpm, an equal or higher N_H is required in the down-pumping mode than in the up-pumping mode. At $N_{helical\ ribbon}$ = 30 rpm a lower N_H is required in the down-pumping mode than in the up-pumping mode, which is also in agreement with the result in high viscosity liquid.

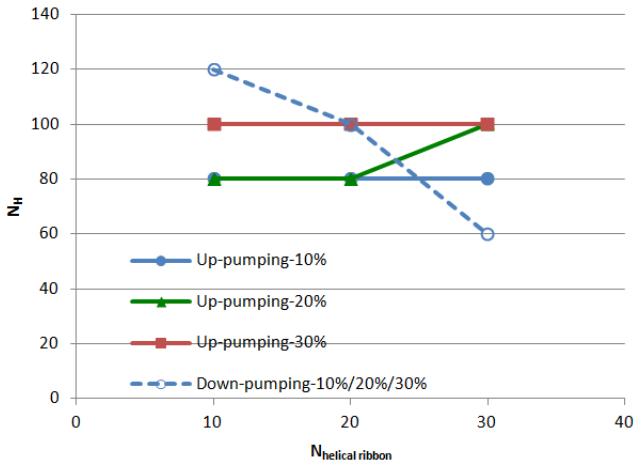

Figure 6.4: Effects of the solids concentration, operating mode, and the speed of the helical ribbon on the homogenization speed of coarse particles (500 μm) in low viscosity liquid (0.1 Pa.s)

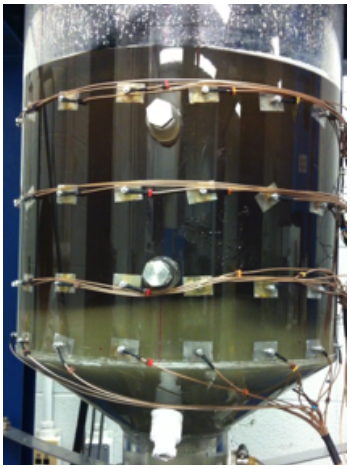

Figure 6.5: Experimental observation of the blocking effect in the up-pumping mode at $N_{Maxblend}$ = 80 rpm, $N_{helical\ ribbon}$ = 30 rpm

6.4.1.3. Distribution of 75 µm particles in 0.1 Pa.s liquid

In this case, the liquid flow lies in the late transitional regime (Re_{liquid} = 784 - 1072 at the speeds studied). Being different from the cases above, the fine particles strictly follow the random liquid flow without settling ($V\emptyset$ = 0.057 - 0.113 m/hour). As Figure 6.6 shows, N_H is 80 rpm regardless of the solids concentrations, rotating modes and $N_{helical\ ribbon}$. The determination of N_H in this case is fairly simple: at all $N_{helical\ ribbon}$, the solid bed on the conical bottom cannot be disrupted and distributed until $N_{Maxblend}$ reaches 80 rpm, and the homogeneous solids distribution can be achieved at this speed. The lifting of the solid bed becomes the bottleneck of accomplishing the homogeneous solids distribution. Even though the up-pumping flow and the hydrodynamic conflict provided by the helical ribbon contributes to the solids distribution, the intense downward flow in the center of the tank provided by the Maxblend impeller is the unique driving force of lifting all the particles off the conical bottom. As a conclusion, in the Superblend mixer N_H of the fine particles in the late transitional regime is limited solely by the speed of the Maxblend impeller. For coarse particles the bottleneck phenomenon does not appear. Therefore, the complete off-bottom suspension is problematic only for fine particles. This can be attributed to the larger amount of fine particles (300 times as many as the coarse particles at the same solids concentration) and the accompanying stronger particle-particle interaction than the coarse particles near the bottom of the tank.

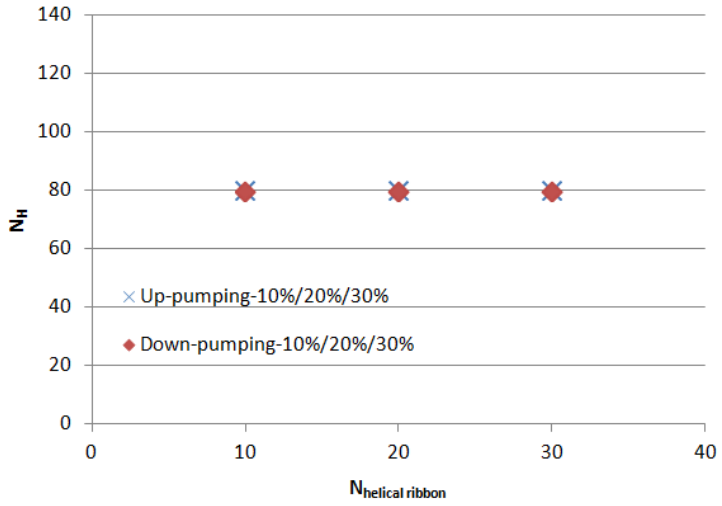

Figure 6.6: The influence of the variables on the homogenization speed of fine particles (75 μm) in low viscosity liquid (0.1 Pa.s)

6.4.1.4. Comparison of distribution of 500 μm particles in 4 Pa.s and 0.1 Pa.s liquids

As discussed in 6.4.1.2, the effect of rotating mode on N_H is equivalent for 500 μm particles in two liquids. Figure 6.7 shows the effect of the speed of the helical ribbon, liquid viscosity and the solids concentration on N_H. Except for the case where the blocking layer is formed, the effect of $N_{helical\ ribbon}$ on N_H is also equivalent in two liquids. Regardless of the rotating mode and the solids concentration, at a given $N_{helical\ ribbon}$ the coarse particles require a higher N_H at 0.1 Pa.s than 4 Pa.s except the case with the solids concentration of 30 wt% in the up-pumping mode. Since the settling velocity of the coarse particles in the low viscosity liquid is 40 times as high as that in the high viscosity liquid, there is no surprise that the extra pumping capacity is required from the Maxblend impeller to overcome the settling of the particles. When the solids concentration rises to 30 wt% in the up-pumping mode, despite the fact that N_H in both viscous liquids become the same, N_H in low viscosity liquid increases by 0%-20% (at 10 and 20 rpm of helical ribbon), while N_H in high viscosity liquid increases by 67%. This demonstrates that the random movement of the extra particles in low viscosity liquid helps lift other particles, and therefore less extra pumping capacity is requested from the Maxblend impeller.

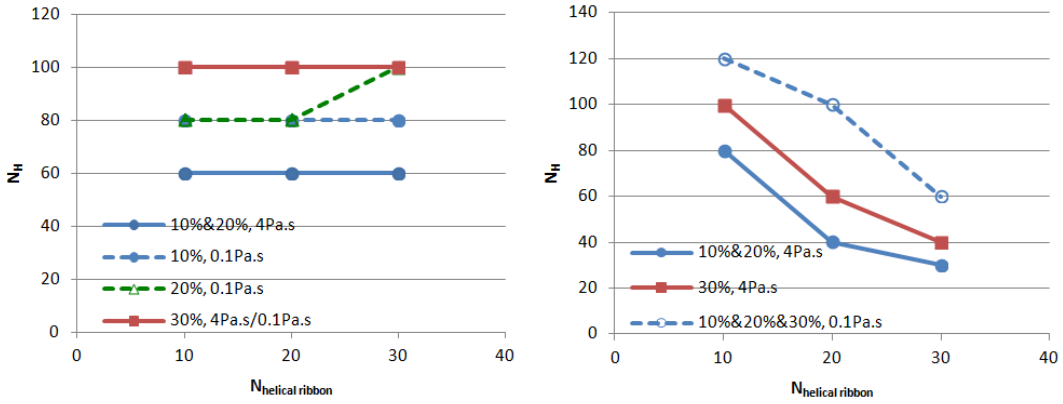

(a) (b)

Figure 6.7: Effects of the speed of the helical ribbon, liquid viscosity and solids concentration on the homogenization speed with 500 μm particles. (a) up-pumping, (b) down-pumping

6.4.1.5. Comparison of distribution of different particles in 0.1 Pa.s liquid

It has been reported (Hosseini et al., 2010; Tahvildarian et al., 2011) that the larger particles require higher speed to be homogeneously suspended at a given solids concentration, which is consistent with the effect of particle size on just suspended speed, N_{js} (Zwietering, 1958). The studies of solids suspension occur in the turbulent regime, where the effect of viscosity is hardly estimated (Atiemo-Obeng et al., 2004). With the viscous fluid of 0.1 Pa.s, late transitional regime is reached. Due to the influence of the viscosity, in the up-pumping mode the coarse particles encounter the blocking effect from the helical ribbon at high rotational speeds and in both rotating modes the fine particles encounter the difficulty of being picked up from the bottom. These complex hydrodynamics result in different mixing mechanisms for the fine and coarse particles. Therefore, with the Superblend mixer the effect of particle size on N_H in viscous fluids is not as simple as the previous researchers suggested (Hosseini et al., 2010; Tahvildarian et al., 2011). The value of N_H for the fine or coarse particles is a strong function of the speed of the helical ribbon, the solids concentration and the rotating mode.

6.4.2 Dimensionless mixing time

6.4.2.1 The effect of variables on the dimensionless mixing time

The effects of the speed of helical ribbon, rotating mode, particle size and solids concentration on the dimensionless mixing time, $N_H \times t_H$, were studied and the results are shown in Figure 6.8. In

all studied cases it is expected that the dimensionless mixing time increases along with the solids concentration and shorter dimensionless mixing time is required with the coarse particles in low viscosity liquid than in the high viscosity liquid.

The dimensionless mixing time is expected to decrease as $N_{helical\ ribbon}$ increases for all the cases. However, in the low viscosity liquid the shortest dimensionless mixing time in the up-pumping mode is obtained at $N_{helical\ ribbon}$ = 20 rpm rather than $N_{helical\ ribbon}$ = 30 rpm. One possible explanation is that the blocking layer formed by the helical ribbon and the viscous slurry is not completely broken down by the increase of $N_{Maxblend}$, and it still reduces the pumping capacity of the Superblend mixer as long as the helical ribbon rotates at high-speeds. In addition, the increasing dimensionless mixing time at $N_{helical\ ribbon}$ = 30 rpm with the fine particles in the low viscosity liquid shows that the blocking layer is present for this case as well. It was not detected in the study of N_H because the blocking effect of the blocking layer for the fine particles is not as strong as that for the coarse particles; however, the reduced pumping capacity still inevitably results in an increase in the dimensionless mixing time. So far it can be concluded that the blocking layer is formed only at high $N_{helical\ ribbon}$ in the up-pumping mode in the low viscosity liquid regardless of the particle size. The second possible explanation is that the transition in the flow regime is achieved above 20 rpm of the helical ribbon and the regime turns turbulent. Hence the very different mixing times. With the results obtained here, there is no clear indication of which explanation to adhere to and only a thorough investigation on the transition between flow regimes can clarify this situation.

The effect of the rotating mode on the dimensionless mixing time is related to the speed of the helical ribbon. At $N_{helical\ ribbon}$ =10 rpm, the dimensionless mixing time in the up-pumping mode is shorter. At $N_{helical\ ribbon}$ =30 rpm, nevertheless, in the down-pumping mode the dimensionless mixing time is shorter. In low-speed rotation the helical ribbon in the down-pumping mode is in the disadvantageous position: due to the hydrodynamic conflict with the Maxblend impeller, the helical ribbon does not produce strong upward flow to lift the particles at all, and weakens the shearing and dispersing capacities of the Maxblend impeller. In high-speed rotation taking advantage of the significant contribution from the helical ribbon to the pumping, shearing and dispersing capacities, the down-pumping mode outperforms the up-pumping mode. The

formation of the blocking layer also prolongs the dimensionless mixing time in the up-pumping mode.

Comparing the dimensionless mixing time for different particles in the same liquid (0.1 Pa.s) in Figure 6.8b and c, it can be seen that the fine particles require longer dimensionless mixing time than the coarse particles. It can be explained from two aspects: first, the number of the fine particles are 300 times as many as that of the coarse particles with the same concentration; second, the particle-particle interaction for the fine particles are stronger and have a hindering effect than the coarse particles, both of which require more dimensionless mixing time to accomplish the homogeneous distribution of the particles.

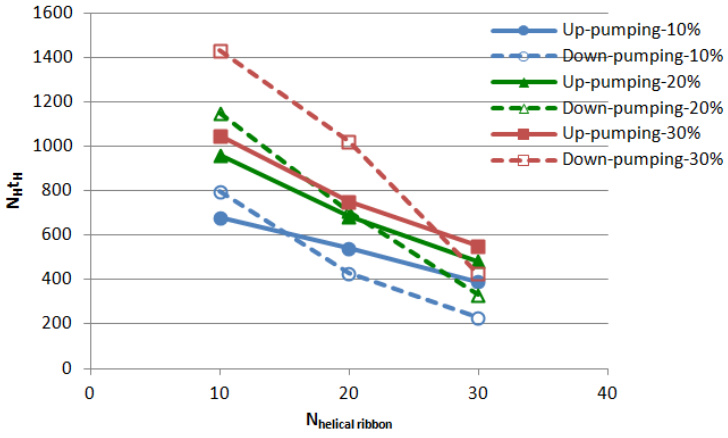

(a)

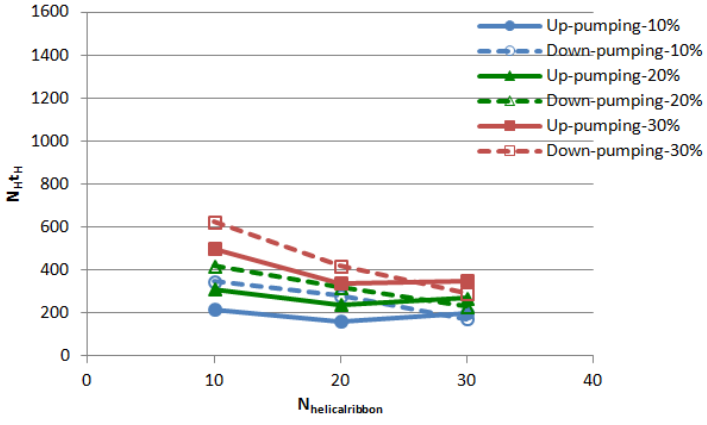

(b)

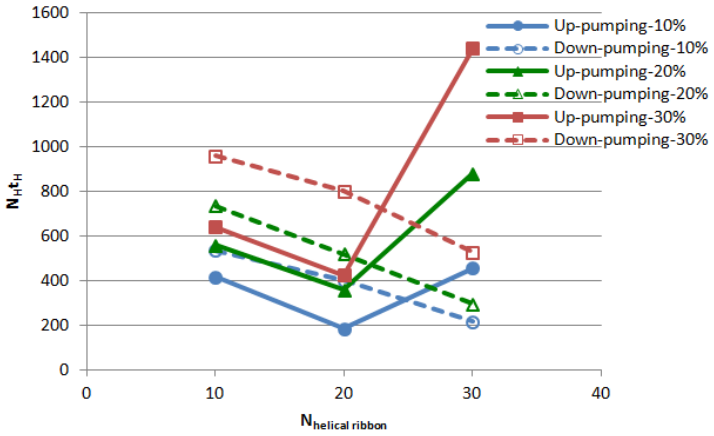

(c)

Figure 6.8: Effects of solids concentration, particle size, operating mode, and speed of the helical ribbon on the dimensionless mixing time. (a) 500 µm particles in 4 Pa.s liquid, (b) 500 µm particles in 0.1 Pa.s liquid, (c) 75 µm particles in 0.1Pa.s liquid

6.4.2.2 Comparison of mixing time in single-phase and solid-liquid systems

Using the dimensionless mixing time in viscous Newtonian fluid that Farhat et al. (2009) and Wang et al. (2012) have published, we calculated the mixing time in single-phase system t_m at the same Reynolds number and impeller speeds as solid-liquid system. Because the speed ratios presented in this work were not all studied by Farhat et al. (2009) (R_N > 10) and Wang et al. (2012) (R_N = 2, 4, 6, 8), only one complete comparison of mixing time between single-phase and solid-liquid systems in terms of mixing time ratio t_H / t_m was obtained at $N_{helical\ ribbon}$ = 10 rpm and varying $N_{Maxblend}$ (N_H) between 60 and 120 rpm. The results given in Figure 6.9 show that the presence of particles significantly increases the mixing time in solid-liquid system: 10 to 68 times as long as the mixing time in single-phase system, and this mixing time ratio increases along with the increase of the solids concentration regardless of the rotating mode. Since with low viscosity liquid the dimensionless mixing time for the fine particles is longer than the coarse particles, the mixing time ratio for the fine particles is also higher than the coarse particles. This shows that the solids concentration has a significant effect on mixing time at all solids concentrations. It should be noted that the techniques for measuring the mixing time are different for the solid-liquid and the single-phase cases. For the solid-liquid case ERT was used, and for the single phase decolorization method was used. The mixing time with the slurry cannot be measured with the

decolorization technique as the vessel becomes opaque, preventing the visualization of possible dead zones in the vessel. However, the ERT has shown very similar mixing time results when used in a comparison with the decolorization in our lab in the past. We are hence confident that the comparison presented here is relevant.

It can be seen in Figure 6.9 that the mixing time ratio with low viscosity liquid is higher than that with high viscosity liquid. This can be explained by the difference in the flow regime. When the viscosity reduces, the system varies from early transitional regime to late transitional regime, where random flow starts to dominate the mixing process. Random flow with momentum convection benefits the single-phase mixing more than the solid-liquid mixing and causes a larger gap between them. As a result, the mixing time ratio is higher with low viscosity liquid. Another possibility is the effect of presence of solids on the viscosity of the slurry. If the presence of solids increase the viscosity of the slurry, that could be reflected in the flow regime of the low viscosity liquid more significantly than the high viscosity liquid. Therefore, the mixing time ratio for the low viscosity liquid would be higher. The steeper slopes between 20 and 30 wt% for 0.1 Pa.s compared to the 4 Pa.s, particularly in the down-pumping mode, support this idea.

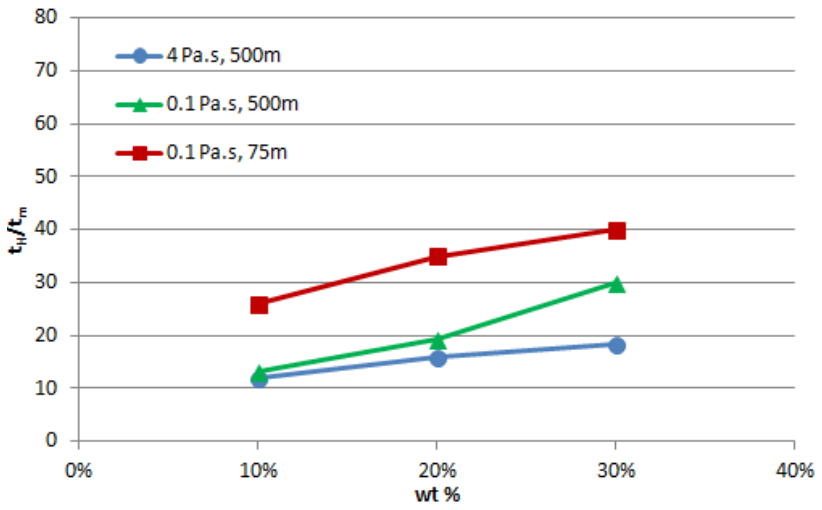

(a)

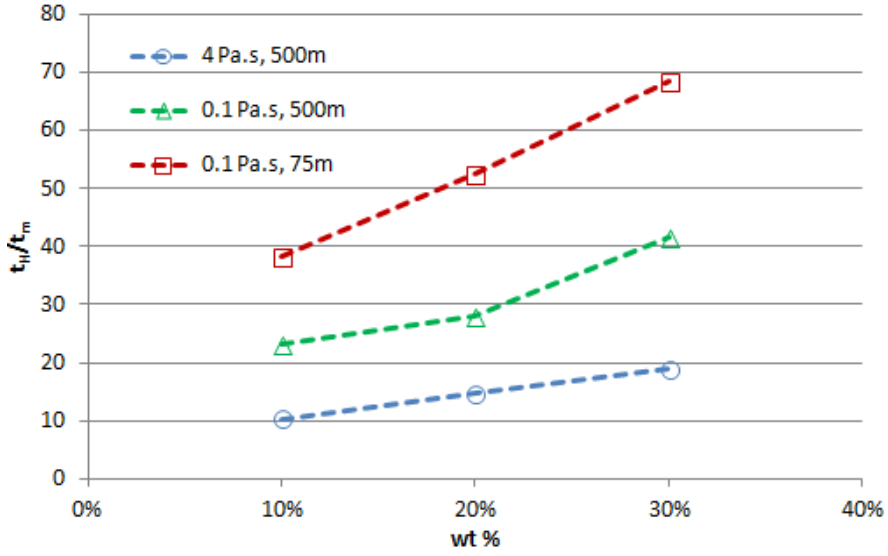

(b)

Figure 6.9: The comparison of mixing time at homogenization speed in single-phase and solid-liquid systems at $N_{helical\ ribbon}$ = 10 rpm and $N_{Maxblend}$ (N_H) varying between 60 and120 rpm. (a) up-pumping mode, (b) down-pumping mode

6.4.3 Energy for Homogenization

In order to evaluate the efficiency of the solids distribution in the Superblend mixer from the perspectives of both the dimensionless mixing time and the specific power consumption (Pv, W/m^3) at a given N_H, energy for homogenization $N_H t_H \times Pv$ is proposed. It can be referred to as an index to compare and derive the optimal operating conditions for the homogeneous solids distribution in different types of mixers on different scales. As shown in Figure 6.10 a, in the high viscosity fluid $N_{helical\ ribbon}$ = 10 rpm in the up-pumping mode is the most efficient operating condition for the solids concentrations of 10 wt% and 20 wt%, while $N_{helical\ ribbon}$ = 30 rpm in down-pumping mode is the most efficient one for the solids concentration of 30 wt%. In the low viscosity fluid the optimal operating condition varies for different particle sizes. For the coarse particles as shown in Figure 6.10 b, $N_{helical\ ribbon}$ = 20 rpm in up-pumping mode is the most efficient operating condition at 10 wt% and 20 wt%, while $N_{helical\ ribbon}$ = 30 rpm in the down-pumping mode is the most efficient one for the solids concentration of 30 wt%. For the fine

particles as shown in Figure 6.10c, $N_{helical\ ribbon}$ = 20 rpm in up-pumping mode is the most efficient operating condition for all the solids concentrations.

The efficiency for a given particle size and a given liquid viscosity can also be seen in Figure 6.10. Comparing Figure 6.10a and b, it is noted that for the coarse particles, regardless of liquid viscosity, the up-pumping mode is more efficient for the solids concentrations of 10 wt% and 20 wt%, and $N_{helical\ ribbon}$ = 30 rpm in the down-pumping mode is the most efficient one at of 30 wt%. Comparing Figure 6.10b and c, in the low viscosity liquid regardless of particle size, $N_{helical\ ribbon}$ = 20 rpm in up-pumping mode is the most efficient operating condition for the solids concentrations of 10 wt% and 20 wt%, whereas there is no universal optimal operating mode for the solids concentration of 30 wt%.

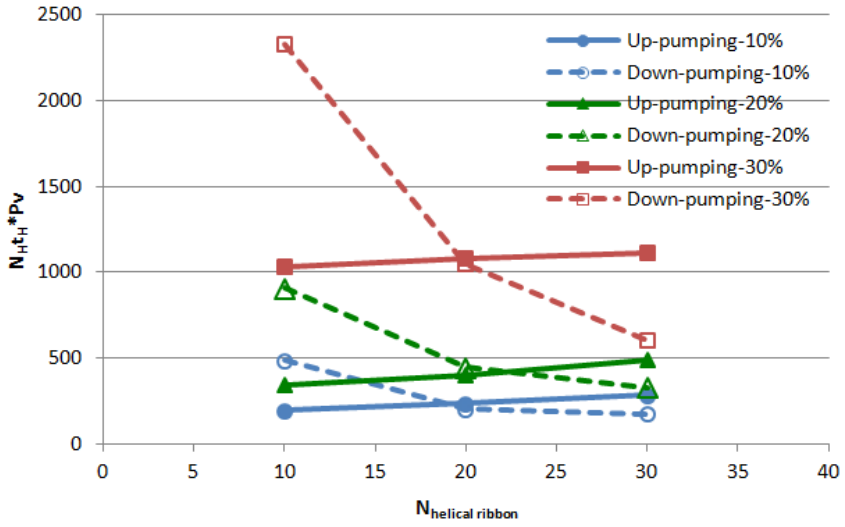

(a)

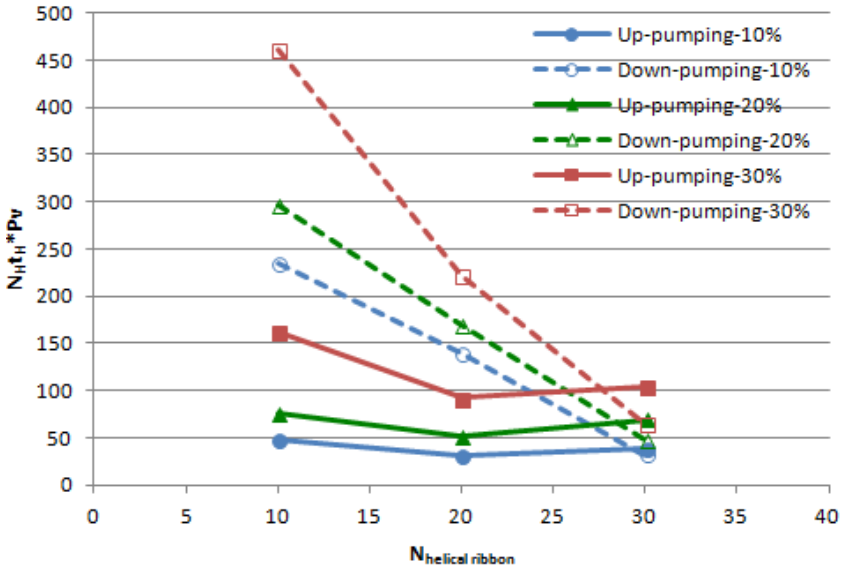

(b)

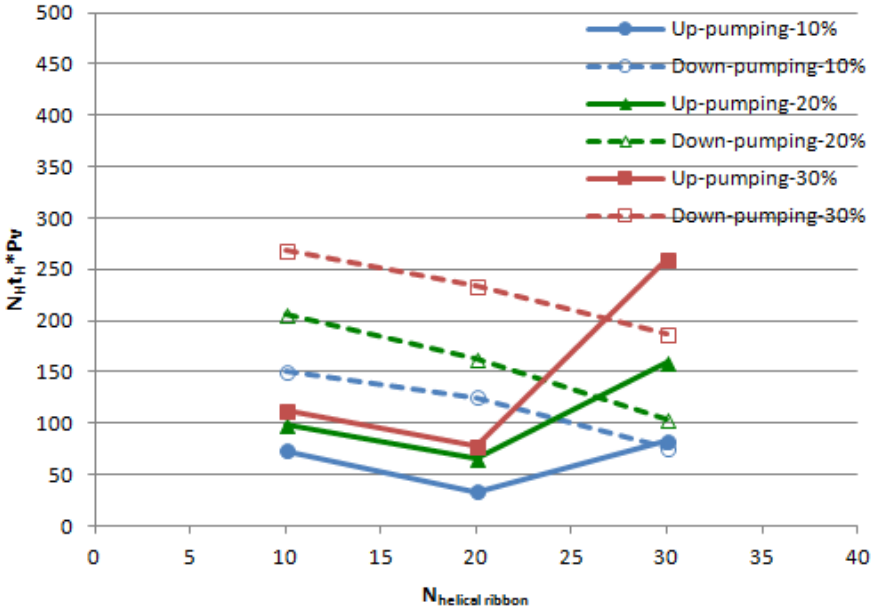

(c)

Figure 6.10: Effects of solids concentration, particle size, operating mode, and speed of the helical ribbon on energy for homogenization. (a) 500 µm particles in 4 Pa.s liquid, (b) 500 µm particles in 0.1Pa.s liquid, (c) 75 µm particles in 0.1 Pa.s liquid

6.5 Conclusion

Electrical resistance tomography allowed for the quantitative characterization of the mixing performance of the Superblend coaxial mixer for homogeneous solids distribution in viscous Newtonian fluids. Homogenization speed and energy for homogenization were introduced to assess the mixing performance. The viscosity of the continuous liquid plays a critical role in the mixing process. Some inconsistencies in the results mainly occur at high solids concentration and indicate that the transition in the rheological behavior, and therefore the flow regime could affect the mixing performance significantly. The Superblend mixer was proven to be overall efficient and easy to operate for homogeneous solids distribution in viscous continuous liquid.

6.6 Reference

ATIEMO-OBENG, V. A., ROY PENNEY, W. and ARMENANTE, P. (2004). Solid-liquid mixing, PAUL, E. L., ATIEMO-OBENG, V. A. and KRESTA, S. M. (2004). Handbook of industrial Mixing: Science and Practice, John Wiley & Sons, Inc., New Jersey, 543-584.

BARAR POUR, S.; FRADETTE, L. and TANGUY, P. A. (2007). Laminar and slurry blending characteristics of a dual shaft impeller system. *Chem. Eng. Res. Des.*, *85* (A9), 1305-1313.

BROWN, D. A. R., JONES, P. N. and MIDDLETON, J. C. (2004). Experimental methods. In: PAUL, E. L., ATIEMO-OBENG, V. A. and KRESTA, S. M. (2004). Handbook of industrial Mixing: Science and Practice. John Wiley & Sons, Inc., Hoboken, New Jersey, 145-256

BUJALSKI, W., TAKENAKA, K., PAOLINI, S., JAHODA, M., PAGLIANTI, A., TAKAHASHI, K., NIENOW, A. W. and ETCHELLS, A. W. (1999). Suspension and liquid homogenization in high solids concentration stirred chemical reactors. *Trans IChemE*., 77(A), 241-247.

FAJNER, D., MAGELLI, F., NOCENTINI, M., and PASQUALI, G. (1985). Solids concentration profiles in a mechanically stirred and staged column slurry reactor. *Chem. Eng. Res. Des.,* 63, 235-240.

FARHAT, M., FRADETTE, L. and TANGUY, P. A. (2008). Revisiting the performance of a coaxial mixer. *Ind. Eng. Chem. Res*., 47(10), 3562-3567.

FARHAT, M., FRADETTE, L., HORIGUCHI, H., YATOMI, R. and TANGUY, P. A. (2009). Experimental Investigation of Superblend Coaxial Mixer. *J. Chem. Eng. Jpn.*, 42(11), 797-803.

GIGUERE, R., FRADETTE, L., D. Mignon and TANGUY, P. A. (2008). ERT algorithms for quantitative concentration measurement of multiphase flows. *Chem. Eng. J.*, 141, 305-317.

GIGUERE, R., FRADETTE, L., D. Mignon and TANGUY, P. A. (2009). Analysis of slurry flow regimes downstream of a pipe bend, Chem. *Eng. Res. Des.*, 87, 943-950.

HARRISON, S. T. L., STEVENSON, R. and CILLIERS, J. J. (2012). Assessing solids concentration homogeneity in Rushton-agitated slurry reactors using electrical resistance tomography (ERT). *Chem. Eng. Sci.*, 71, 392-399.

HOLDEN, P. J., WANG, M., MANN, R., DICKIN, F. J. and EDWARDS, R. B. (1998). Imaging stirred-vessel macromixing using electrical resistance tomography. *AIChE J.*, 44(4), 780-790.

HOSSEINI, S., PATEL, D., EIN-MOZAFFARI, F. and MEHRVAR, M. (2010). Study of solid–liquid mixing in agitated tanks through electrical resistance tomography. *Chem. Eng. Sci.*, 65, 1374-1384.

KRAUME, M. (1992). Mixing times in stirred suspensions. *Chem. Eng. Tech.*, 15, 313-318.

KURATSU, M., NISHIMI, H., YATOMI, R., SATO, H. and MISHIMA, M. (1994). Mixing Reactor "Superblend" applied to wide range of viscosity. *Sumitomo Heavy Industries Technical Review.*, *42* (124), 82-85.

MANN, R., WILLIAMS, R. A., DYAKOWSKI, T., DICKIN, F. J. and EDWARDS, R. B. (1997). Development of mixing models using electrical resistance tomography. *Chem. Eng. Sci.*, 52(13), 2073-2085.

MICHELETTI, M., NIKIFORAKI, L., LEE, K. C. and YIANNESKIES, M. (2003). Particle concentration and mixing characteristics of moderate-to-dense solid–liquid suspensions. *Ind. Eng. Chem. Res.*, 42, 6236-6249.

OCHIENG, A. and ALISON, E. L. (2006). Nickel solids concentration distribution in a stirred tank. *Miner. Eng.,* 19, 180-189.

OZCAN-TASKIN, G. and WEI, H. (2003). The effect of impeller-to-tank diameter ratio on draw down of solid. *Chem. Eng. Sci*., 58, 2011–2022.

PAUL, E. L., ATIEMO-OBENG, V. A. and KRESTA, S. M. (2004). Handbook of industrial Mixing: Science and Practice. John Wiley & Sons, Inc., Hoboken, New Jersey.

RAGHAV RAO, K. S. M. S. and JOSHI, J. B. (1998). Liquid-phase mixing and power consumption in mechanically agitated solid–liquid contactors. *Chem*. *Eng*. *J*., 39(2), 111-124.

RICHARDSON, J. F. and ZAKI, W. N. (1954). Sedimentation and fluidisation: Part 1. *Trans. IChemE.*, *32*, 35-53.

TAHVILDARIAN, P., NG, H., D'AMATO, M., DRAPPEL, S., EIN-MOZAFFARI, F. and UPRETI, S. R. (2011). Using electrical resistance tomography images to characterize the mixing of micron-sized polymeric particles in a slurry reactor. *Chem*. *Eng*. *J*., 172, 517-525.

WANG, M., DORWARD, A., VLAEC, D. and MANN, R. (2000). Measurements of gas–liquid mixing in a stirred vessel using electrical resistance tomography (ERT). *Chem*. *Eng*. *J*., 77(1-2), 93-98.

WANG, X., FRADETTE, L., TAKENAKA, K. and TANGUY, P. A. (2012). Effect of operating parameters on the mixing performance of the Superblend coaxial mixer. *Ind. Eng. Chem. Res.*, *51* (4), 1826-1833.

ZWIETERING, T. (1958). Suspending of solid particles in liquid by agitators. *Chem. Eng. Sci.*, 8, 244-253.

CHAPTER 7: GENERAL DISCUSSION, CONCLUSION AND RECOMMENDATIONS

7.1 General discussion

The Superblend coaxial mixer is specifically developed for making a real breakthrough in industrial process for handling rheologically complex applications involving single-phase blending with highly viscous Newtonian and non-Newtonian fluids and homogeneous solid-liquid distribution in viscous Newtonian fluid in multiphase systems. Taking advantage of innovative measurement technologies such as decolorization and electrical resistance tomography, the role played by the mixing hydrodynamics generated by the Superblend mixer was revealed. It allows the researchers and the industries to identify the handles and the locks that control the process efficiency and the mixing performance of the Superblend mixer. The synthetical utilization of the scientific information is capable of helping in the design and optimization of mixing operations and the improvement of existing mixing processes. The methodologies applied in this investigation are not limited to the selected mixer, and they should also be extended to other types of configurations and experimental conditions.

7.2 Conclusion

- Fluid mixing with complex rheological behaviors has been a challenge to the mixing community for many years. The Superblend coaxial mixer has been proposed as a promising technology to cope with this situation. To validate its mixing performance and better understand the mixing hydrodynamics, the effect of speed ratio, rotating mode and rheological behavior on the flow field, mixing evolution, mixing time, power consumption and Metzner-Otto constant was investigated in this work. Decolorization-image-processing technique was used to measure the mixing time. Results proved that the Superblend mixer is qualified to handle and accomplish such complex and challenging mixing goals. It possesses an excellent mixing efficiency outperforming other multi-shaft mixers, including coaxial and dual shaft mixers with a variety of impellers, in terms of mixing time and mixing energy. Referring to the power contribution of each impeller, the

Maxblend impeller does not dominate the power consumption at all speed ratios and the helical ribbon contributes more to the power consumption at $R_N \leq 3.3$. From the perspective of the mixing time, the optimal operating conditions are to apply a low speed ratio with high viscosity Newtonian fluids and to increase the speed ratio with low Newtonian viscosity fluids. Due to the influence of rheological behaviour, the mixing performance with shear-thinning fluids is significantly different from the one observed with Newtonian fluids in terms of mixing evolution, mixing time and power consumption. The pumping capacity of the Superblend mixer was discussed based on the mixing curves obtained by using decolorization-image-processing technique. As the power-law index decreases, less power is needed, and the Metzner-Otto constant drops in the up-pumping mode but increases in the down-pumping mode. On the basis of the comparison of the mixing energy, the mixing efficiency with shear-thinning fluids outperforms that with Newtonian fluids. $R_N = 4$ in the up-pumping mode and $R_N = 2$ in the down-pumping mode are proposed as the optimal operating conditions for both Newtonian and non-Newtonian fluids in a wide range of Reynolds numbers ($10<Re<1000$).

- Characteristic parameters in the multi-shaft mixers are used to investigate and compare the mixing performance in different multi-shaft mixers on the basis of uniform criteria. Due to the complexity of the configuration, the definitions of the characteristic parameters have been controversial. In search of reliable and universal definitions, the applicability of the correlations proposed by Farhat et al. (2008) was extended to the dual shaft and Superblend mixers. Overall results proved that single power curve could be obtained by using these correlations, which indicated they are well suited for coaxial mixers, dual shaft mixers and the Superblend mixer. Taking advantage of the universal applicability, a general approach was first introduced to predict the power constant in the multi-shaft mixers. When two impellers have low power constants, the power constant of any coaxial mixer can be predicted as the power constant of the high-speed impeller. The limitations of the new correlations were revealed and discussed through the extensive application on the Superblend mixer at low speed ratios and rotor stator-Paravisc dual shaft mixer. They are applicable when the high-speed impeller is the largest contributor to the fluid circulation in the tank.

- Uniform solids distribution in high viscosity fluids is significant for processes such as crystallization. However, existing studies only focus on uniform solids distribution in water, and there are no reports in the literature that deal with the viscous continuous media. To fill this scientific blank and seek a solution for this operation, an initial investigation on the homogeneous solids distribution in viscous liquids was carried out in Superblend coaxial mixer. Meanwhile, the application of ERT technology in coaxial mixer was also first reported, though the complex configuration causes drastic interference and difficulty. Homogenization speed and energy for homogenization were introduced to assess the mixing performance of the Superblend mixer for homogeneous solids distribution, and the development of the quantitative measurement of the homogenization speed and mixing time for ERT was demonstrated. A series of investigations on the impact of the particle size and concentration, the viscosity of the fluid and the operating conditions of the Superblend mixer on the homogeneous solids distribution were carried out. Results proved that the value of homogenization speed or mixing time is a strong function of the particle size and concentration, the viscosity of the fluid, the speed of the helical ribbon and the rotating mode. The effect of the rotating mode on homogenization speed and mixing time is strongly conditioned by the speed of the helical ribbon. Especially in the up-pumping mode the helical ribbon in high-speed rotation results in a restraining effect to the solids distribution in low viscosity liquid. The optimum conditions were derived in terms of energy for homogenization from the perspectives of both the dimensionless mixing time and the specific power consumption. In contrast with solids suspension in turbulent regime, the viscosity of the liquid plays a critical role in the entire mixing process. Some inconsistencies in the results mainly occur at high solids concentration and indicate that the transition in the rheological behavior, and therefore the flow regime could affect the mixing performance significantly. The Superblend mixer was proven to be overall efficient and easy to operate for homogeneous solids distribution in viscous continuous liquid.

7.3 Recommendations

- From the perspective of product formulation, the strongly rheologically evolving process with the extreme shearing-thinning effect in the single-phase mixing and the homogeneous solids distribution in shear-thinning fluid are of broad industrial interest. Therefore, the extensive exploration and validation in such cases ought to be carried out in the future study of the Superblend mixer.

- As an effective and non-intrusive imaging measurement technique, decolorization method has shown to be a versatile technique to both qualitatively and quantitatively detect not only the macro mixing time but also the mixing evolution in the single-phase blending. So far, the application of decolorization method merely based on 2D imaging information from the front view of the mixer, which is not qualified to describe the full-scale mixing evolution throughout the tank. To make it more precise and reliable, 3D measurement and analysis ought to be explored.

- ERT technique has penetrated to the experimental study of multiphase mixing. A quantitative evaluation of the homogeneous solids distribution with viscous Newtonian fluids was developed in this investigation. Due to the non-transparent process occurs in multiphase mixing, decolorization method can be hardly applied in multiphase mixing. However, ERT technique has been used in single-phase blending with non-Newtonian fluids in recent works (Leica Pakzad, 2013; Dineshkumar Patel, 2013). Therefore, the application of ERT technique in the study of the fluid mixing in the Superblend mixer should be taken into account. The comparison between the performance of decolorization method and ERT technique on the characterization of the fluid mixing is able to provide new knowledge and understanding to both the application of each technique and the comprehensive application of the two techniques.

REFERENCE

ATIEMO-OBENG, V. A., ROY PENNEY, W. and ARMENANTE, P. (2004). Solid-liquid mixing, PAUL, E. L., ATIEMO-OBENG, V. A. and KRESTA, S. M. (2004). Handbook of industrial Mixing: Science and Practice, John Wiley & Sons, Inc., New Jersey, 543-584.

BAKKER, A. and GATES, L. E. (1995). Properly Choose Mechanical Agitators for Viscous Liquids. *Chem. Eng. Prog.*, 91(12), 25-34.

BAO, Y., YANG, B., XIE, Y., GAO, Z., ZHANG, Z., LIU, T. and Gao, X. (2011). Power demand and mixing performance of coaxial mixers in non-Newtonian fluids. *J. Chem. Eng. Jpn.*, 44, 57-66.

BARAR POUR, S.; FRADETTE, L. and TANGUY, P. A. (2007). Laminar and slurry blending characteristics of a dual shaft impeller system. *Chem. Eng. Res. Des.*, *85* (A9), 1305-1313.

BONNOT, S., CABARET, F. FRADETTE, L. and TANGUY, P. A. (2007). Characterization of Mixing Patterns in a Coaxial Mixer. *Chem. Eng. Res. Des.*, 85(A8), 1129-1135.

BRITO-DE LA FUENTE, E., CHOPLIN, L. and TANGUY P. A. (1997). Mixing with helical ribbon impellers: Effect of highly shear thinning behavior and impeller geometry. *Chem*. *Eng*. *Res*. *Des*., 75, 45-52.

BROWN, D. A. R., JONES, P. N. and MIDDLETON, J. C. (2004). Experimental methods. In: PAUL, E. L., ATIEMO-OBENG, V. A. and KRESTA, S. M. (2004). Handbook of industrial Mixing: Science and Practice. John Wiley & Sons, Inc., Hoboken, New Jersey, 145-256.

BUJALSKI, W., TAKENAKA, K., PAOLINI, S., JAHODA, M., PAGLIANTI, A., TAKAHASHI, K., NIENOW, A. W. and ETCHELLS, A. W. (1999). Suspension and liquid homogenization in high solids concentration stirred chemical reactors. *Trans IChemE*., 77(A), 241-247.

CABARET, F., BONNOT, S., FRADETTE, L. and TANGUY, P. A. (2007). Mixing Time Analysis Using Colorimetric Methods and Image Processing. *Ind. Eng. Chem. Res.*, 46(14), 5032-5042.

CABARET, F., RIVERA, C., FRADETTE, L., HENICHE, M. and TANGUY, P. A. (2007). Hydrodynamics performance of a dual shaft mixer with viscous Newtonian liquids. *Chem. Eng. Res. Des.*, *85* (A5), 583-590.

CHAVAN, V. V. (1983). Close-clearance Helical Impeller: A Physical Model for Newtonian Liquids at Low Reynolds Numbers, *AIChE J*., 29(2), 177.

DIEULOT, J. Y., DELAPLACE, G., GUERIN, R., BRIENNE, J. P. and LEULIET, J. C. (2002). Laminar Mixing Performances of A Stirred Tank Equipped with Helical Ribbon Agitator Subjected to Steady and Unsteady Rotational Speed. *Trans IChemE*., 80(A), 335-344.

ESPINOSA-SOLARES, T., BRITO-DE LA FUENTE, E., TECANTE, A. and TANGUY, P. A. (2001). Flow Patterns in Rheologically Evolving Model Fluids Produced by Hybrid Dual Mixing Systems. *Chem. Eng. Technol*., 24(9), 913-918.

FAJNER, D., MAGELLI, F., NOCENTINI, M., and PASQUALI, G. (1985). Solids concentration profiles in a mechanically stirred and staged column slurry reactor. *Chem. Eng. Res. Des.,* 63, 235-240.

FARHAT, M., RIVERA, C., FRADETTE, L., HENICHE, M. and TANGUY, P. A. (2007). Numerical and Experimental Study of Dual-shaft Coaxial Mixer with Viscous Fluids. *Ind. Eng. Chem. Res.*, 46(14), 5021-5031.

FARHAT, M., FRADETTE, L. and TANGUY, P. A. (2008). Revisiting the performance of a coaxial mixer. *Ind. Eng. Chem. Res.*, 47(10), 3562-3567.

FARHAT, M., FRADETTE, L., HORIGUCHI, H., YATOMI, R. and TANGUY, P. A. (2009). Experimental Investigation of Superblend Coaxial Mixer. *J. Chem. Eng. Jpn.*, 42(11), 797-803.

FOUCAULT, S., ASCANIO, G. and TANGUY, P. A. (2004). Coaxial mixer hydrodynamics with Newtonian and Non-Newtonian fluids. *Chem. Eng. Technol.*, 27(3), 324-329.

FOUCAULT, S., ASCANIO, G. and TANGUY, P. A. (2005). Power characteristics in coaxial mixing: Newtonian and Non-Newtonian fluids. *Ind. Eng. Chem. Res.*, 44, 5036-5043.

FOUCAULT, S., ASCANIO, G. and TANGUY, P. A. (2006). Mixing times in coaxial mixers with Newtonian and non-Newtonian fluids. *Ind. Eng. Chem. Res.*, 45(1), 352-359.

FRADETTE, L., THOME, G., TANGUY, P. A. and TAKENAKA, K. (2007). Power and Mixing Time Study Involving A Maxblend Impeller with Viscous Newtonian and Non-Newtonian Fluids. *Chem. Eng. Res. Des.*, 85(A11), 1514-1523.

GIGUERE, R., FRADETTE, L., D. Mignon and TANGUY, P. A. (2008). ERT algorithms for quantitative concentration measurement of multiphase flows. *Chem. Eng. J.*, 141, 305-317.

GIGUERE, R., FRADETTE, L., D. Mignon and TANGUY, P. A. (2008). Characterization of slurry flow regime transitions by ERT. *Chem. Eng. Res. Des.*, 86, 989-996.

GIGUERE, R., FRADETTE, L., D. Mignon and TANGUY, P. A. (2009). Analysis of slurry flow regimes downstream of a pipe bend, Chem. *Eng. Res. Des.*, 87, 943-950.

GUNTZBURGER, Y., FONTAINE, A., FRADETTE, L. and BERTRAND, F. (2013). An experimental method to evaluate global pumping in a mixing system: Application to the Maxblend™ for Newtonian and non-Newtonian fluids. *Chem. Eng. J.*, 214, 394-406.

IRANSHAHI, A., DEVALS, C., HENICHE, M., FRADETTE, L., TANGUY, P. A. and TAKENAKA, K. (2007). Hydrodynamics Characterization of the Maxblend Impeller. *Chem. Eng. Sci.*, 62, 3641-3653.

FAJNER, D., PINELLI, D., GHADGE, R. S., MONTANTE, G., PAGLIANTI, A. and MAGELLI, F. (2008). Solids distribution and rising velocity of buoyant solid particles in a vessel stirredwith multiple impellers. *Chem.l Eng. Sci.*, 63, 5876-5882.

FURLING, O., TANGUY, P. A., HENRIC, P., DENOEL, D. and CHOPLIN, L. (2001). New dispersing turbines for the preparation of concentrated suspensions. *J. Chem. Eng. Jpn.,* 34(5), 634-639.

HARRISON, S. T. L., STEVENSON, R. and CILLIERS, J. J. (2012). Assessing solids concentration homogeneity in Rushton-agitated slurry reactors using electrical resistance tomography (ERT). *Chem. Eng. Sci.*, 71, 392-399.

HOLDEN, P. J., WANG, M., MANN, R., DICKIN, F. J. and EDWARDS, R. B. (1998). Imaging stirred-vessel macromixing using electrical resistance tomography. *AIChE J.*, 44(4), 780-790.

HOSSEINI, S., PATEL, D., EIN-MOZAFFARI, F. and MEHRVAR, M. (2010). Study of solid–liquid mixing in agitated tanks through electrical resistance tomography. *Chem. Eng. Sci.*, 65, 1374-1384.

JIN, H., WANG, M., and WILLIAMS, R. A. (2007). Analysis of bubble behaviors in bubble columns using electrical resistance tomography. *Chem. Eng. J.*, 130, 179-185.

KHOPKAR, A., FRADETTE, L. and TANGUY, P. A. (2007). Hydrodynamics of a dual shaft mixer with Newtonian and non-Newtonian fluids. *Chem. Eng. Res. Des.*, *85*, 863-871.

KIM, S., NKAYA, A. N. and DYAKOWSKI, T. (2006). Measurement of mixing of two miscible liquids in a stirred vessel with electrical resistance tomography. *Int. Commun. Heat Mass Transfer*, 33, 1088-1095.

KOHLER, S. and HEMMERLE, W. (2003). Analysis of the power characteristic of a coaxial agitator with varied diameter and speed ratio inner and outer mixing device. *11th European Conference on Mixing*, Bamberg, 14-17.

KRAUME, M. (1992). Mixing times in stirred suspensions. *Chem*. *Eng*. *Tech*., 15, 313-318.

KURATSU, M., NISHIMI, H., YATOMI, R., SATO, H. and MISHIMA, M. (1994). Mixing Reactor "Superblend" applied to wide range of viscosity. *Sumitomo Heavy Industries Technical Review.*, *42* (124), 82-85.

KURATSU, M., YATOMI, R. and SATO, H. (1995). Design of versatile reactors. *Chem. Equipment.*, 8, 86-92.

MACHADO, M. B., NUNHEZ, J. R., NOBES, D. and Kresta, S. M. (2012). Impeller Characterization and Selection: Balancing Efficient Hydrodynamics with Process Mixing Requirements. *AIChE J*., *58* (8), 2573-2588.

MANN, R., WILLIAMS, R. A., DYAKOWSKI, T., DICKIN, F. J. and EDWARDS, R. B. (1997). Development of mixing models using electrical resistance tomography. *Chem. Eng. Sci.*, 52(13), 2073-2085.

METZNER, A. B. and OTTO, R. E. (1957). Agitation of non-Newtonian fluids. *AIChE J.*, 3(1), 3-10.

MICHELETTI, M., NIKIFORAKI, L., LEE, K. C. and YIANNESKIES, M. (2003). Particle concentration and mixing characteristics of moderate-to-dense solid–liquid suspensions. *Ind. Eng. Chem. Res.*, 42, 6236-6249.

NORMAN, J. T. and BONNECAZE, R. T. (2005). Measurement of solids distribution in suspension flows using electrical resistance tomography," *Can. J. Chem. Eng*, 83, 24-36.

OCHIENG, A. and ALISON, E. L. (2006).Nickel solids concentration distribution in a stirred tank. *Minerals Engineering,* 19, 180-189.

OLDSHUE, J. Y. (1983). Fluid Mixing Technology, McGraw-Hill, New York.

OZCAN-TASKIN, G. and WEI, H. (2003). The effect of impeller-to-tank diameter ratio on draw down of solid. *Chem. Eng. Sci*., 58, 2011–2022.

PAKZAD, L., EIN-MOZAFFARI, F., UPRETI, S. R. and LOHI, A. (2013). Evaluation of the mixing of non-Newtonian biopolymer solutions in the reactors equipped with the coaxial mixers through tomography and CFD. *Chem. Eng. J.*, 215-216, 279-296.

PATEL, D., EIN-MOZAFFARI, F. and MEHRVAR, M. (2013). Using tomography technique to characterize the continuous-flow mixing of non-Newtonian fluids in stirred vessels. *Chemical Engineering Transactions*, 32, 1465-1470.

PAUL, E. L., ATIEMO-OBENG, V. A. and KRESTA, S. M. (2004). Handbook of industrial Mixing: Science and Practice. John Wiley & Sons, Inc., Hoboken, New Jersey.

PINELLI, D., MONTANTE, G. and MAGELLI, F. (2004). Dispersion coefficients and settling velocities of solids in slurry vessels stirred with different types of multiple impellers. *Chem. Eng. Sci.*, 59, 3081-3089.

RAGHAV RAO, K. S. M. S. and JOSHI, J. B. (1998). Liquid-phase mixing and power consumption in mechanically agitated solid–liquid contactors. *Chem. Eng. J.*, 39(2), 111-124.

RAZZAK, S. A., ZHU, J. X. and BARGHI, S. (2009). Particle shape, density, and size effects on the distribution of phase holdups in an LSCFB Riser. *Chem. Eng. Technol*, 32(8), 1236-1244.

RICHARDSON, J. F. and ZAKI, W. N. (1954). Sedimentation and fluidisation: Part 1.

Trans. IChemE., *32*, 35-53.

RIEGER, F. and NOVAK, V. (1973). Power consumption of agitators in highly viscous non-Newtonian liquids. *Trans. IChemE.*, 51, 105-111.

RIVERA, C., FOUCAULT, S., HENICHE, M., ESPINOSA-SOLARES, T. and TANGUY, P.A. (2006). Mixing Analysis in a Coaxial Mixer. *Chem Eng Sci*., 61(9), 2895–2907.

RUDOLPH, L., SCHAFER, M., ATIEMO-OBENG V. and KRAUME, M. (2007). Experimental and numerical analysis of power consumption for mixing of high viscosity fluids with a co-axial mixer. *Chem. Eng. Res. Des.*, 85(A5), 568-575.

STEVENSON, R., HARRISON, S. T. L., MILES, N. and CILLIERS, J. J. (2006). Examination of swirling flow using electrical resistance tomography. *Powder Technol*, 162, 157-165.

TAHVILDARIAN, P., NG, H., D'AMATO, M., DRAPPEL, S., EIN-MOZAFFARI, F. and UPRETI, S. R. (2011). Using electrical resistance tomography images to characterize the mixing of micron-sized polymeric particles in a slurry reactor. *Chem. Eng. J.*, 172, 517-525.

TAKENAKA, K., YATOMI, R., MORINAGA, S. and TANGUY, P. A. (2006). Comparison of Solid-mixing Performance Between A Pitched Blade Turbine and the Maxblend Impeller. *Proceedings of the 12th European Conference on Mixing,* Bologna, Italy.

TANGUY, P. A., THIBAULT, F., BRITO-DE LA FUENTE, E., ESPINOSA-SOLARES, T. and TECANTE, A. (1997). Mixing performance induced by coaxial flat blade-helical ribbon impellers rotating at different speeds. *Chem. Eng. Sci.*, 52(11), 1733-1741.

TANGUY, P. A. and THIBAULT, F. (2002). Power consumption in the turbulent regime for a coaxial mixer. *Can. J. Chem. Eng.*, 80(4), 601-603.

THIBAULT, F. and TANGUY, P. A. (2002). Power-draw analysis of coaxial mixer with Newtonian and non Newtonian fluids in the laminar regime. *Chem. Eng. Sci.*, 57, 3861-3872.

VIJAYAN, M., SCHLABERG, H. I. and WANG, M. (2007). Effects of Sparger geometry on the mechanism of flow pattern transition in a bubble column. *Chem. Eng. J*, 130, 171-178.

WANG, M., DORWARD, A., VLAEC, D. and MANN, R. (2000). Measurements of gas–liquid mixing in a stirred vessel using electrical resistance tomography (ERT). *Chem. Eng. J.*, 77(1-2), 93-98.

WANG, X., FRADETTE, L., TAKENAKA, K. and TANGUY, P. A. (2012). Effect of operating parameters on the mixing performance of the Superblend coaxial mixer. *Ind. Eng. Chem. Res.*, *51* (4), 1826-1833.

WILLIANMS, R. A. and BECK, M. S. (1995). Process tomography: principles, techniques and applications. *Butterworth-Heinemann Ltd*, Oxford, UK.

YAO, W., MISHIMA, M. and TAKAHASHI, K. (2001). Numerical Investigation on Dispersive Mixing Characteristics of Maxblend and Double Helical Ribbons. *Chem. Eng. J.*, *84*, 565–571.

YATOMI, R., TAKENAKA, K., MORINAGA, S., TAKAHASHI, K. and TANGUY, P.A. (2006). Large Paddle Impeller for Enhancing Surface Aeration: Application to Polymerization Reactor with Liquid Level Change. *Proceedings of the 12th European Conference on Mixing*, Bologna, Italy.

ZWIETERING, T. (1958). Suspending of solid particles in liquid by agitators. *Chem. Eng. Sci.*, 8, 244-253.